Ultrasound-Induced Cavitation for Controlled Drug Release from Thermosensitive Liposomes

by

Anni Pan

A thesis
presented to the University of Waterloo
in fulfillment of the
thesis requirement for the degree of
Master of Applied Science
in
Electrical and Computer Engineering

Waterloo, Ontario, Canada, 2022

Author's Declaration

I hereby declare that I am the sole author of this thesis. This is a true copy of the thesis, including any required final revisions, as accepted by my examiners.

I understand that my thesis may be made electronically available to the public.

Abstract

Ultrasound-induced cavitation of microbubbles has increased anticancer drug Doxorubicin (DOX) release from thermosensitive liposomes (TSL). Yet, the influence of liposomal formulations and their responses toward cavitation on controlled drug release of TSL is inadequately investigated. This novel research evaluates the contribution of heating and cavitation in enhancing drug release of biotinylated, doxorubicin-loaded thermosensitive liposomes (TSL-DOX) by changing liposomal formulations and ultrasound conditions. We have found that combining heating and cavitation triggers the maximum cumulative DOX release (80%~100%) than heating or cavitation only. The final cumulative drug release percentages are mainly dependent on the membrane compositions, which are influenced by changing the molar ratios of DSPE-PEG2K-biotin. Heating TSL-DOX to the phase transition temperature (T_m: ~ 42 ºC) is the driving force of DOX release (~ 70%). However, when the temperature is below T_m, cavitation can also trigger more DOX release of 10~20%. Cavitation (ultrasound frequency: 1 MHz, 10% duty cycle, 1kHz pulse repetition frequency, and 10 s exposure period) increased more DOX release by 20 ~ 25% after heating at 37 ºC and 42 ºC. Without cavitation, changing ultrasound parameters: burst cycles and exposure periods slightly influenced DOX release. Interestingly, increasing the molar ratios of DSPE-PEG2K-biotin decreased DOX release% even treating with cavitation and heating. To further evaluate the influence of cavitation on TSL-DOX, we also developed liposome-conjugated microbubbles (TSL-MB) *via* biotin-avidin-biotin linkage. DiO-labeled TSL-DOX have been shown to conjugate to the surface of DiD-labeled microbubbles. After treating with heating and cavitation, TSL-MB improved DOX release within 5 min of heating, compared to TSL-DOX. In summary, we successfully proved that combining cavitation and heating can improve drug release, and heating to T_m is the major incentive to control drug release. These findings would support the development of novel liposomal drug control-release methods using both cavitation and heating.

Acknowledgements

I would like to thank those who help me during my master's study at the University of Waterloo. First, I would like to gratefully thank my supervisor professor Alfred Yu, who offered me the chance to study at the University of Waterloo and supported me during my research. I would also like to thank the lab mates of LTMUS for discussing research problems and for sharing the lab experience with me.

Second, I would like to extend my sincere thanks to professor Xiaosong Wang, who gives me research suggestions and supports me by sharing his lab resource. I also gratefully acknowledge professor Juewen Liu for his kindness in providing me the access to some experimental instruments. I would like to acknowledge the assistance of the group members of both Prof. Wang's group and Prof. Liu's group.

Third, I would like to thanks to the faculties in the Writing and Communication Center for giving me suggestions and helping me rephrasing my thesis.

Finally, I would like to thank my parents and my fiancé Yulin. The completion of my dissertation would not be possible without their moral and spiritual supports.

Table of Contents

List of Figures

List of Tables

List of Abbreviations

C_3F_8	Perfluoropropane
C_4F_{10}	Perfluorobutane
Chol	Cholesterol
DC	Duty cycle
DiD	1,1'-dioctadecyl-3,3,3',3'-tetramethylindodicarbocyanine perchlorate
DiO	3,3′-dioctadecyloxacarbocyanine perchlorate
DLS	Dynamic light scattering
DPPC	1,2-dipalmitoyl-snro-3-phosphocholine
DSPC	1,2-distearoyl-sn-glycero3-phosphocholine
DSPE-PEG2000-PE	1,2-distearoyl-sn-glycero-3-phosphoethanolamine-N-[methoxy(polyethylene glycol)-2000
DSPE-PEG2000-Biotin	1,2-distearoyl-sn-glycero-3-phosphoethanolamine-N-[biotinyl(polyethylene glycol)-2000
DOX	Doxorubicin
EE	Encapsulation efficiency
E.P.R.	Enhanced Permeation and Retention
FDA	Food and Drug Administration
FRET	Fluorescence resonance energy transfer
HA	Hyperthermia
HIFU	High-intensity focused ultrasound
MB	Microbubble
MI	Mechanical Index
MR	Magnetic resonance
mRNA	Messenger ribonucleic acid
MSPC	1-tetradecanoyl-2-octadecanoyl-sn-glycero-3-phosphocholine
MW	Molecular weights
PEG	Polyethylene glycol
PEG40S	Polyoxyethylene (40) stearate
PRF	Pulse repetition frequency
RT	Room temperature
siRNA	Small interfering ribonucleic acid

SF_6	Sulphur hexafluoride
SHM	Staggered herringbone micromixer
RCF	Relative centrifugal force
RPM	Revolutions per minute
TI	Thermal Index
T_m	Phase transition temperature
TSL	Thermosensitive liposomes
TSL-DOX	DOX-loaded thermosensitive liposomes
TSL-MB	DOX-loaded thermosensitive liposomes conjugated microbubbles

List of Symbols

A	Cross-sectional area
c_o	Speed of sound
f	Center frequency of the transducer
F_o	The initial fluorescent intensity of TSL-DOX solution at room temperature
F_t	The fluorescent intensity of TSL-DOX solution which was heated at different temperature
F_{tx}	The fluorescent intensity of TSL-DOX solution after treated with 1% TritonX-100
ρ_o	Density
p	Spatial peak pressure
I_o	The fluorescent intensity of the mixed solution of TSL-DOX and unloaded DOX before purification
I_t	The fluorescent intensity of TSL-DOX solution after purification
I_{SPPA}	Spatial-peak, pulse-averaged intensity
I_{SPTA}	Spatial-peak, time-averaged intensity
δ	Duty cycle
Q	Flow rate
Q_a	Flow rate of aqueous solvent
Q_o	Flow rate of organic solvent
υ	Flow velocity
W	Acoustic power
W_{deg}	Acoustic power that rises 1 ºC of the temperature

Chapter 1 Introduction

1.1 Chapter Overview

Ultrasound-induced cavitation has been applied to increase anticancer drug: doxorubicin (DOX) release using thermosensitive liposomes (TSL) and liposome-conjugated microbubbles (TSL-MB). As one of temperature-sensitive drug carrying systems, TSL are designed to release the loaded drugs when the environmental temperature has increased to the phase transitions temperature (T_m) of the lipid membrane. Biotinylated lipids are used to develop TSL-MB to increase DOX release by combining both heating and cavitation. However, two essential points about DOX release are unknow: 1) the impacts on drug release after the insertion of biotinylated lipids into TSL; 2) the exact contribution on drug release from heating and cavitation, respectively. To understand the potential influence factors behind cavitation and heating in controlled drug release from TSL. It is necessary to understand what ultrasound-induced cavitation is, what TSL is, and how do TSL release loaded drug. Therefore, in section 1.2, I will introduce the background knowledge about ultrasound-induced cavitation and TSL from four directions: 1) introduced the applications of ultrasound-mediated drug delivery for cancer treatments. 2) explained the fundamental principles of ultrasound-induced cavitation, the safety indexes, and the ultrasound setups. 3) introduced TSL and its preparation; 4) introduced ultrasound-induced cavitation mediated drug release. As the background information has been explained, section 1.3 will introduce the scientific gaps, research motivations, hypothesis, and research objectives.

1.2 Background

1.2.1 Ultrasound-mediated drug delivery in cancer treatment

Cancer is one of the leading causes of death worldwide, which is estimated to lead to ~9.5 million deaths in 2018(Bray et al., 2018). Although nanomedicine (1 ~ 100 nm) increases the drug accumulation of ~5% of the administrated dose in tumor tissue based on the Enhanced Permeation and Retention (E.P.R.) effect in comparison to the free drug, only the < 1% of the injected dose is delivered to a solid tumor(Wilhelm et al., 2016; Boissenot et al., 2016). To improve therapeutic efficacy, some smart drug delivery systems were developed to control drug release and to enhance the local concentrations of anticancer drugs at the tumor sites by some environmental stimulations(Pham et al., 2020). These stimulations include pH, oxidation state, temperature, and physical disruptions(Pham et al., 2020). Among the external control-drug release techniques for cancer treatments, ultrasound has advantages like being non-invasive, controllable, and economically accessible(Meng et al., 2021). As a non-invasive external controlled-drug release technique,

ultrasound can propagate and transport acoustic energy into the tissue medium, generating different bioeffects: cavitation, hyperthermia, thermoablation, and histotripsy(Leighton, 2007). Among these bioeffects, ultrasound-induced cavitation can: 1) mechanically disrupt and increase the permeability of the local blood vessel wall *in vivo*(L. Duan et al., 2020); 2) induce perforation of the cell membrane *in vitro*(Hu et al., 2013); 3) increase endocytosis of the perforated cells *in vitro*(De Cock et al., 2015); 4) change the cell proliferation cycle *in vitro*(Zhong et al., 2011); 5) induce immune effects both *in vivo* and *in vitro*(Tu et al., 2018); 6) mechanically disrupts the drug-carrying systems(Gasca-Salas et al., 2021; Small et al., 2011). Combined with different therapeutic agents, ultrasound-induced cavitation has been applied to increase drug delivery for cancer treatments(Sirsi & Borden, 2014). However, these environmental stimulations like cavitation also add the difficulties in predicting the drug release processes, whose distributions change dynamically along with the cavitation process. It is even harder to predict the drug release behavior of some sensitive drug-carrying systems when they were treated with multiple stimulations like heating and cavitation.

1.2.2 Ultrasound and energy transfer into tissue

Medical ultrasound is generated by a transducer with a center frequency that is above 20 kHz(Leighton, 2007). Depending on the center frequency, the amplitude of the ultrasound intensity attenuates (i.e. attenuation coefficient) differently along with the propagation in the tissue(Leighton, 2007). Ultrasound attenuation happens because of scattering, reflection, and refraction during the propagation in the inhomogeneous tissue where there is bone or gas that causes strong acoustic impedance mismatch. A higher center frequency or a larger acoustic impedance leads to a faster ultrasound attenuation in the tissue(Bamber & Hill, 1979). For therapeutic purposes, the center frequency of the transducer can be 0.5 to 2.5 MHz, allowing ultrasound transmitted into tissue with certain depths(Goss et al., 1979; Grazia Andreassi et al., 2007). The Food and Drug Administration (FDA) has an exposure limit of the ultrasound spatial-peak temporal-average intensity of 720 mW/cm^2 and spatial-peak, the pulse-average intensity of 190 W/cm^2(Nelson et al., 2009). Theoretically, the amplitude level of the ultrasound intensity at the interface area of different depths can be evaluated by the spatial peak pressure (p), speed of sound (C_o) in the transmitting medium, and density (ρ_o) of the medium. As shown in Figure 1, a spatial-peak, pulse-averaged intensity (I_{SPPA}) and a spatial-peak, time-averaged intensity (I_{SPTA}) can be used to evaluate the spatial ultrasound intensity distribution of one ultrasound pulse and a pulse repetition period respectively. This scheme (Figure. 1) is developed based on the previous papers(X. X. Duan et al., 2019; Leighton, 2007; Nelson et al., 2009). Increasing the duty cycle (δ), which is the ratio of pulse period to the entire pulse

repetition period, can increase the I_{SPTA}, allowing more acoustic energy transporting in one pulse repetition period. Increasing the pulse repetition frequency (PRF) or the exposure duration time also increases the total acoustic energy delivery by increasing more ultrasound pulses. Overall, both I_{SPPA} and I_{SPTA} are important indicators to describe the acoustic energy that is delivered to a specific spatial area for therapeutic applications of ultrasound(Leighton, 2007). The control of the acoustic intensity in the targeted tissue can be achieved by adjusting the number of duty cycles, PRF, and the total exposure duration time.

Equation 1

$$\text{pulse repetition period} = \frac{1}{\text{pulse repetition frequency (PRF)}}$$

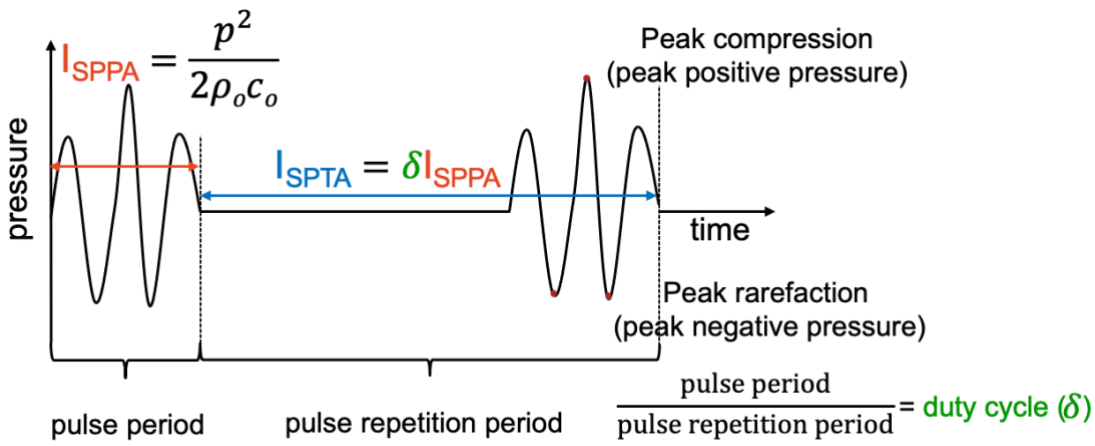

Figure 1 Schematic of the relationship between spatial-peak, pulse-averaged intensity (I_{SPPA}) and spatial-peak, temporal-averaged intensity (I_{SPTA}) in one pulse repetition period.

1.2.3 Ultrasound-induced cavitation of microbubbles

1.2.3.1 The ultrasound contrast agent: microbubbles

An ultrasound contrast agent is a gaseous microbubble, which can scatter ultrasound and enhances the intravascular contrast of the ultrasound signal, improving the image quality. Microbubbles are formed by a monolayer of phospholipids and a gas core. The microbubbles are usually with 1-10 μm of size and an inert low solubility gas core. (Stride et al., 2020). The microbubbles can be prepared after mechanical agitation with a concentration of 10^8-10^9 bubbles/mL and are usually administrated with 2 mL by intravenous injection(Stride et al., 2020). The currently approved clinically used microbubbles include SonoVue®, Difinity®, and Sonazoid®, which are all phospholipids-coated shells with the gas core as perfluoropropane

(C_3F_8) or sulfur hexafluoride (SF_6)(Ignee et al., 2016). Although the lipid-shell and the low solubility gas improved the stability of microbubbles, the *in vivo* circulation half-life of a microbubble is still shot (<5 min)(Stride et al., 2020). As a result, microbubbles have limited the drug delivery efficiency. Some studies have incorporated drug-carrying particles (e.g., thermosensitive liposomes) into microbubbles to control drug release(Zhang et al., 2020). Yet, there is lack of understanding of the enhancing drug release mechanisms regarding the ultrasound conditions such drug carrying systems.

1.2.3.2 Ultrasound-induced cavitation

Ultrasound-induced cavitation is a process of volumetrically oscillation and collapse of microbubbles with gas nucleus. As shown in Figure. 2, during cavitation, microbubbles expand at a negative ultrasound pressure phase and contract at a positive ultrasound pressure phase after ultrasound exposure. Cavitation mechanically disrupts the nearby environment based on microstreaming, micro-jet, oscillation, or shockwave of the microbubbles(Coussios et al., 2007; Tung et al., 2010). Cavitation can be further categorized into stable cavitation and inertial cavitation(Gu et al., 2016). Both types of cavitation can induce bioeffects like perforation of the cell membrane or increased permeability of the targeted blood vessel wall(Dong et al., 2018; Wang et al., 2018). Based on these bioeffects, for *in vivo* studies, ultrasound-induced cavitation has been applied to increase drug delivery into the brain by temporally opening the blood-brain barrier in the latest clinical trial to treat glioblastoma(Idbaih et al., 2021) and Parkinson's disease with dementia(Gasca-Salas et al., 2021). For *in vitro* studies, ultrasound-induced cavitation induces perforation of the cell membrane, which increases the intracellular delivery of therapeutic agents(Leighton, 2007; Stride et al., 2020).

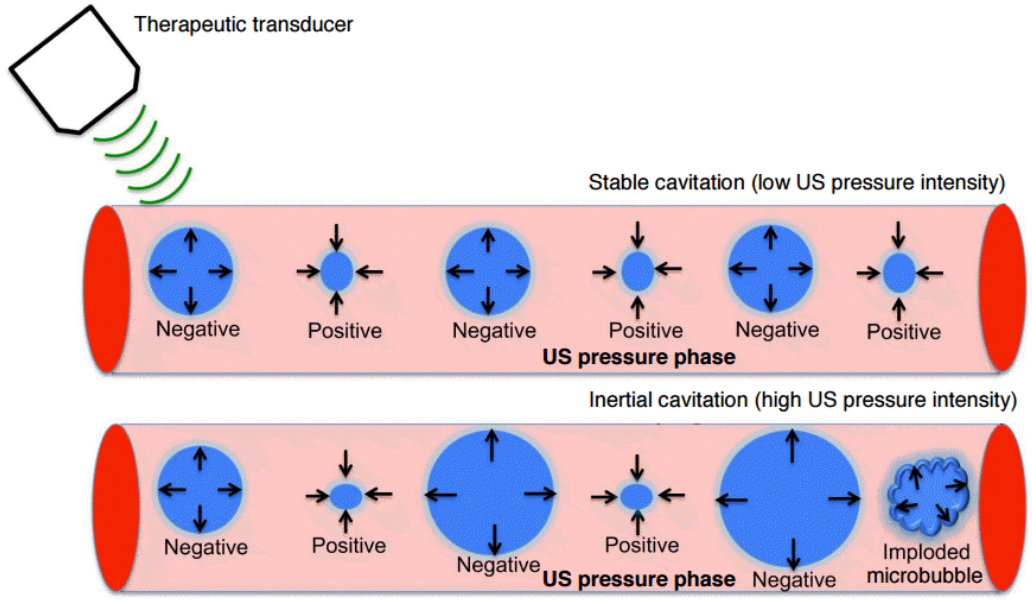

Figure 2 Schematic drawing of the principles of stable and inertial cavitation.

1.2.3.3 Parameters for ultrasound-induced cavitation

Ultrasound with a center frequency of 1 ~ 2 MHz and a peak negative pressure of 0.1 ~ 0.5 MPa is commonly used to induce cavitation(Hu et al., 2013; Suzuki et al., 2009; Yang et al., 2008). As shown in Figure 2, with strong ultrasound power inrushes the liquid at the peak rarefaction pressure, the inertial cavitation can induce gas cavities and collapse of the generated bubbles, generating strong mechanical disruptions that damage the tissue or the blood vessel(W.-S. Chen et al., 2003; Mullick Chowdhury et al., 2017). With sub-harmonic (e.g. 0.5 f_o) or ultra-harmonic responses (1.5 f_o), the stable cavitation also generates mechanical disruption during the oscillation process of microbubbles(Gu et al., 2016; Mullick Chowdhury et al., 2017). The ultrasound intensity, pulse length, and duration time will influence the cavitation effect, which could either improve drug delivery or generate side effects like tissue damage(Chang et al., 2001; Mullick Chowdhury et al., 2017). Therefore, controlling the ultrasound conditions to trigger drug release is significant.

1.2.3.4 The safety indexes: medical index (MI) and thermal index (TI)

The Mechanical Index (MI) and the Thermal Index (TI) are commonly used to further specify the safety requirements of acoustic exposures(Duck, 2007). These two indices can be calculated as follow(Duck, 2007):

Equation 2

$$\mathrm{MI} = \frac{p}{\sqrt{f}}$$

Equation 3

$$\mathrm{TI} = \frac{\mathrm{W}}{W_{deg}}$$

Where W is the acoustic power; W_{deg} is the acoustic power that rises 1 ºC of the temperature at the focal area. p is the spatial peak pressure. f is the center frequency of the transducer.

The medical index (MI) defines the inertial cavitation threshold that limits the ultrasound-induced mechanical disruptions level of the targeted tissue to avoid shock waves and shear that can strongly damage tissue(Duck, 2007; Grazia Andreassi et al., 2007). According to the FDA standard, the maximum MI is 1.9, except for ophthalmology(Leighton, 2007). In this research, we are focusing on cavitation (MI < 1.9) with the presence of a lipid shell-covered, C_4F_{10} gas-based microbubble.

Heat transfer into the tissue is the endpoint of ultrasound attenuation, resulting in the local temperature rise at the targeted region. The thermal index (TI) defines the temperature rise threshold when the acoustic energy was absorbed by the targeted tissue. According to the FDA standard, the maximum TI is 6.0, except for fetus or ophthalmology(Leighton, 2007). Therefore, in this research, we use low-intensity ultrasound that theoretically causes no thermal effect.

1.2.4 The ultrasound setups

An ultrasound setup is a platform that adjusts the ultrasound parameters to induce bioeffects (i.e. cavitation or heat) at the focal tissue or cell suspension. For either *in vivo* or *in vitro*, an ultrasound platform should provide controllable experimental conditions and repeatable therapeutic results(Hensel et al., 2011). There are four necessity parts of an *in vitro* ultrasound platform: 1) a signal generator that adjusts the ultrasound parameters: a duty cycle and pulse repetition period; 2) a power amplifier that amplifies the generated signal; 3) a transducer that received the signals and pulses ultrasound to the focal region; 4) a sample chamber that contains the sample solutions and receives the acoustic energy generated from the transducer(X. Chen et al., 2013; X. X. Duan et al., 2019; Hensel et al., 2011). However, the reproducibility of the experimental results varies a lot by using different kinds of ultrasound setups(Hensel et al., 2011). Coupling gel or water is commonly used to match the acoustic impedance between the transducer and the medium, facilitating the propagation of ultrasound(Leighton, 2007; Nelson et al., 2009). Therefore, the transducer is usually placed in a water tank or is connected to a waveguide which contains coupling gel to match the acoustic impedance

between the transducer and the sample chamber(Hu et al., 2013). To achieve a harmonic acoustic pressure, the distance between the transducer and the sample chamber should be equal to the geometry focal length of the transducer. As shown in Figure 3, four different kinds of ultrasound setups are commonly used in the *in vitro* experiment: 1) a transducer is under the cell culture well, whose bottom is attached with the coupling gel; 2) a transducer is under the cell culture well, whose bottom is attached to water surface; 3) a transducer is under a sealed cell chamber, both are immersed in water; 4) a transducer is above the cell culture well, immerged in the cell culture medium(Hensel et al., 2011).

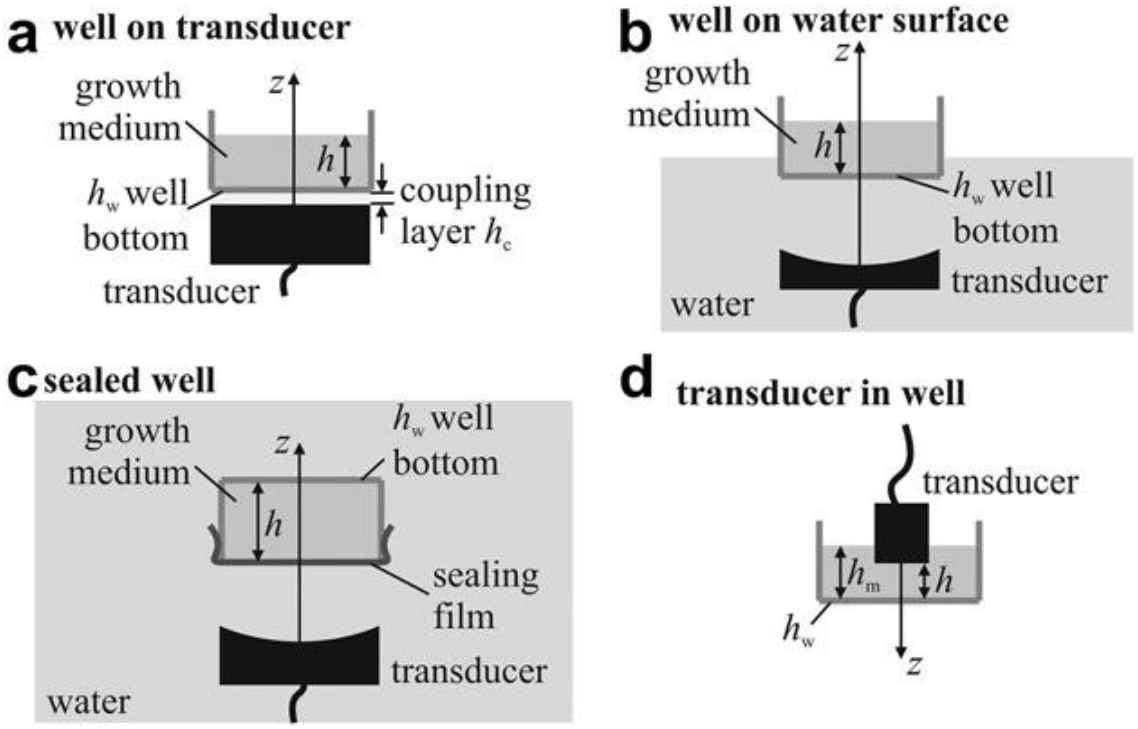

Figure 3 Different approaches of *in vitro* ultrasound therapy.

Since the microbubbles are highly susceptive to the change of acoustic pressure, the ultrasound setup should be designed to keep a homogenous acoustic pressure field(X. X. Duan et al., 2019). Therefore, in this research, I used an ultrasound setup (i.e. type-3 sealed well) that is based on the lab's previous published paper to investigate the cavitation of microbubbles(X. X. Duan et al., 2019). This type of setup helps to achieve a homogenous acoustic pressure field from two aspects: 1) avoid acoustic reflection; 2) minimize the acoustic impedance between the transducer and the sample solution.

1.2.5 A drug loaded thermosensitive liposome

1.2.5.1 Introduction of liposomes

A liposome, a hollow spherical vesicle, was firstly developed in 1965 by Bangham *et al*(Jesorka & Orwar, 2008). Liposomes are formed when amphipathic molecules, mostly phospholipids, rearrange with the hydrophilic part of the molecules facing the aqueous phase, while the hydrophobic part of the same molecule faces each other (Carugo et al., 2016). Liposomes are produced with a structure of a bilayer (~ 5 nm) of phospholipids and an aqueous core (0.02 – 250 um)(Swaay & deMello, 2013). Criteria of liposomes include size distribution, lipid membrane composition, lamellarity, and encapsulation efficiency of the loaded cargo(Kotouček et al., 2020; Evers et al., 2018). Liposomes have been used to load different kinds of therapeutic agents: proteins, peptides, genes, and small molecule drugs by inserting these agents into the lipid bilayer membrane or loading them into the aqueous core("Doxil® — The First FDA-Approved Nano-Drug: Lessons Learned," 2012; Swaay & deMello, 2013). So far, liposomes are one of the widely clinically used carrier systems to load anticancer therapeutic agents.

1.2.5.2 Introduction of thermosensitive liposomes

To meet the needs of spatially specific drug release at the targeted point and minimize the toxicity side effect on the normal organs, the temperature-sensitive liposomes (TSL) were firstly developed in 1978 by Yatvin et al(Yatvin et al., 1978). The lipid compositions of the TSL included 1,2-dipalmitoyl-snro-3-phosphocholine (DPPC) and 1,2-distearoyl-sn-glycero3-phosphocholine (DSPC) with a molar ratio of 3:1. The TSL can response to and release the loaded cargo at the external temperatures from 40 to 45 ºC(Kneidl et al., 2014; Landon et al., 2011). To have a higher drug encapsulation efficiency, longer *in vivo* circulation time, and a faster drug release, the low-temperature sensitive liposomes (LTSL) were developed in 1996(Landon et al., 2011). The polyethylene glycol (PEG) modified lipids, cholesterol, and a lysolipid (i.e. 1-tetradecanoyl-2-octadecanoyl-sn-glycero-3-phosphocholine (MSPC)) were incorporated into the lipid bilayer to develop LTSL, leading to an ultra-fast release 80% of the loaded drugs in 20s at 41.3 ºC (Kneidl et al., 2014). As one of the clinically related LTSL, the Thermodox® (Celsion, USA), firstly reported by Needham *et al* in 2000, is the first thermal sensitive liposome that has reached Phase-III trial(Regenold et al., 2022).

1.2.5.3 Drug release and membrane compositions of thermosensitive liposomes

The drug release from TSL is highly dependent on the integrity and the arranging state of the lipid bilayers. Four major factors illustrate the integrity changes of lipid bilayers: 1) membrane penetration by inserting

proteins through the lipid bilayer(Harayama & Riezman, 2018); 2) membrane defects because the incorporation of small molecules (cholesterol or hydrophobic drugs) between lipid bilayers(Fahr et al., 2005; Guion & Fayer, n.d.); 3) membrane perforation induced by incorporation of surfactants(Kneidl et al., 2014; Needham et al., 2013); 4) adjust the thickness of the membrane using special lipids (Lyso-lipids)(Needham et al., 2013). Regarding the state of the lipid bilayer, the phase transition temperature (T_m) of phospholipids plays a key role. As shown in Figure 4, three drug release mechanisms are related to the phase changes of the lipid bilayers of TSL(Kneidl et al., 2014). First, there is low permeability of the loaded drugs (yellow pentagon) to diffuse across the lipid bilayer into the external environment when the temperature is much lower than T_m. Second, the highest permeability of the loaded drugs is achieved when the temperature is close to T_m. Third, a high permeability is achieved when the temperature is much higher than T_m(Kneidl et al., 2014). The temperature changes influence the arrangement of lipid bilayer from ordered gel phase to disorder liquid phase, which allows the packed drugs to diffuse from the aqueous core to the external environment(W. Chen et al., 2018; Kneidl et al., 2014). Ultrasound-induced cavitation mechanically affects the integrity of lipid membranes, while the heating effect can also change the lipid arrangement states. Therefore, theoretically both cavitation and heating can influence the drug release. To better combine these two effects for controlled-drug release, it is crucial to know which effect is the key factor.

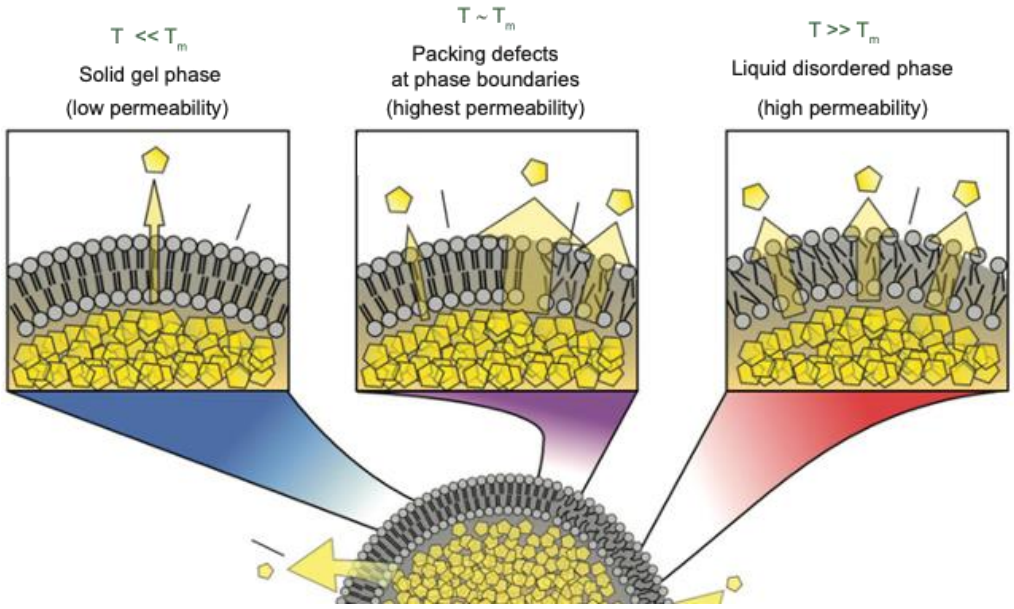

Figure 4 Phase changes and drug release from thermosensitive liposomes.

1.2.5.4 Preparation methods of liposomes

The preparation method impacts the qualities of liposomes, which in turn further influences the drug encapsulation efficiency. The conventional methods for liposome production include thin-film hydration, reverse-phase evaporation, and solvent (commonly ethanol) injection(Dua et al., n.d.). The ethanol injection method, reported in 1970, can be used for macroscale production of liposomes with low degradation of phospholipids while providing acceptable homogeneous size distribution(Batzri & Korn, 1973; Charcosset et al., 2015). However, the ethanol injection method as well as the other conventional methods have limited reproducibility among different batches. In contrast, microfluidic mixing provides fine-tune quality control of liposome production with higher reproducibility and material usage efficiency (Swaay & deMello, 2013). The microfluidic methods for liposome production include extrusion, pulsed jetting, and transient membrane ejection(Carugo et al., 2016). Currently, three new microfluidic mixing methods for liposome production include staggered herringbone mixing (SHM), T-junction mixing, and microfluidic hydrodynamic focusing (MHF)(Evers et al., 2018). Reported in 2002, the SHM microfluidic channel design showedd advantages in increasing the mixing efficiency of different solvents by chaotic advection, based on the patterned herringbone grooves at the bottom of the channel(Stroock et al., 2002). Curretnly, SHM is also used to produce DOX-loaded liposomes with narrow size distribution and high agent encapsulation efficiency >80%(Cheung et al., 2020). Therefore, I used a SHM micromixer to produce TSL.

1.2.5.5 Production of liposome by a staggered herringbone micromixer

Liposomes produced by microfluidic mixers are affected from two aspects: 1) the geometry of the mixing channel; 2) the flow rate and diffusion coefficient of the aqueous and organic solvents. Flows that inside the microfluidic mixer are laminar flow, which has a low Reynolds (Re) number of 13.5 << 2000(Yu et al., 2009). Though a laminar flow has no disruptions between fluid layers, staggered herringbones increase the chaotic rotations inside the channel. In addition to the geometry of the mixing channel, both the total flow rate (TFR) and the flow rate ratio (FRR) of the aqueous and organic solvents also influence the size distribution and polydispersity index (PDI) of liposomes. TFR is the sum of flows inside the mixing channel; FRR is the flow rate ratio of the aqueous solvent and the organic solvent.

Equation 4

$$Flow\ rate\ (Q) = \upsilon A$$

Equation 5

$$Flow\ rate\ ratio(FRR) = \frac{Q_a}{Q_o}$$

Equation 6

$$Total\ flow\ rate(TFR) = Q_a + Q_o$$

Where Q_a is the flow rate of aqueous solvent; Q_o is the flow rate of organic solvent; υ is flow velocity, A is cross-sectional vector area.

Based on different structural designs of micromixers, different TFR and FRR have been adjusted to produce liposomes. However, TFR ≥ 10 mL/min and FRR ~3 are commonly used to produce liposome, which can produce liposomes with a size of 100 to 150 nm and a PDI < 0.2(Jahn et al., 2008). The encapsulation efficiency of the therapeutic agents (e.g. DOX) of a liposome is as high as 80-90%(Cheung et al., 2020; Jahn et al., 2008). Therefore, in this research, I produced the drug loaded thermosensitive liposomes with the TFR of 6~10 mL/min and FRR of 3.

1.2.6 Ultrasound-induced cavitation mediated drug release from liposomes

1.2.6.1 Ultrasound-induced cavitation mediated drug release and cellular uptake

The ultrasound-induced cavitation of microbubbles that causes perforation on the cell membrane with a size of nanometers to micrometers, has been shown to improve the intracellular delivery of multiple types of therapeutic agents(De Cock et al., 2015; Leow et al., 2015). With different acoustic pressures (~0.5 MPa), ultrasound-induced cavitation can perforate the membrane of cells, with pore sizes ranging from nanometers (diameter: ~10 - 500 nm) to micrometers (~1 - 4.3 μm) (Hu et al., 2013; Yang et al., 2008; Zeghimi et al., 2012). Ultrasound-induced cavitation facilitates intracellular transportation of therapeutic agents with a wide range of molecular weights (MW) from 4.4 to 500 kDa(Takahashi et al., 2019). The maximum MW of the delivered agents can reach up to 2000 kDa(Takahashi et al., 2019). Therefore, some studies also applied cavitation to improve uptake of drug loaded nanoparticles like liposomes(De Temmerman et al., 2011).

1.2.6.2 Ultrasound-induced drug release from liposomes

Cells and liposomes share similar structures as a vesicle formed by a bilayer phospholipid membrane and an aqueous core(Lasic, 1992). However, as artificial vesicles, liposomes are different from the cell in two respects: the physical and the chemical properties, which can be manually changed. These physical properties include size, membrane stiffness, and surface tension. The chemical properties include shell

chemistry, lipid compositions, and ligand conjugations(Harayama & Riezman, 2018; Kneidl et al., 2014). With diverse physical and chemical properties, the drug release of liposomes varies in response to ultrasound-induced cavitation(Daeichin et al., 2017; Small et al., 2012; Stride et al., 2020). Ultrasound-induced cavitation has been used to enhance drug release from liposomes(Boissenot et al., 2016; Couture et al., 2014). Yet, no study has investigated cavitation and heating-mediated controlled drug release from thermosensitive liposomes by changing their membrane formulations and ultrasound conditions.

1.2.6.3 Ultrasound-induced cavitation mediated drug release from liposome-conjugated microbubbles

Microbubbles are essential to achieve the ultrasound-induced cavitation effect. However, liposomes are better drug carriers than microbubbles regarding their *in vivo* stability and their *in vitro* long-term storage(Stride et al., 2020). To better combine cavitation and heating for controlling drug release, thermosensitive liposome-conjugated microbubbles (TSL-MB) were developed(De Temmerman et al., 2011; Zhang et al., 2020). To develop TSL-MB, the drug-loaded liposomes are conjugated to the surface of the microbubbles via linkages: biotin-avidin or maleimide-thiol(Cool et al., 2013; De Cock et al., 2016; Dewitte et al., 2014). Both kinds of linkages are commonly used for bioconjugations, forming a stable conjugation(LI et al., 2014; Sapra & Allen, 2003). Theoretically, 600-1300 of the liposomes (diameter: ~100 nm) can be linked to the surface of one microbubble (diameter: ~4 μm)(Luan et al., 2012) through biotin-avidin conjugations. In the current study, $1.32*10^{12}$ of the liposome-conjugated microbubbles (20 mg/m^2 of liposomes) are given *in vivo* to the tumor-bearing mice(Lentacker et al., 2010). Though the anticancer efficacy has been improved, these studies did not investigate how does the biotinylated lipids influence the drug release of liposomes and how much contribution of increasing the drug release is from cavitation. In this research, I used biotin-avidin linkage to prepare doxorubicin-loaded thermosensitive liposome-conjugated microbubbles (TSL-MB) to investigate DOX release after heating and cavitation. On one hand, TSL-MB can respond to ultrasound because one of its components: microbubble is necessary to induce the cavitation. On the other hand, the attached doxorubicin-loaded thermosensitive liposomes (TSL-DOX) can release the loaded DOX when they are heated to the phase transition temperature. Using TSL-MB as the drug-carrying system, cavitation can directly impact the nearby liposomes because of the conjugation between microbubbles and liposomes. In comparison to the previous studies, in this research I changed the molar ratios of the biotinylated lipids on TSL-DOX to investigate how the membrane compositions will affect the drug release when combined heating and cavitation.

1.3 Outline of thesis study

1.3.1 Motivation and hypothesis

Ultrasound-induced cavitation of microbubbles has increased anticancer drug Doxorubicin (DOX) release from thermosensitive liposomes (TSL). However, in practical applications, both heating and cavitation are combined to enhance DOX release. Since microbubble is required to induce cavitation, two drug delivery systems are used: 1) mixed solutions of drug loaded TSL and microbubbles(Shen et al., 2020); 2) drug loaded TSL-conjugated microbubbles(Lentacker et al., 2007). Since drug release will affect the final efficacy of cancer treatments, it is necessary to know either heating or cavitation is the major incentive in triggering drug release. This is also important for developing new functional drug-carrying systems like thermosensitive liposomes-conjugated microbubbles (TSL-MB) to combine heating and cavitation for increasing drug release. For the preparation of TSL-MB, some studies used biotin-avidin linkage to conjugate the DOX-loaded, biotinylated thermosensitive liposomes (TSL-DOX) to biotinylated microbubbles (De Temmerman et al., 2011; Zhang et al., 2020). However, it is unclear how do biotinylated lipids affect DOX release from TSL-DOX. The insertion of biotinylated lipids to the membrane of TSL might influence the phase transition temperature, which is directly related to the thermal sensitivity and drug release. Yet, no study has investigated how will the drug release behavior change after changing the molar ratios of biotinylated lipids on the membrane of TSL. When combined heating and cavitation to increasing DOX release from TSL-DOX or TSL-MB, it is unknow how much contribution is from ultrasound-induced cavitation? Is heating or cavitation the primary cause in triggering DOX release? Will different ultrasound conditions affect the enhancement of drug release? Will the enhancement of DOX release change if the membrane formulations of TSL were different even with the help of cavitation? Whether TSL-MB is a better drug-carrying system than TSL-DOX to releaser more drugs after heating and cavitation? This research project is motivated to investigate the above questions to find out how cavitation and heating will affect drug release when the ultrasound parameters and membrane formulations of TSL were changed. We hypothesize that increasing temperature to the phase transition temperature (T_m) of TSL-DOX is the driving force of DOX release, while cavitation helps to further increase the cumulative DOX release after heating. The sub hypothesis is that TSL-DOX, formed with different molar ratios of biotinylated lipids, will respond differently to cavitation and heating regarding drug release.

1.3.2 Research objectives

The overall goal of this research project is to investigate the drug release mechanisms of combining heating and ultrasound-induced cavitation to increase doxorubicin (DOX) release from DOX-loaded thermosensitive liposomes (TSL-DOX) that are formed with different molar ratios of biotinylated lipids. To achieve this goal, three research objectives have been exploited: 1) the preparation of TSL-DOX and evaluation of their drug release treating with heating only; 2) analysis of drug release of TSL-DOX, with different membrane compositions, after heating and cavitation; 3) develop TSL-MB and investigate their DOX release behavior after heating and cavitation. Details of each research objective are introduced as below:

1. Develop TSL-DOX, with different molar ratio of biotinylated lipids on the membrane, using a microfluidic method. Characterized the prepared TSL-DOX with the criteria of size, stability, polydispersity, encapsulation efficiency (EE) of DOX, and DOX release at different temperatures.
2. Develop biotinylated microbubbles and evaluate the cavitation of them after ultrasound exposures. Evaluate the DOX release from TSL-DOX triggered by heating and ultrasound-induced cavitation of microbubbles by changing the heating conditions (e.g. temperatures and duration time) and ultrasound parameters (e.g. pulse cycles, pulse repetition frequency, and exposure duration time).
3. Develop a new ultrasound-responsive drug-carrying system: doxorubicin-loaded thermosensitive liposome conjugated microbubbles (TSL-MB). Evaluate size, morphology, and conjugation of TSL-MB. Compare the DOX release of TSL-MB and TSL-DOX after heating and cavitation.

1.3.3 Significance and contributions

This research project proved that heating is the driving force of controlled drug release of TSL-DOX, while the combination of cavitation and heating can further increase the drug release. Another drug-carrying system DOX-loaded thermosensitive liposome conjugated microbubble (TSL-MB) has also been prepared. We also proved that combing heating and cavitation might improve the drug release at the early heating time. This drug-carrying system can also be used to investigate the drug releaser kinetics of ultrasound-induced cavitation on other drug loaded liposomes. In summary, the results of this project provide more thoughts in developing a new drug-controlled release method combining cavitation and heating.

Chapter 2 Materials and Methods

2.1 Chapter overview

This chapter introduced the materials and experimental methods to achieve three research objectives. Specific methods for each research objective were introduced as below:

Research objective 1: Develop TSL-DOX using the microfluidic method and characterize the prepared doxorubicin-loaded thermosensitive liposomes (TSL-DOX); section 2.2 introduced the preparation of TSL-DOX using the microfluidic method. Section 2.2 ~ 2.4 introduced the methods for evaluations of TSL-DOX including size, stability, polydispersity, encapsulation efficiency (EE) of DOX, and DOX release percentages at different temperatures, using Dynamic Light Scattering (DLS) and fluorescent spectrophotometer.

Research objective 2: Triggering DOX release from TSL-DOX by combing heating and ultrasound-induced cavitation to. Section 2.5 introduced the methods for evaluations of DOX release when TSL-DOX were heated at different temperatures or the phase transition temperature (T_m). After that, section 2.6 introduced the evaluations of DOX release after cavitation and heating by changing the ultrasound parameters using an ultrasound setup.

Research objective 3: Develop and evaluate another drug-carrying system doxorubicin-loaded thermosensitive liposome conjugated microbubbles (TSL-MB). Section 2.7 introduced the preparation of TSL-MB by conjugating TSL-DOX to biotinylated microbubbles. Finally, section 2.8 introduced how to test the size, morphology, and conjugation of TSL-MB using fluorescent microscopy.

In summary, this chapter has introduced how to prepare different drug-carrying systems and how to gain the initial results of controlled-DOX release by combining cavitation and heating. I will introduce the test results in the next chapter.

2.2 Preparation of thermosensitive liposomes

2.2.1 Geometry of a micromixer and the setup

The production of liposomes is related to the designs of microfluidic chips(Joshi et al., 2016; Swaay & deMello, 2013). Before using the microfluidic method to prepare thermosensitive liposomes, I first evaluated the geometry of the micromixer. The channel geometry of the staggered herringbone micromixer (Fluidic 187, Microfluidic ChipShop, Germany) was detected by a fluorescent microscopy platform using a 10X objective (Axio Observer Colibri 5, Carl Zeiss, Germany). Based on the optical results, I developed

a scheme image of the two microfluidic channels of the staggered herringbone micromixer (SHM) using COMSOL Multiphysics®. Figure 5 showed the structures of the channels. Channel 1&2 are consisted of staggered oblique ridges and herringbones. Differently, channel 3 is formed by staggered herringbones. As shown in Figure 5b, there are 20 grooves in each channel, equaling to 4 cycles of mixing per channel. Table 1 showed the physical dimensions of specific parts of the SHM chip, which has 600 μm of mixing length of each channel. The width of each channel is 300 μm. For both staggered oblique ridges and herringbones, the height of grooves was 25 μm, while the height of the cover lid was 175 μm. The join angle between inlets was 120º, while the join angle of the herringbones was 90º.

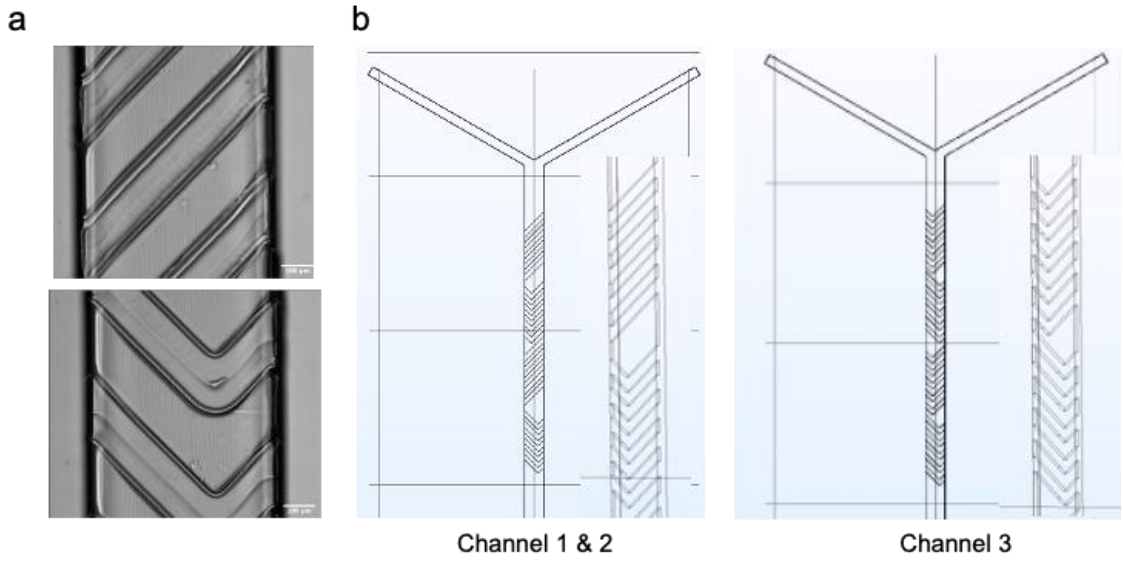

Figure 5 (a)Structures and (b)channel geometries of a staggered herringbone micromixer. Scale bar = 100 μm.

Table 1 Channel geometries of a staggered herringbone micromixer

	Category name	**Units**
Width	Herringbone mixer	600 μm
	Channel	300 μm
	Inlets	300 μm
	Herringbones	130 μm
	Distance between two herringbones	130 μm
Length	Outlets	600 μm

Hight	Herringbone grooves	25 µm
	Lid	175 µm
Angle	Join of inlets	120º
	Join of herringbones	90º

According to the literature, 15 cycles provide a better mixing effect to produce liposomes(Stroock et al., 2002). Therefore, three channels are connected in series to achieve the maximum mixing effect of 12 cycles. As shown in Figure 6a, two outlets of channel 1&2 were blocked (the red crosses) to prevent leaking of the solution. All inlets and outlets were connected with the nuts (green connectors) that were further connected to silicon tubes. The silicon tubes were connected to the syringes by 25G needles. Figure 6b shows more details that all channels were connected from No. 1 to No.3. The organic and aqueous solutions were injected into two inlets of channel 3, and the prepared liposomes were collected from the outlet of channel 1.

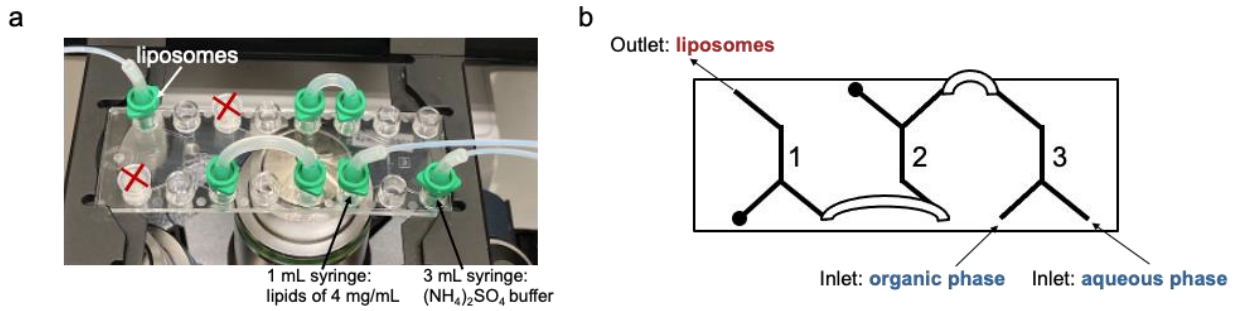

Figure 6 (a) Channel connection and (b) connecting sequence of a staggered herringbone micromixer.

2.2.2 The flow estimations in a SHM and the microfluidic setup

The schematic of liposome preparation using a staggered herringbone micromixer (SHM) was shown in Figure7a. The lipids in ethanol and $(NH_4)_2SO_4$ buffer are mixed inside the micromixer, generating liposomes. In Figure 7b, the simulations of the flow inside the SHM showed that the herringbones at the bottom can guide the flow from X, Y, and Z directions. In the XY-plane, the flow changed from straight to zigzag directions. In the YZ-plane, the flow also changed from horizontal to fluctuate. Finally, the flow direction also changed at the XZ-plane when the flow went into the herringbone grooves. These simulation results showed that the flow become more chaotic once it went through the micromixer, making a homogenous mixing of the lipids and the aqueous buffer. Theoretically, the lipids materials will form

liposomes in such a homogenous mixing. Therefore, I used this kind of micromixer to produce liposomes in the follow experiment.

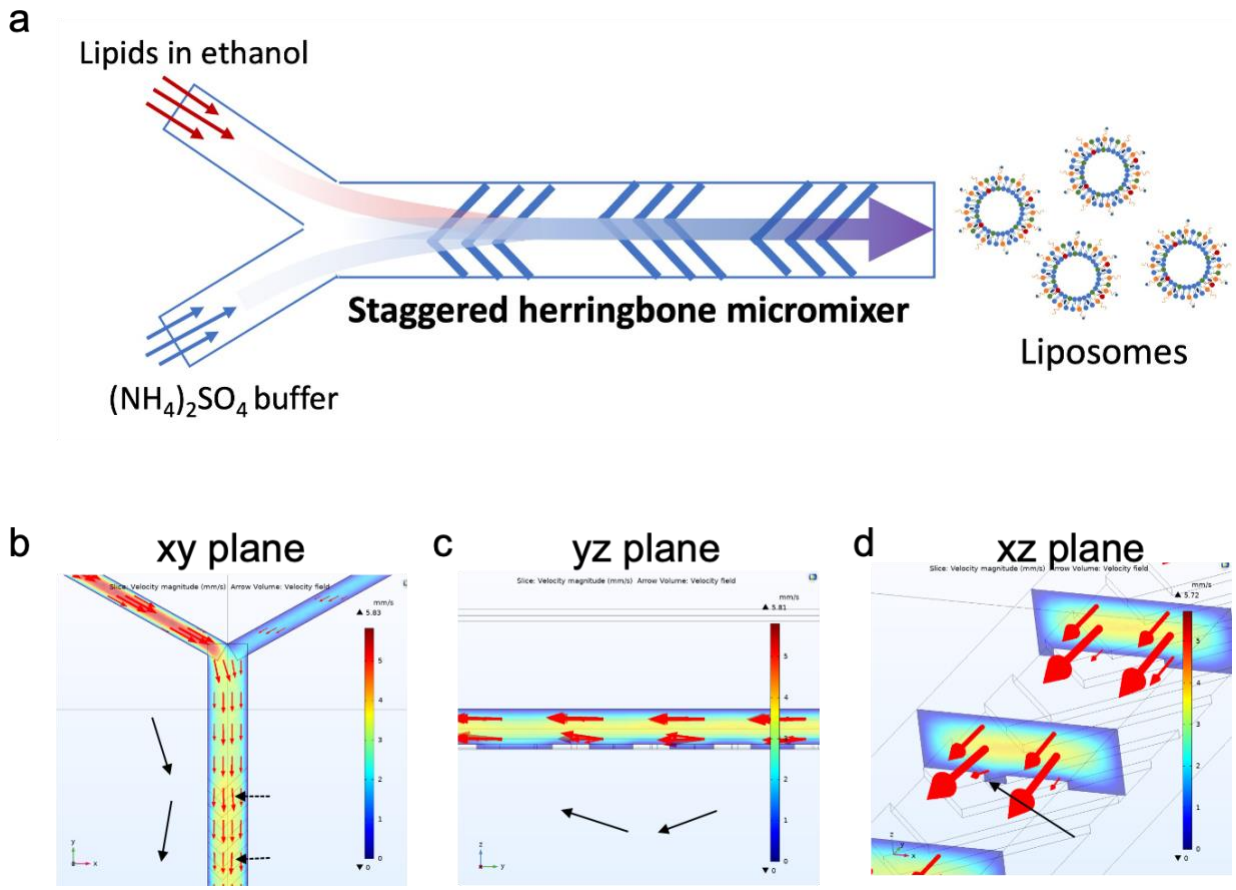

Figure 7 (a) Schematic of liposomes preparation using a staggered herringbone micromixer; Simulations of flows inside the micromixer from (b) xy-plane, (c) yz-plane, and (d) xz-plane.

Figure 8 showed the microfluidic setup. Two syringes were respectively installed on two syringe pumps with the plunger flanges attached to the pusher of each pump. All connections were checked for leakage and washed with DI water by turning on two syringe pumps for 1 min.

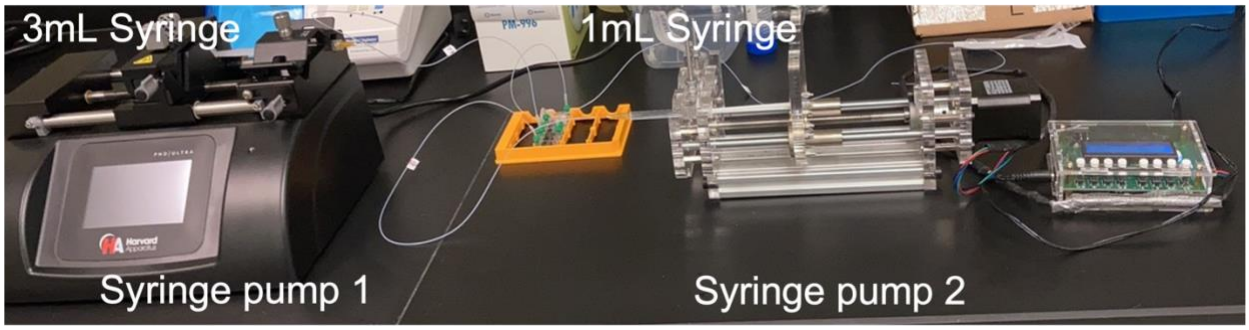

Figure 8 Microfluidic setup of producing liposomes using a staggered herringbone micromixer.

2.2.3 Preparation of TSL using the staggered herringbone micromixer

Thermosensitive liposomes (TSL) were prepared using a staggered herringbone micromixer (SHM). 1,2-dipalmitoyl-sn-glycero-3-phosphocholine (DPPC), 1,2-distearoyl-sn-glycero-3-phosphocholine (DSPC), 1,2-distearoyl-sn-glycero-3-phosphoethanolamine-N-[methoxy(polyethylene glycol)-2000] (DSPE-PEG2000-PE), 1,2-distearoyl-sn-glycero-3-phosphoethanolamine-N-[biotinyl(polyethylene glycol)-2000] (DSPE-PEG2000-Biotin), and cholesterol (Chol) are all from Avanti Polar Lipids, Sigma-Aldrich), Canada. Two fluorescent dyes were used to label the TSL: 3,3′-dioctadecyloxacarbocyanine perchlorate (DiO, excitation: 484 nm, emission: 501 nm, Vybrant™, ThermoFisher, Canada) and 1,1'-dioctadecyl-3,3,3',3'-tetramethylindodicarbocyanine perchlorate (DiD, excitation: 644 nm, emission: 665 nm, ThermoFisher, Canada). All lipids and the fluorophore were dissolved in ethanol and added into a 10 mL glass bottle at a molar ratio: DPPC:DSPC:Chol:DSPE-PEG2000-PE:DSPE-PEG2000-Biotin:dye = 53:26:16:x:5-x:0.1 with a total lipid concentration of 4 mg/mL. Figure 9 showed the arrangement of all lipid materials of a doxorubicin (DOX) loaded liposome. The bilayer lipids formed a vesicle with DOX loaded in the aqueous core.

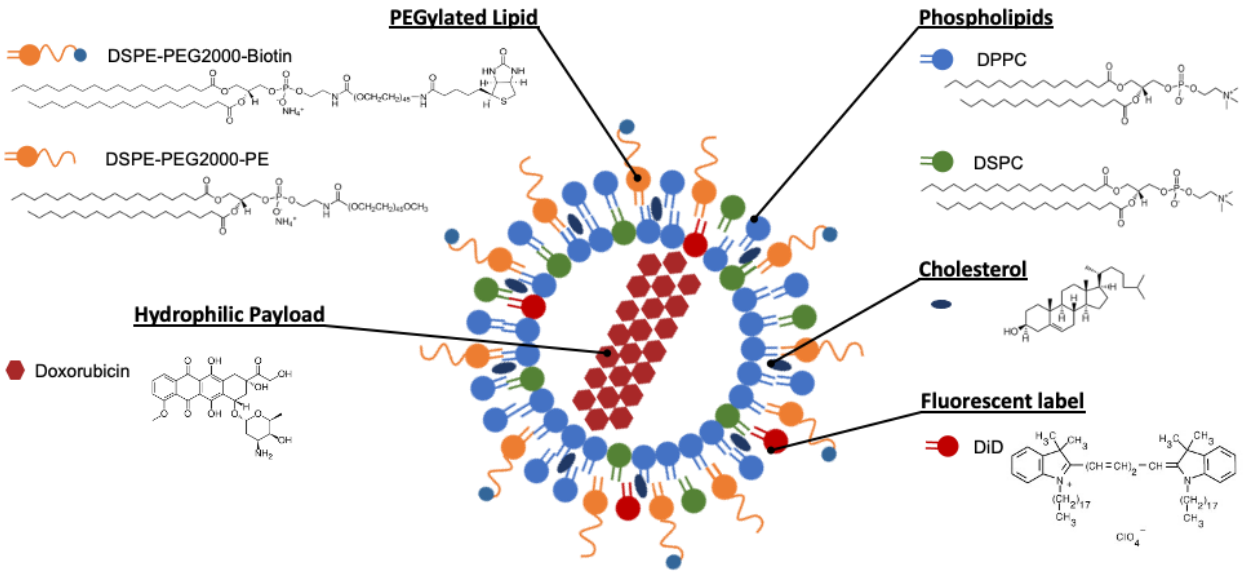

Figure 9 Schematic of a DOX-loaded thermosensitive liposome (TSL-DOX).

The $(NH_4)_2SO_4$ buffer (250 mM) was prepared and heated to 60 °C using a water bath. Then, the lipid mixture solution and the pre-heated $(NH_4)_2SO_4$ buffer were withdrawn using a 1mL syringe and a 3 mL syringe, respectively. Install the syringes to two syringe pumps and run the syringe pumps. For the 3 mL syringe, the pushing rate of the syringe pump (PHD UlTRA™, Harvard Apparatus) was set to 3 ml/min; For the 1 mL syringe, the pushing rate of the syringe pump was set to 1mL/min. The flow rate ratio is set to 3 and the total flow rate is set to 3~10 mL/min. All solutions were pumped into the SHM chip. The resulting TSL solution was collected into a 20 mL glass bottle from the outlet. The mixture solution was then using a probe tip sonifier (SFX250, Branson Ultrasonics, US) at a pulsed wave with a 10% power for 5s for 6 times with 5s of cooling after each exposure. The TSL solution was then transferred into a 15 mL centrifugal filter unit (3 KDa, Sigma-Aldrich, Canada) and was washed using 1X PBS (Sigma-Aldrich, Canada) three times by centrifugation at 4500 rpm for 1h per time. The upper filtered TSL solution was collected and stored at -4 °C for DOX remote loading.

2.3 Remote loading DOX into TSL

Doxorubicin (DOX) (Sigma-Aldrich, Canada) was loaded into the aqueous core of TSL based on the transmembrane ammonium sulfate gradient ("Doxil® — The First FDA-Approved Nano-Drug: Lessons

Learned," 2012). As shown in Figure 10, the ionized DOX will transmit into the aqueous cores of TSL and from precipitate (i.e. $[(DOX\text{-}NH_3)_2SO_4$).

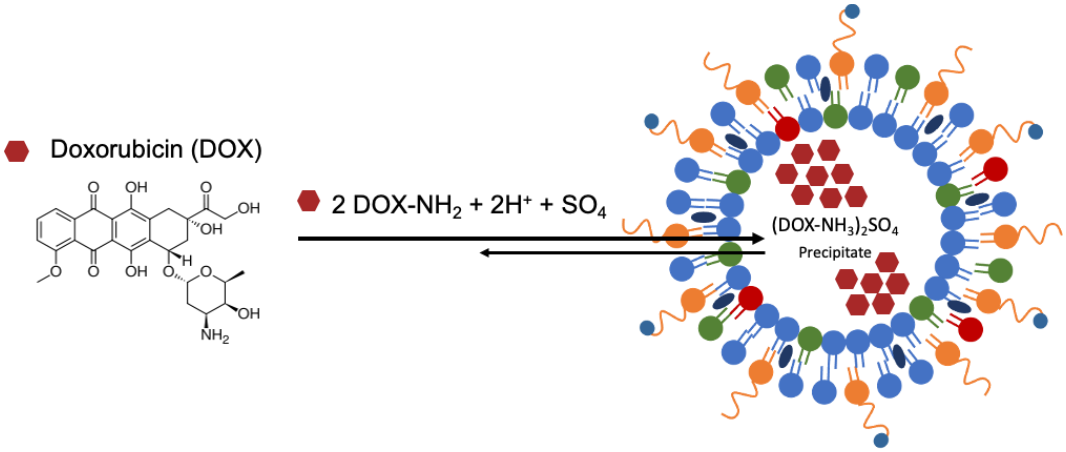

Figure 10 Schematic of remote loading of DOX into a liposome.

The TSL in $(NH_4)_2SO_4$ buffer (pH 5.34) was extruded through a polycarbonate membrane (Millipore, Sigma-Aldrich, Canada) with 0.1 µm pore size to remove the large vesicles. Then the extruded liposome solution was passed through a Sephadex (G-50) column (Sigma-Aldrich, Canada) and washed with 1X PBS (pH 7.43) to form the ammonium sulfate gradient (i.e. $[(NH_4)_2SO_4]_{liposome} >> [(NH_4)_2SO_4]_{medium}$). The pH values of 1X PBS and DOX $(NH_4)_2SO_4$ buffer were detected by a pH meter (S210-Uni-Kit, Mettler Toledo, Canada). DOX solution was then added to the liposome solution at 1:0.05 (w/w, total lipids: DOX), and the mixture solution was incubated in a water bath at 37 °C overnight for DOX remote loading. Finally, the mixture solution was passed through Sephadex (G-50) column and washed with 1X PBS again to remove the unloaded DOX. The resulted solution was further sterilized by passing through the 0.1 µm filter (Millipore, ThermoFisher, Canada). The sizes of DOX-loaded liposomes were measured by Dynamic Light Scattering (DLS), (Malvern, Nano S90, United Kingdom). The ultra-violet (UV) abortion and fluorescent emission of DOX were detected by a UV-visible spectrophotometer (GENESYS 150, ThermoFisher, Canada). DOX (excitation: 490 nm, emission: 600 nm). Therefore, the fluorescent DOX was tested using a fluorescent spectrophotometer (Cary Eclipse, Agilent Technologies, US).

2.4 Encapsulation efficiency of DOX

After remote-loading doxorubicin (DOX) into TSL to form doxorubicin-loaded thermosensitive liposomes (TSL-DOX), the solution was purified by passing through the Sephadex (G-50) column to remove the unloaded DOX. Both 1 mL of the solutions before and after purification were respectively treated with 1%

Triton X-100 (Sigma, Canada) that can disrupt the integrity of the liposome membrane and fully release the loaded DOX. The fluorescent intensity of the resulted solutions was detected. The encapsulation efficiency (EE) of DOX was calculated according to the following equation:

Equation 7

$$\text{EE } (\%) = \frac{I_t}{I_o} \times 100$$

Where I_o: the fluorescent intensity of the mixture of TSL-DOX with unloaded DOX before purification. I_t: the fluorescent intensity of TSL-DOX solution after purification.

2.5 DOX release of DOX-TSL

According to the fluorescent spectrum of both free DOX and TSL-DOX, the DOX release percentage was calculated based on their fluorescent intensity according to the following equation:

Equation 8

$$\text{DOX release } (\%) = \frac{F_t - F_o}{F_{tx} - F_o} \times 100$$

Where F_o: the initial fluorescent intensity of TSL-DOX solution at room temperature. F_t: the fluorescent intensity of TSL-DOX solution which was heated at different temperatures. F_{tx}: the fluorescent intensity of TSL-DOX solution after treated with 1% Triton X-100.

2.6 An ultrasound setup to induce cavitation

The impact of ultrasound on the DOX release of TSL-DOX was evaluated using an ultrasound setup. This ultrasound setup is selected because it can adjust different ultrasound parameters(X. X. Duan et al., 2019). As shown in Figure 11, the ultrasound setup was immersed in a water tank (length*width*height: 51.4*26.7*32.1 cm, Aqueon, Amazon, Canada) with a heater (hygger, Amazon, Canada) to control the water temperature as 37 ºC. The setup was composed of three panels: 1) the bottom panel holds the transducer to pulse ultrasound out toward the chamber; 2) the middle panel holds the chamber that contains samples; 3) the top panel cover the upper space above the chamber. The distance between the chamber and the transducer was adjusted, according to the focal length (11 cm) of the transducer. Acoustic absorbers (5 mm rubber) were attached to the bottom of both the middle and the bottom panels to absorb ultrasound

reflections, which impact the homogeneity of the acoustic field and the cavitation effects. A signal generator (SDG 2042X, Siglent, China) was connected to an RF power amplifier (A075, Electronics & Innovation, Ltd, USA), which was then connected to the transducer. The ultrasound parameters were adjusted in the signal generator with a center frequency: 1 MHz, an output voltage burst periods: 1 ms, and burst cycles: 5 to 100. The mixed solutions of TSL-DOX and microbubbles were added into the chamber, which was then sealed. The relative position of the ultrasound transducer and the sample chamber on panels was shown in Figure 12. Geometries of the ultrasound transducer and sample chamber were shown in Table 2. The water inside the tank was previously heated up to 37 °C or 42 °C. TSL-DOX were previously heated to 37 °C or 42 °C for different time and were then cooled in a cold-water bath to prevent further DOX release. The sample solution: ~600 µL of microbubbles ($4.35 \times 10^8 \pm 1.05 \times 10^8$) and TSL-DOX (1 mg/mL) was injected into the chamber using a 1 mL syringe. The chamber was sealed with tape to prevent leakage and was then fixed on the middle panel with two caps, see Figure 12c. The ultrasound was pulsed out toward the chamber with different parameters by turning on the power amplifier. The resulted solution was collected and detected for the fluorescent intensity. The DOX release percentage was calculated according to Equation 7.

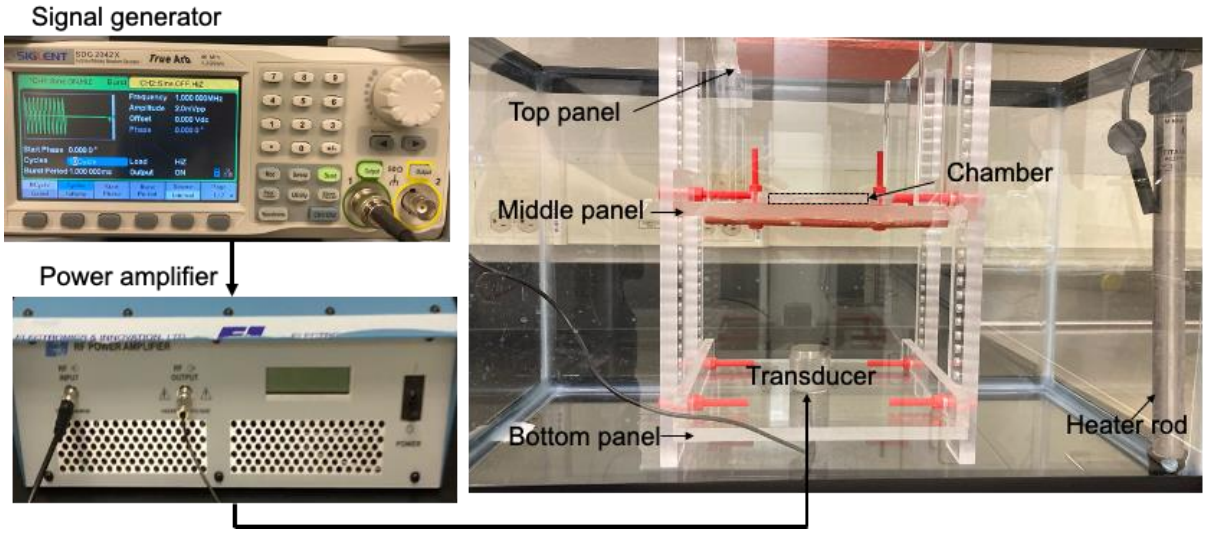

Figure 11 Ultrasound setup to induce cavitation of microbubbles.

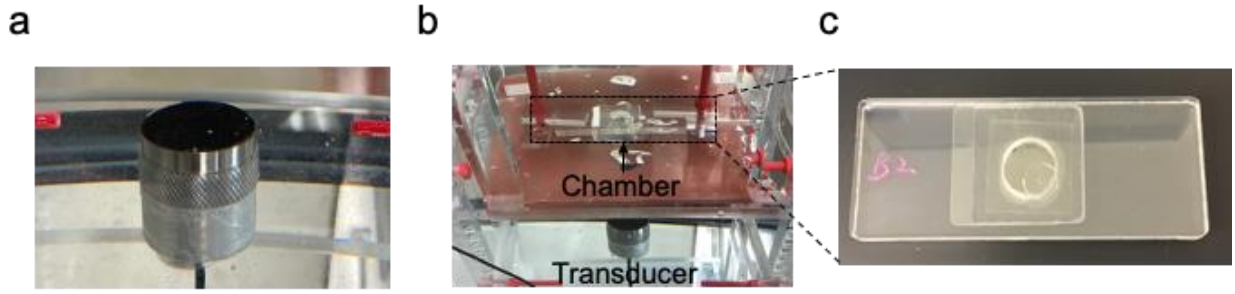

Figure 12 (a) The ultrasound transducer; (b)Position of the sample chamber in the setup; (c)Geometries of the chamber.

Table 2 Geometries the ultrasound transducer and sample chamber

	Category name	**Units**
Ultrasound transducer	Geometry length	3.5 cm
	Diameter	3.0 cm
	Focal length	11~11.5 cm
Chamber	Inner diameter	12 mm
	Height	5 mm
	Thickness of cover slides	0.13 mm

2.7 Preparation of biotinylated microbubbles

Several lipid membrane formulations have been tried to prepare biotinylated microbubbles. DSPE-PEG2000 or DSPE-PEG2000-Biotin were used as the emulsifier, and DSPC or DPPC were used as the main coating lipids, see Figure 13 and Table 3. All materials were dissolved in ethanol at different molar ratios (see Table 3) with a total lipid concentration of 2 mg/mL. The lipid film was formed by evaporating ethanol with a steady nitrogen stream in a 10 mL glass vial. The hydration solution (i.e. DI water: propylene glycol: glycerol = 7:2:1) was prepared and was heated up at a water bath to 60 °C, which is above the phase transition temperature (T_m) of the main lipid DSPC (i.e. 55 °C). The lipid film was hydrated in a solution with a final concentration of 1 mg/mL by sonicating the solution with a probe tip sonifier. The resulted solution was further sterilized by passing through a 0.22 μm filter into a 2 mL glass vial (Sigma-Aldrich, Canada) and was sealed with an open-top aluminum crimp cap (PTFE/red rubber septa, Sigma-Aldrich, Canada). The perfluorobutane (C_4F_{10}, 99 wt%, FluoroMed) gas (i.e. 2 mL in a 3 mL syringe) was injected

into the vial and completely exchanged the air (i.e. 1 mL gas space and 1 mL lipid solution). The vials, with the lipid solutions and saturated C_4F_{10} gas, were stored in 4 °C fridge. The biotinylated microbubbles are produced by mechanical agitation of the vials using a capsule mixer (G8O, Aphrodite, USA) at 4200 Hz for 30s. The resulted milky solution (i.e. microbubble suspension) inside the vial was withdraw by a 1 mL syringe and was diluted with 1X PBS to 5 mL in a glass bottle. Since the ultrasound-induced cavitation effect is relate to the size of the targeted microbubbles(Stride et al., 2020). We aim to prepare a biotinylated microbubble with the a suitable size distribution (i.e. 1~2 μm) for cavitation. According to Table 3, the membrane formulations of biotinylated microbubbles were finally optimized as DSPC:DSPE-PEG2000-PE:DSPE-PEG2000-Biotin:DiD with a molar ratio: 90:5:5:0.1. A DiD-labeled, biotinylated microbubble was prepared. Size distribution of the biotinylated microbubbles was detected by DLS and fluorescent microscopy. The numbers of microbubbles were quantified using a hemacytometer (Bright-Line™, Sigma-Aldrich, Canada).

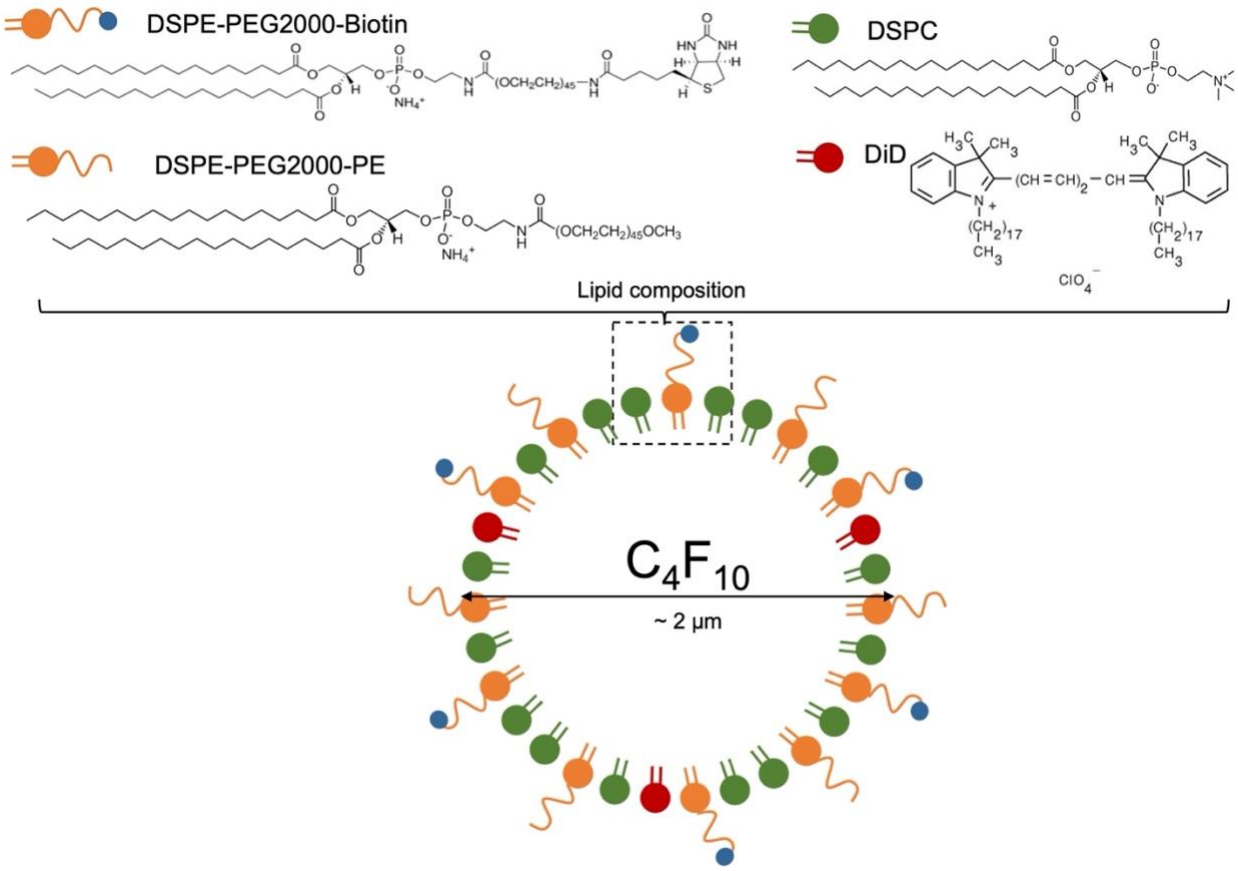

Figure 13 Schematic of a biotinylated microbubble.

Table 3 Size detection of a biotinylated microbubble with different lipid compositions

Main coating lipid (molar ratio%)	Emulsifier (molar ratio%)		Hydrated solution	Dynamic light scattering (DLS)
DSPC	DSPE-PEG_{2000}	DSPE-PEG_{2000}-Biotin	1:2:7 gly-pro-H_2O	Z-Avg Size (N = 3)
90	10	/	+	944.1 ± 379.2 nm
90	9	1	+	636.5 ± 93.3 nm
92	7	1	+	606.6 ± 63.2nm
95	4	1	+	516.4 ± 40.5nm
97	2	1	+	624.9 ± 167.7nm

2.8 Preparation of TSL-MB

Thermosensitive liposomes conjugated microbubbles (TSL-MB) were developed by linking a biotinylated TSL-DOX to a biotinylated microbubble via biotin-avidin-biotin linkage (see Figure 14). After agitation, the biotinylated microbubbles solution was collected and incubated with 20 µL (300 nM) of streptavidin (Sigma-Aldrich, Canada) in a 20 mL glass bottle. The bottle was gently shaken on an orbital shaker (VEVOR, Canada) for 1 h at 120 RPM at room temperature. After that, TSL-DOX solution (1 mg/mL) was added and incubated with the biotinylated microbubbles solution for another 1 h to produce the TSL-MB. The TSL-MB solution was diluted to 5 mL. The size distribution and morphology of microbubbles before and after centrifugation were detected by 20X and 60X objectives of a fluorescent microscopy platform. Three fluorescent channels were used: DiO, DoxRub, and DiD to detect the conjugation of TSL with microbubbles.

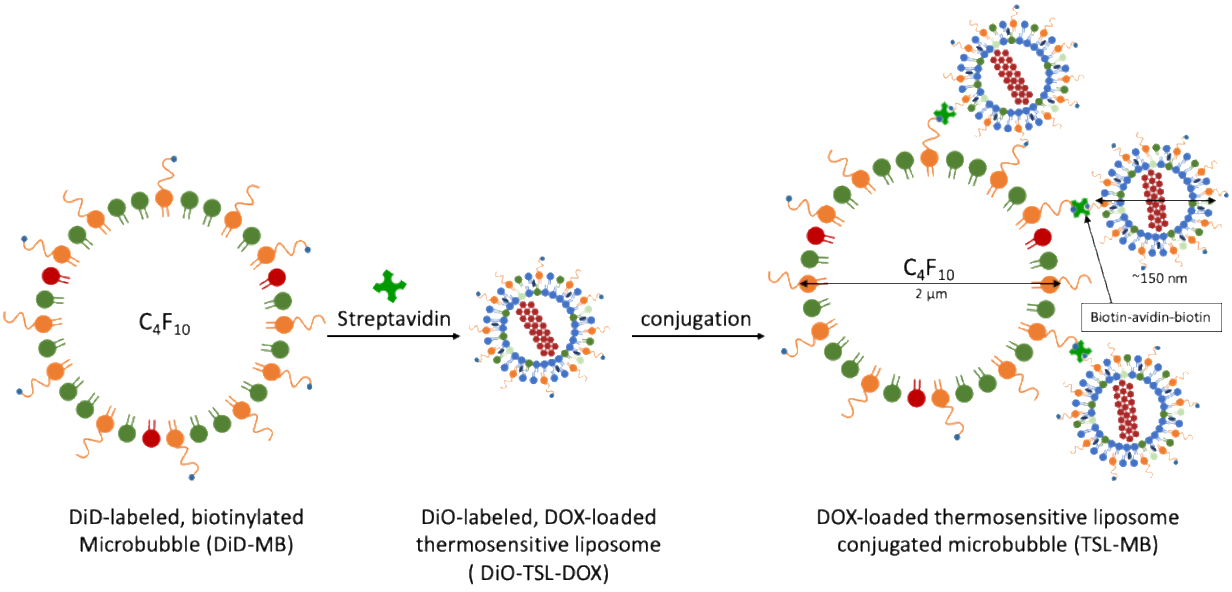

Figure 14 Schematic of production of a thermosensitive liposome conjugated microbubble.

2.9 Statistical analyses

The results were expressed as the mean ± standard deviation (SD). Student's t-test was used to analyze the data between two groups. Two-way analysis of variance (ANOVA) was used to analyze multiple comparisons. *$p < 0.05$, ** $p < 0.01$, and *** $p < 0.001$ were considered statistically significant and very significant.

Chapter 3 Experimental Results

3.1 Chapter overview

This chapter introduced the initial results that support three research objectives. Specific evaluation criteria for each research objective were introduced as below:

Research objective 1: Develop TSL-DOX using the microfluidic method and characterize the prepared TSL-DOX. Characterizations of TSL-DOX including size, stability, polydispersity, and encapsulation efficiency of DOX were introduced in section 3.2. After that, section 3.3 introduced DOX release percentage induced by heating at different temperatures and at the phase transition temperature.

Research objective 2: Combing heating and ultrasound-induced cavitation to trigger DOX release from TSL-DOX. Section 3.4 introduced characterizations of microbubbles. Before combining cavitation and heating to control DOX release, it is necessary to know whether ultrasound and heating influence drug

release without cavitation. Therefore, section 3.5 first introduced DOX release of TSL-DOX formed with different membrane formulations after heating and ultrasound exposures without cavitation. To investigate the cavitation of microbubbles, ultrasound-induced microbubble destruction was then evaluated by changing ultrasound parameters: pulse cycles and pulse repetition frequency. Finally, DOX release of TSL-DOX was evaluated after treating with both heating and cavitation.

Research objective 3: Develop and evaluate an ultrasound-responsive drug-carrying system: doxorubicin-loaded thermosensitive liposome-conjugated microbubbles (TSL-MB). Section 3.6 introduced the tests to prove the conjugation of TSL-DOX and a biotinylated microbubble stepwise: 1) proved the conjugation between DiO-labeled TSL (without DOX loading) and non-fluorescent labeled microbubbles. 2) further evaluated the conjugation efficiency by changing the biotinylated molar ratios of both DiO-labeled TSL and microbubbles. 3) evaluated the conjugation between DiO-labeled TSL-DOX (with DOX loading) and DiD-labeled microbubbles. 4) confirmed the successful development of TSL-MB by evaluating the colocalization of fluorescent signals of TSL, loaded DOX, and microbubbles. Finally, the DOX release of TSL-MB and TSL-DOX were compared after combining heating and cavitation.

3.2 Characterization of DOX-loaded thermosensitive liposomes

3.2.1 Size distribution of TSL-DOX

Doxorubicin-loaded liposomes (TSL-DOX) were prepared and evaluated for size and polydispersity index (PDI). These two factors are the common evaluation indicators of nanoparticles. Figure 15 showed one representative size distribution and the PDI of a TSL in $(NH_4)_2SO_4$ solution before drug loading, detected by DLS. After loading with doxorubicin (DOX), the size and PDI of TSL-DOX were 173.7 ± 11.2 nm and 0.282 ± 0.06, respectively (see Table 5). With different preparation conditions, the sizes of TSL-DOX increased to ~ 200 nm. According to Table 6, the sizes of TSL in PBS and in $(NH_4)_2SO_4$ solutions were stable for three months. However, the size of TSL-DOX was increased to ~ 75 nm after one month.

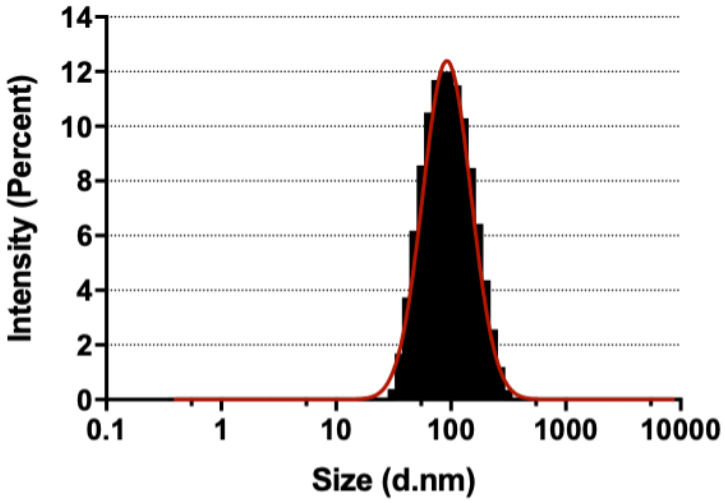

Figure 15 Size distribution of thermosensitive liposomes.

Table 4 Size detection of liposomes prepared by the staggered herringbone micromixer

Name	Flow conditions (mL/min)	Size (Z-Ave d.nm)	PDI
TSL	TFR[a]:4; FRR[b]:3	197.4 ± 9.44*	0.316 ± 0.082*
TSL	TFR:5; FRR:3	179.65 ± 6.13*	0.250 ± 0.033*
	TFR:6; FRR:3	152.5	0.382
	TFR:8; FRR:3	203.5	0.288
	TFR:10; FRR:3	186.9	0.260
	TFR:12; FRR:3	196.6	0.314

a: TFR: total flow rate; b: FRR: flow rate ratio. *: N = 6

Table 5 Long term stability test of the size changes of a TSL

Sample	Freshly prepared (Z-Ave d.nm/Pdl)	1 month after (Z-Ave d.nm/Pdl)	2 month after (Z-Ave d.nm/Pdl)	3 month after (Z-Ave d.nm/Pdl)
TSL in PBS	130.5 nm/0.187	155 nm/0.084	171.1 nm/0.047	179.0 nm/0.045
TSL in $(NH_4)_2SO_4$	243.4 nm/0.204	238.4 nm/0.179	238.2 nm/0.212	246.1 nm/0.120

TSL-DOX	98.37 nm/0.152	174.0 nm/0.271	-	-

3.2.2 The absorption and fluorescence emission of DOX

The fluorescent signal of DOX is important to identify the DOX release. Therefore, in this section, the absorption and fluorescence emission spectrum of DOX was respectively detected by a UV-Vis and a fluorescent spectrophotometer. The absorption spectrum helps identify the best fluorescent excitation condition of DOX. As shown in Figure 16a, the peak absorption of DOX is 480~490 nm. After excitation at 490 nm, the fluorescent emission spectrum of DOX was shown in Figure 16b. The fluorescent emission spectrum provides specified peaks (~560 and ~600 nm) of DOX, which helps to identify DOX in a fluorescent emission spectrum when we detected the DOX release from TSL-DOX.

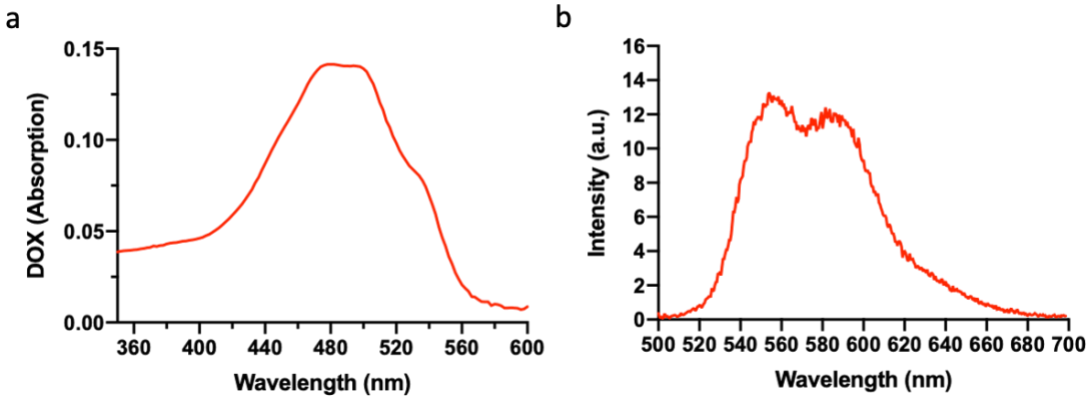

Figure 16 The (a) absorption and (b) fluorescence emission of DOX in PBS solution.

3.2.3 Lipid membrane disruption of TSL-DOX

To evaluate the DOX release of TSL-DOX at different temperatures, it is necessary to have a positive control group that indicated 100% release of the loaded DOX from TSL. TritonX-100 was used to control and fully release the loaded DOX from TSL-DOX. Two different concentrations (0.1% and 1%) of TritonX-100 solution have been reported to release DOX from TSL-DOX (Hertz & Barenholz, 1977). Therefore, to confirm the experimental condition, both 0.1% and 1% of TritonX-100 solutions were used to dilute TSL-DOX to control the DOX release. As shown in Figure 17, in 1% TritonX-100 solution, DOX was fully released immediately. As a control, the fluorescence of TSL-DOX is low in PBS at room temperature (RT) because the fluorescence of DOX was quenched inside TSL. In contrast, 0.1% TritonX-100 solution help to increase DOX release, increasing the fluorescent signal. However, 0.1% TritonX-100 solution did not

fully release DOX, compared to the 1% TritonX-100 group (see Figure 17). Therefore, 1% TritonX-100 solution is chosen in the following experiment to fully release the loaded DOX from TSL-DOX.

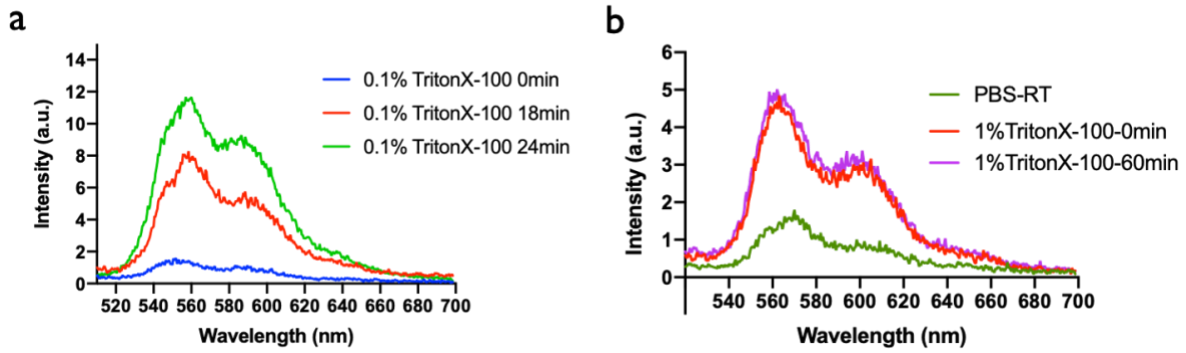

Figure 17 DOX release of TSL-DOX treated with (a) 0.1% or (b) 1% TritonX-100.

3.2.4 Encapsulation efficiency of DOX

The TSL and the unloaded DOX mixed solution (TSL + DOX) was passed through a SephadexG50 column to remove the unloaded DOX. As shown in Figure 18a, the unloaded DOX passed slower than TSL-DOX, indicating the separation. After purification, the color of TSL-DOX was lighter than the mixed solution TSL+DOX but was stronger than the unloaded DOX. After purification, both the TSL+DOX mixed solution and TSL-DOX solution were collected and treated was with 1% TritonX-100 to fully release the loaded DOX. As shown in Figure 18b, the fluorescent peaks of TSL-DOX and TSL+DOX were similar. The intensity of TSL-DOX (red curve) was also similar to that of TSL+DOX (green curve). In contrast, the fluorescent intensity of TSL-DOX in PBS (blue curve) is low, indicating a signal quench of DOX.

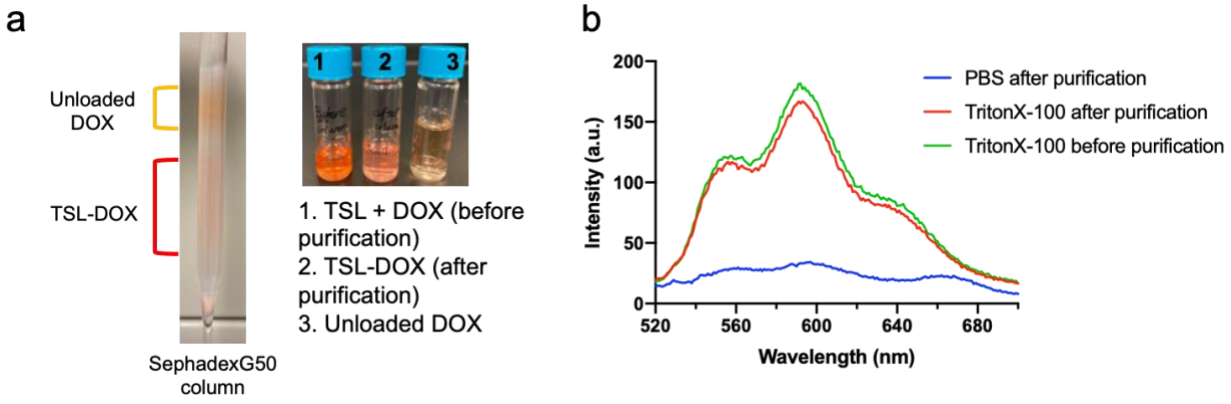

Figure 18 (a) Appearance and (b) the fluorescent spectrum of a TLS-DOX in PBS or TritonX-100 solution.

The quenching effect happens when two DOX molecules are closed together and form an energy donor and receptor pair, decreasing the fluorescent intensity(Barenholz et al., 1993). DOX can form crystallization in the core of a TSL, causing the fluorescent quenching effect. The results proved that DOX was successfully loaded into TSL. As shown in Figure19 a, the encapsulation efficiency (EE) of DOX can reach ~ 80%. The DOX loading efficiency increased along with the total flow rate (TFR) from 2 mL/min to 6 ml/min. However, when TFR was higher than 6 ml/min, the EE of DOX does not increase. Figure 19b showed that the increase of DSPE-PEG2000-Biotin lipids molar ratio on the membrane of TSL has slightly influence of DOX EE. The highest DOX EE reached ~ 95% for TSL with 3 mol% of DSPE-PEG2000-Biotin. Overall, adding DSPE-PEG2000-Biotin into the bilayer membrane slightly increased DOX EE. However, there is no obvious trend of the increase of DOX EE along with the increase of membrane molar ratio of DSPE-PEG2000-Biotin lipids.

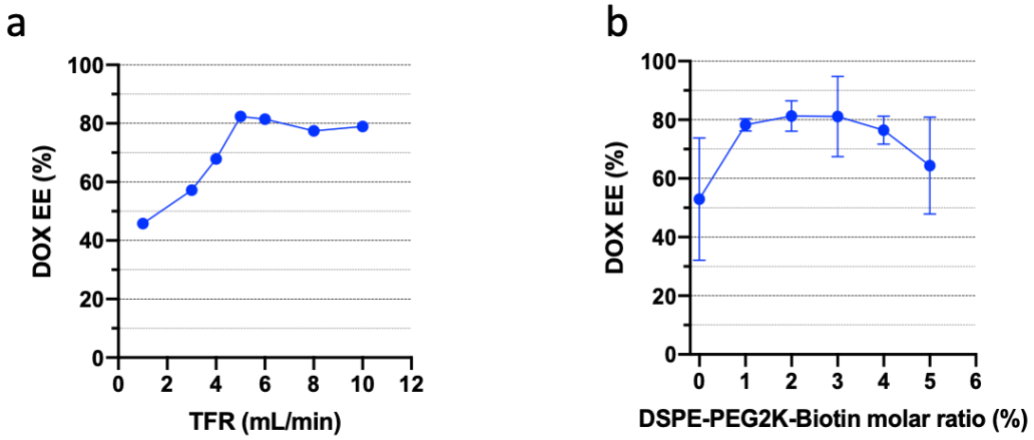

Figure 19 DOX encapsulation efficiency (EE) of TSL-DOX (a) prepared by different microfluidic conditions and (b) prepared with different membrane compositions. EE: encapsulation efficiency; TFR: total flow rate.

3.2.5 Stability of TSL-DOX

In addition to testing the size changes of TSL-DOX, the fluorescent intensity change is another indicator to show whether TSL-DOX is stable after preparation. As the fluorescent signal of DOX was quenched in TSL-DOX, the leakage of DOX from TSL-DOX can be detected based on the fluorescent intensity increase. The encapsulation of DOX inside TSL was further indirectly proved based on the fluorescence resonance

energy transfer (FRET) effect that happens when two fluorophores are close (< 10 nm). Therefore, I prepared DiD-labeled thermosensitive liposomes (DiD-TSL-DOX). DiD can insert into the lipid bilayer and label the membrane of a liposome with low disassociation(Münter et al., 2018). The labeled TSLs were loaded with DOX and formed DiD-TSL-DOX. As shown in Figure 20, with the only one excitation of DOX (490 nm), both the special emission peaks of DOX (~560nm and ~600 nm) and DiD (~668 nm) were detected, indicating a FRET effect between DOX (the core of TSL) and DiD (lipid membrane of TSL). After one week of storage, the fluorescent intensity of DOX (peak1: 560 nm and peak2: 600 nm) slightly increased. However, the FRET effect of DOX and DiD is similar, indicating a stable state of the loaded DOX inside the DiD-TSL-DOX. The peak positions of both DOX and DiD were constant, indicating no obvious degradations of the chemicals. The noise of the fluorescent curve of DiD-TSL-DOX indicated a strong fluorescent quench effect of DOX inside DiD-TSL-DOX.

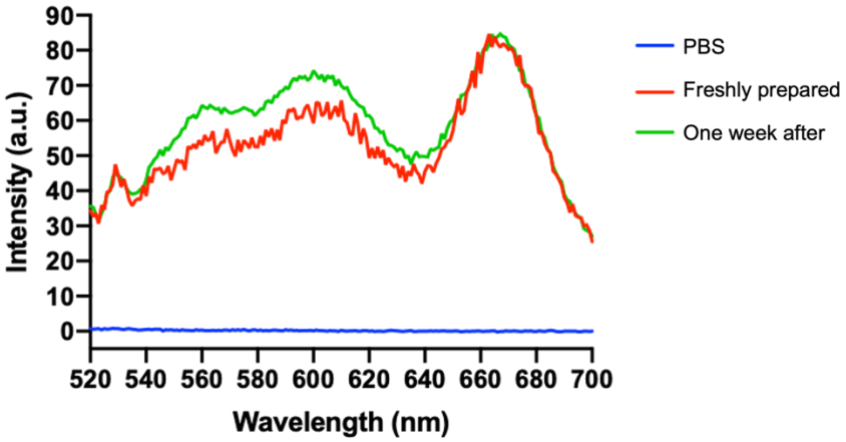

Figure 20 Fluorescence stability of DiD-TSL-DOX.

3.3 DOX release of TSL-DOX

After proving loading efficiency of DOX and the loaded state in TSL, the thermal sensitivity of TSL-DOX was investigated by detecting DOX release at different conditions: heating at 37 °C or 42 °C for different time and heating at 37 to 45 °C for the same time.

3.3.1 DOX release of TSL-DOX at 37 °C or 42 °C

The thermal sensitivity of TSL-DOX was examined by changing the environmental temperatures. The fluorescent intensity changes were indicators of DOX release from the TSL-DOX. As shown in Figure 21a, the fluorescent intensity of TSL-DOX maintained low for 10 min at 37 °C, like the PBS group at room

temperature. As the molar fractions of biotinylated lipids increase from 1% to 5%, the final cumulative DOX release percentages of all TSL-DOX were still < 10% at 37 °C. The DOX release percentage was calculated based on the fluorescent intensities, according to Equation 7. In contrast, the fluorescent intensity of TSL-DOX increased after 1 min of heating at 42 °C (Figure 21b). As shown in Figure 21, the DOX release percentage was increased to 20 ~ 70% in 3 min at 42 °C. As the molar fractions of biotinylated lipids increase from 1% to 5%, the final cumulative DOX release percentages of TSL-DOX decreased from 69.84 ± 7.80 % to 18.90 ± 5.39%. This result indicates that DOX release is related to the molar fractions of biotinylated lipids on the membrane of TSL.

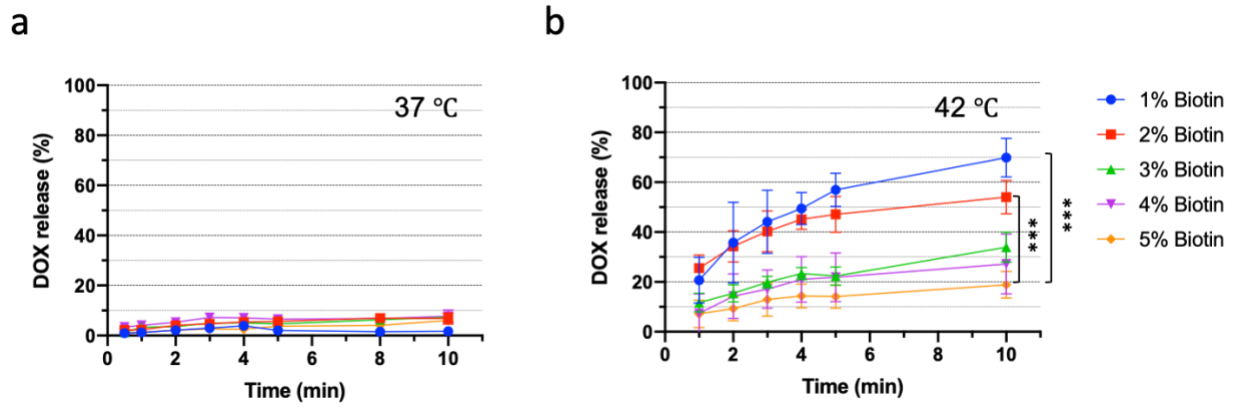

Figure 21 DOX release percentage of TSL-DOX with different molar ratio of biotin-lipids at (a) 37 °C or (b) 42 °C. N = 3, ***P < 0.001.

3.3.2 DOX release of TSL-DOX at different temperatures

Although the DOX release of TSL-DOX has been proved at 42 °C, the responsive temperature range is still unknown. Therefore, in this section, the DOX release of TSL-DOX was evaluated at different temperatures. Moreover, to further investigate the states of TSL-DOX, size changes were also detected when TSL-DOX was heated or was cool to room temperature (RT). As shown in Figure 22a, the DOX release obviously increased at 40 °C. However, the DOX release percentage reach peak at a higher temperature (42°C to 43°C) when the membrane molar ratios of biotin-lipids increased from 1% to 5%. The maximum DOX release percentage reached 100% for TSL-DOX (1% biotinylated-DSPE-PEG) at 42 °C. With the increase of biotin mole ratios from 2% to 5%, the maximum DOX release was decreased from 80% to ~40% at 42 °C. The size of liposomes also increased ~ 60 nm from 37 °C to 42 °C than that were cooled to room temperature. After heating at different temperatures then cooling to room temperature, the final sizes of the TSL-DOXs were ~ 200 nm. Heating increased the sizes of TSL-DOX by 50 ~ 70 nm, but the size changes are reversible

when cooling to the room temperature. According to these results, TSL-DOX was proved to be thermo-sensitive, and its best sensitivity range was 40 ~ 42 °C, which is in line with expectations.

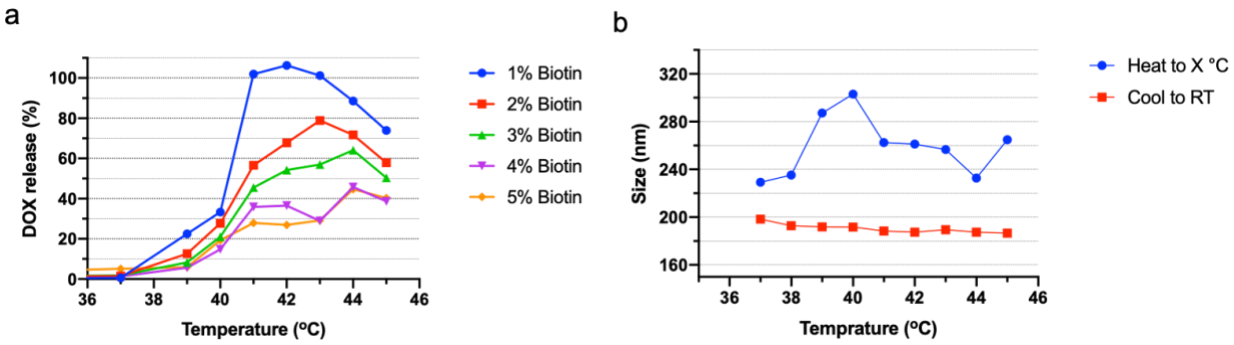

Figure 22 (a) DOX release percentage of TSL-DOX with different membrane combinations at 37~45 °C and (b) Size changes of TSL-DOX at different temperatures.

3.4 Characterization of a biotinylated microbubble

The characterizations of the biotinylated microbubbles were evaluated stepwise: 1) investigate the morphology, size distribution, and stability. 2) investigate the size distribution change of the microbubbles after washing with PBS by centrifugation. Based on the completed experiment, the state of a prepared microbubble and the impacts of the post-processing procedures on the microbubbles were evaluated. These results supported the preparation of TSL-DOX conjugated microbubble.

3.4.1 Morphology, size distribution, and stability of microbubbles

Both DLS and microscopy have been used to detect the size of microbubbles. As shown in Figure 23, detected by DLS, the sizes of commercialized microbubbles: USphere™ (Trust Biosonics) and the prepared microbubbles were 1,380 μm and 1,072 μm, respectively. As shown in Figure 24, the biotinylated microbubbles were successfully labeled with DiD (red) on the membranes. Based on the results detected by fluorescent microscopy, the main size distribution of the freshly prepared biotinylated microbubbles is 0.5-3.5 μm with an average mean size ~2 μm (Figure 24c). After storing at 4 °C for 24h, the microbubbles became small with an average mean size of 1~1.5 μm (Figure 24b and Figure 24d).

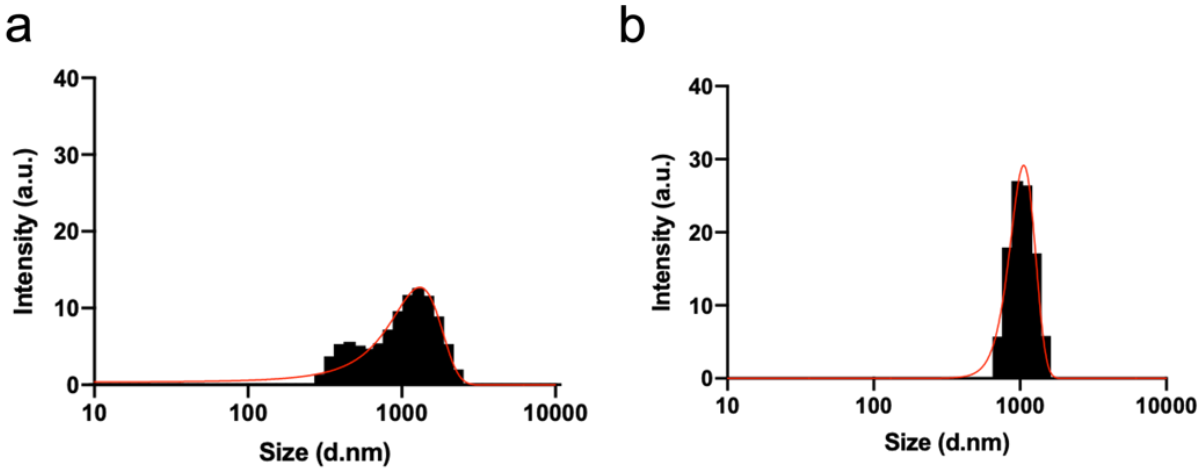

Figure 23 Sized distribution of (a) commercialized microbubbles: USphere™ and (b) prepared microbubbles.

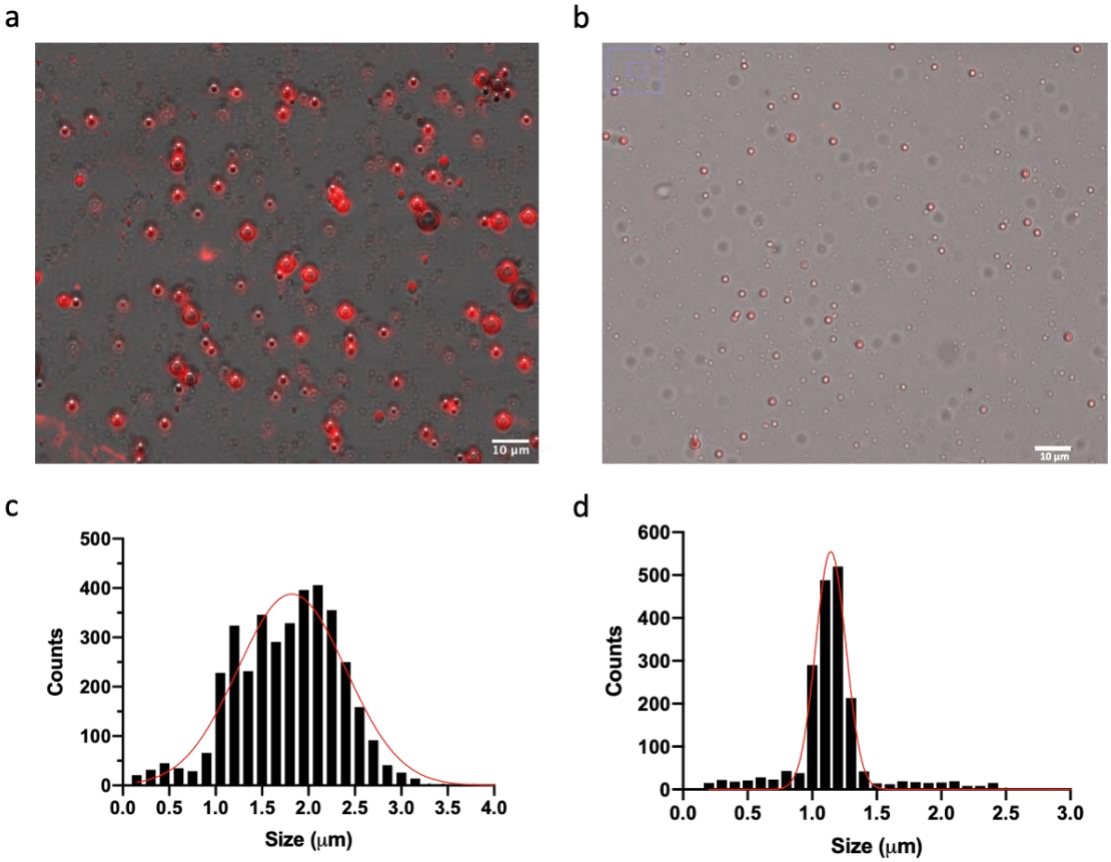

Figure 24 Morphology and sized distribution of DiD-labeled microbubbles that are fleshly prepared(a), (c) or are freshly prepared and stored in -4 °C after 24h(b), (d).

3.4.2 Size distribution of microbubbles after different times of washing

The size distribution of the biotinylated microbubbles was evaluated after washing for different times in a 5 mL syringe at 250 RCF for 1 min per time. According to calculation, the upper cut-off size of microbubbles will be ~2.2 μm(Feshitan et al., 2009). The sizes of microbubbles are detected using a 20X objective of microscopy. As shown in Figure 25 a-c, the size distribution range after washing became narrower when the washing times increased. Figure 25d gave a clear comparison of the sized distribution range and median. Washing by centrifugation decreased the large microbubbles, the average mean of the size was around 1~1.5 μm. After three times of washing, three segments of the solution in the syringe were collected and tested for the sizes (see Figure 26). The sized distributions of microbubbles in these three segments are similar. After centrifuging for once, the size distribution of microbubbles has been limited < 2.2 μm, which is in line with the results from the literature.

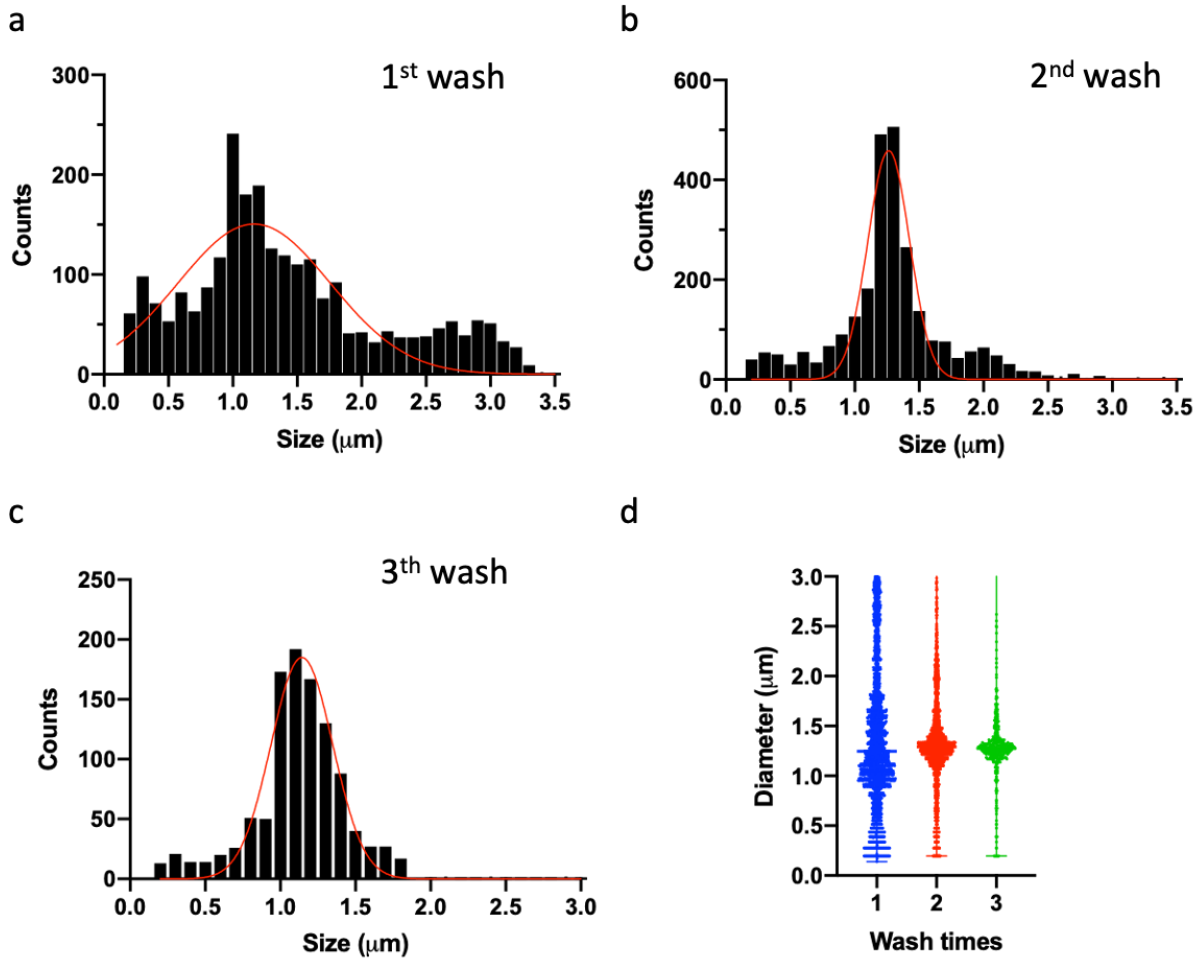

Figure 25 Size distribution of biotinylated microbubbles after (a) the first, (b) the second, and (c) the third time of washing at 250 RCF by centrifugation. (d) The medians of size distribution of microbubbles after each washing.

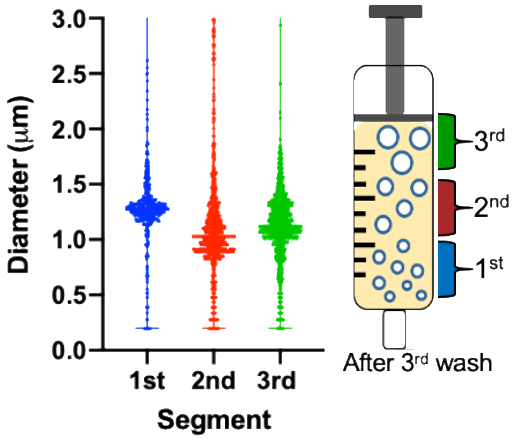

Figure 26 Size distribution of different segments of microbubbles in the syringe after the third time of washing.

3.5 Ultrasound-induced cavitation and DOX release of TSL-DOX

3.5.1 DOX release of TSL-DOX after treated with different ultrasound burst cycles

In addition to temperatures, the doxorubicin (DOX) release from DOX-loaded thermosensitive liposomes (TSL-DOX) was slightly influenced by ultrasound. TSL-DOX with different membrane formulations were treated with ultrasound burst cycles 5 to 100 cycles, frequency: 1MHz, 100 cycles, burst repetition time: 1 ms, duration:10 s. According to the scheme shown in Figure 1, increasing ultrasound burst cycles in each ultrasound pulse will increase the spatial peak time-averaged intensity (I_{SPTA}). As shown in Figure 27, the DOX release percentages of TSL-DOX are increased to ~10% at 37 ºC after ultrasound exposure with 5 to 10 cycles. However, DOX release did not further increase after treated with 50 and 100 cycles of ultrasound at 37 ºC. In contrast, the DOX release percentage is chaotic at 42 ºC when the ultrasound burst cycles are < 20. The DOX release percentage from TSL-DOX was ~15% after being treated with 50 to 100 cycles of ultrasound at 42 ºC for 2 min.

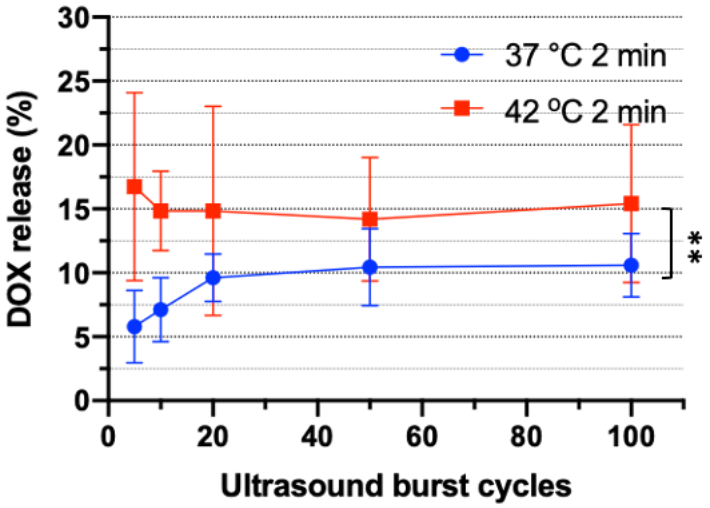

Figure 27 DOX release percentage of TSL-DOX at 37 ºC or 42 ºC with different ultrasound burst cycles. ** P < 0.01.

The sizes and PDI of TSL-DOX did not obviously change when they were treated with different ultrasound pulse cycles (see Figure 28). After ultrasound exposure, the sizes of TSL-DOX were 197.2 ± 4.84 nm, while the PDI was 0.210 ± 0.054, indicating a homogenous dispersity. The sizes are close to the freshly prepared TSL-DOX (173.7 ± 11.2 nm) without ultrasound exposures.

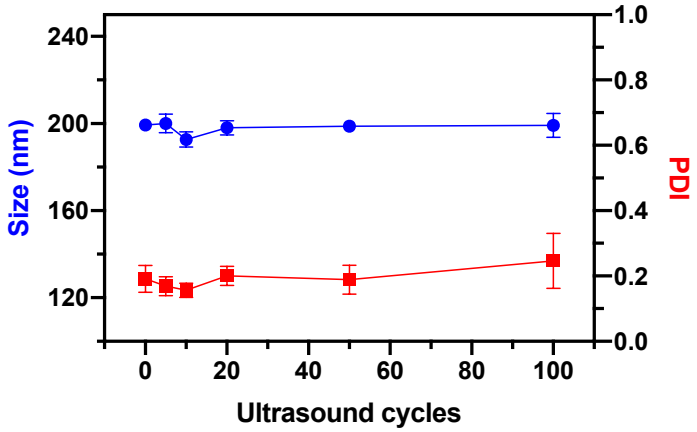

Figure 28 Size (blue) and PDI (red) changes of TSL-DOX after treated with different ultrasound pulsed cycles. N = 3

3.5.2 DOX release of TSL-DOX after treated with different ultrasound exposure duration times

Doxorubicin-loaded thermosensitive liposomes (TSL-DOX), with different membrane molar fractions of DSPE-PEG2K-Biotin lipids, were sealed in the sample chamber with the final concentration of 1 mg/mL. To evaluate the DOX release percentage, the sample solutions were heated at 42 ºC for 10 min. As shown in Figure 29, TSL-DOX (1% DSPE-PEG2K-Biotin) released 58.82 ± 6.55% of the loaded doxorubicin (DOX) without ultrasound exposures. As the molar fractions of DSPE-PEG2K-Biotin on TSL-DOX increased, the DOX release percentages decreased. TSL-DOX (5% DSPE-PEG2K-Biotin) released DOX 2 times less than TSL-DOX with 1% biotinylated lipids at 42 ºC. A similar trend was found after combining ultrasound exposure and environmental heating when TSL-DOX were treated with different ultrasound exposure duration times from 10s to 30s. For TSL-DOX (1% DSPE-PEG2K-Biotin), the DOX release slightly increased and reached a peak (73.78 ± 7.69%) at an ultrasound exposure duration of 20 s. After that, increasing ultrasound exposure duration time did not further enhance DOX release. The cumulative release percentage was 70.39 ± 6.88% after 30s of ultrasound exposure, which is still ~10% higher than that without ultrasound treatment. For TSL-DOX with 2~4% DSPE-PEG2K-Biotin, ultrasound exposure did not increase the DOX release even when the exposure time was prolonged. Interestingly, TSL-DOX with 5% of DSPE-PEG2K-Biotin also slightly increased the DOX release after ultrasound exposure. However, the of drug release was similar. Based on these findings, TSL-DOX with 1% DSPE-PEG2K-Biotin released more loaded DOX than other groups after treating with heating and ultrasound exposures.

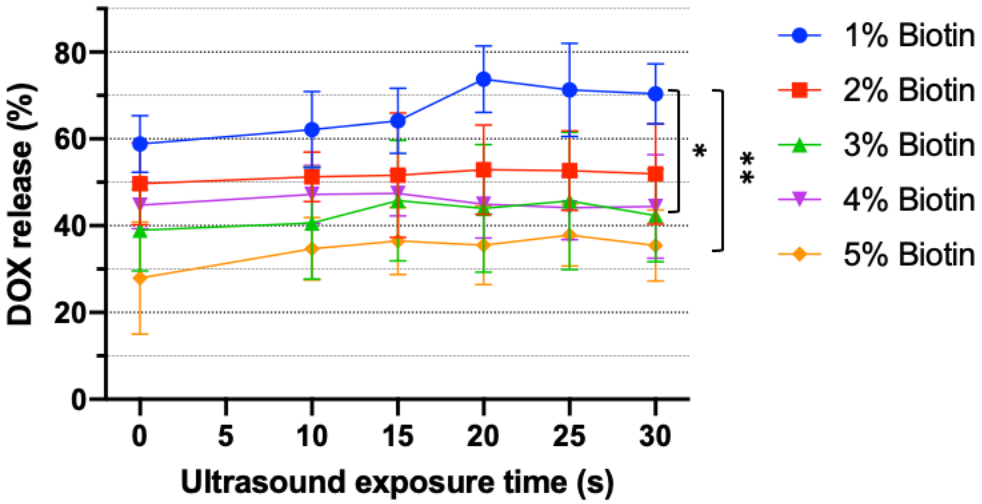

Figure 29 DOX release percentage of TSL-DOX at 42 ºC with different ultrasound exposure time. N = 3. * P < 0.05; ***P < 0.01.

3.5.3 Ultrasound-induced cavitation and microbubble destruction percentage

The microbubble destruction percentage was calculated based on the number of microbubbles in 6 different microscopy views in one test. Three independent tests were done to gain the average destruction percentage for each point in Figure 30. According to the result in Figure 30, with the increase of ultrasound burst cycles, the destruction percentage of microbubbles (MBs) increased at both 37 ºC and 42 ºC. With < 50 ultrasound pulse cycles, the destruction ratio of microbubbles is similar at 37 ºC or at 42 ºC. However, the final destruction percentage of microbubbles (1.386×10^{10}) at 42 ºC was 76.77 ± 8.81%, which is slightly higher than that at 37 ºC (60.43 ± 13.41%) when the microbubbles were treated with 100 pulse cycles of ultrasound. However, there was no statistically difference between the microbubbles' destruction rates at 37 ºC and 42 ºC treating with different ultrasound exposures.

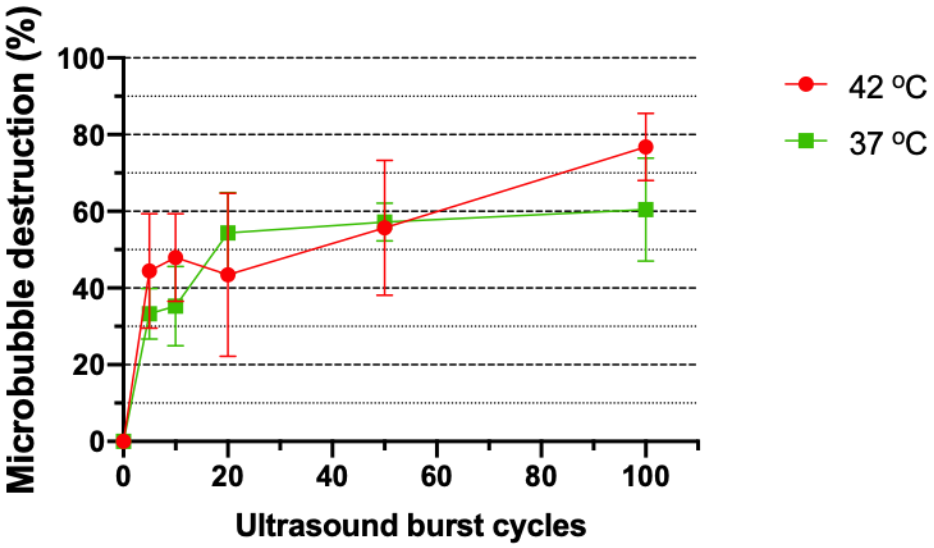

Figure 30 Microbubble destruction percentage at 37 ºC or 42 ºC with different ultrasound burst cycles. N = 3.

3.5.4 Size detection of biotinylated microbubbles after ultrasound exposure

As shown in Figure 31, the initial size range of microbubbles at 42 ºC was larger than that at 37 ºC when there was no ultrasound exposure. Most of the large microbubbles (diameter > 5 μm) were destroyed when they were heated at 42 ºC and then were treated with ultrasound. With different ultrasound burst cycles, the size range of microbubbles becomes narrower than that were without ultrasound exposure. No obvious

difference in microbubbles size distributions when they were treated with different ultrasound pulse cycles. Both the size distribution ranges of microbubbles at 37 ºC and 42 ºC were similar. Based on these results, an ultrasound cycle number of 100 was selected for the following experiment to induce cavitation.

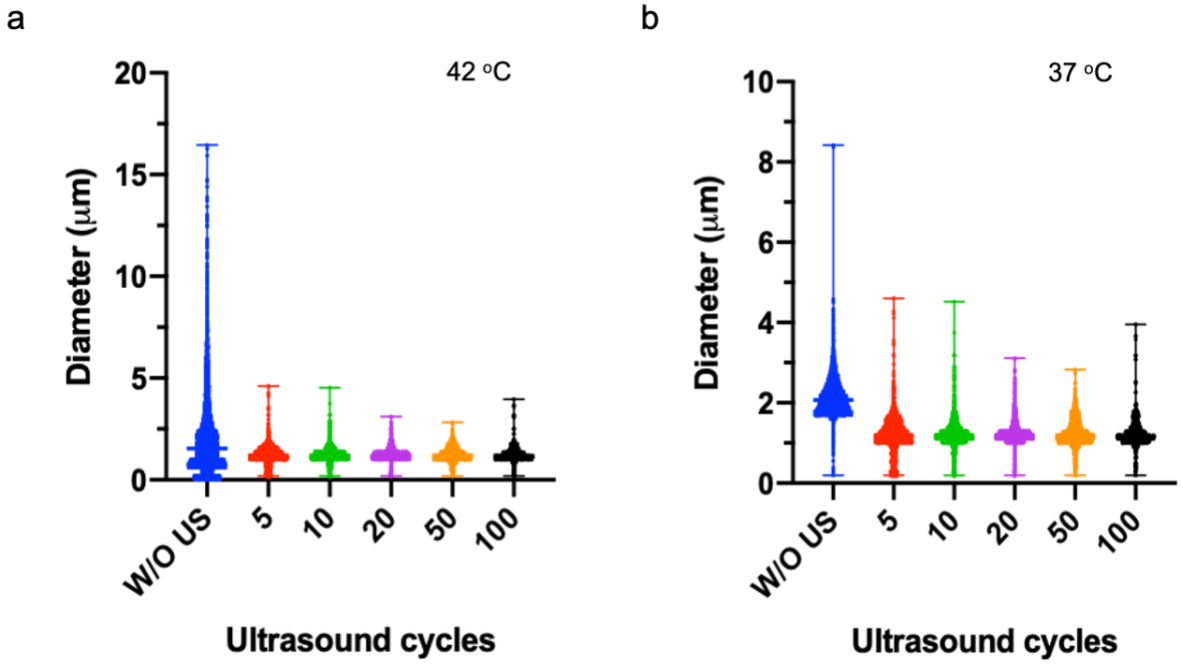

Figure 31 Size change of biotinylated microbubbles under different ultrasound pulsed cycle lengths at (a) 37 ºC or (b) 42 ºC.

In addition to changing the ultrasound cycle numbers in each pulse. The ultrasound pulse repetition frequency (PRF) also could potentially influence the cavitation of microbubbles, which could finally affect the DOX release. Therefore, it is necessary to evaluate the destruction rate of microbubbles when they were treated with different PRF. According to Equation 1, a higher PRF will provide a shorter pulse repetition period. As the scheme shown in Figure 1, with the same length of pulse period, decreasing the pulse repetition period will lead to the increase of duty cycle. Finally, the spatial-peak, time-averaged intensity (I_{SPTA}) will increase, while the pulse-averaged intensity (I_{SPPA}) was constant. As shown in Figure 32, when PRF was < 100 Hz, destruction rates of microbubble were ~37.5%. However, when PRF was increased to 1000 Hz, destruction rates of microbubble were increased to > 45%. Based on these results, PRF of 1 kHz was selected for the following experiment to induce cavitation.

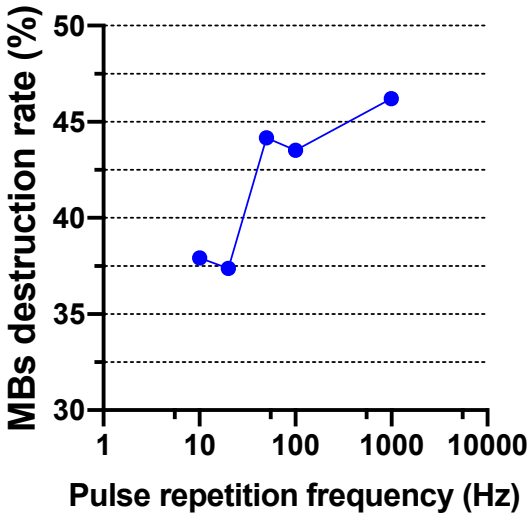

Figure 32 Microbubble destruction percentage under different ultrasound pulse repetition frequencies.

3.5.5 Ultrasound-induced cavitation and DOX release of TSL-DOX

Based on the previous experiment, doxorubicin-loaded thermosensitive liposomes (TSL-DOX) have been proven to release of ~70% the loaded doxorubicin (DOX) at 42 ºC. With different membrane molar fractions of biotinylated lipids, the TSL-DOX responded differently to release DOX. Therefore, in this section, I further evaluated the influence of ultrasound-induced cavitation on drug release of TSL-DOX. Before proceeding to examine the DOX release of TSL-DOX, it is important to introduce the differences in the experimental conditions in this section. Different from the previous experiment, in this section, microbubbles were added along with TSL-DOX in preparing the sample solution to induce the cavitation effect. DOX release of TSL-DOX has been tested under three research conditions: heating only, heating (blue curve) + ultrasound (red curve), and heating + cavitation (green curve). As shown in Figure 33a, TSL-DOX, with a 1~5% molar fraction of biotinylated lipids, release only ~5% of DOX at 37 ºC for 10 min. When treated with ultrasound exposure, the DOX release of TSL-DOX (1% biotinylated lipids) did not change. In contrast, TSL-DOX with 2~5% biotinylated lipids increased DOX release in comparison to the control groups without ultrasound exposure. Interestingly, when combined heating and cavitation, all types of TSL-DOX increased ~5 times of DOX release, see the green curve in Figure 33a. Among five types of TSL-DOX, the TSL-DOX, with 1% biotinylated lipids on the membrane, showed the highest DOX release after treating with heating and cavitation. The increase of DOX release also happened when TSL-DOX were heated to 42 ºC for 10 min. As shown in Figure 33b, the DOX release percentages are close when

TSL-DOX (1% & 2% biotinylated lipids) were treated with only heating (blue curve) or heating plus ultrasound exposure (red curve). However, for TSL-DOX (3~5% biotinylated lipids), the DOX release slightly increased in comparison to that were treated with only heating. Interestingly, when TSL-DOX were treated with both heating and cavitation (green curve), DOX release percentages were increased for all five types of TSL-DOX, in comparison to other control groups: W/O US and US. DOX release percentages are shown relative to the membrane molar ratio of biotinylated lipids. In three experimental groups, as the molar ratio of biotinylated lipids increased from 1% to 5%, DOX release dropped. For all five types of TSL-DOX that were treated with cavitation, the DOX release at 37 ºC was 30~40%, which was still lower than that at 42 ºC (50% ~ 80%). Though cavitation helps further increase DOX release, heating to the phase transition temperature (42 ºC) of TSL is the incentive for controlling DOX release.

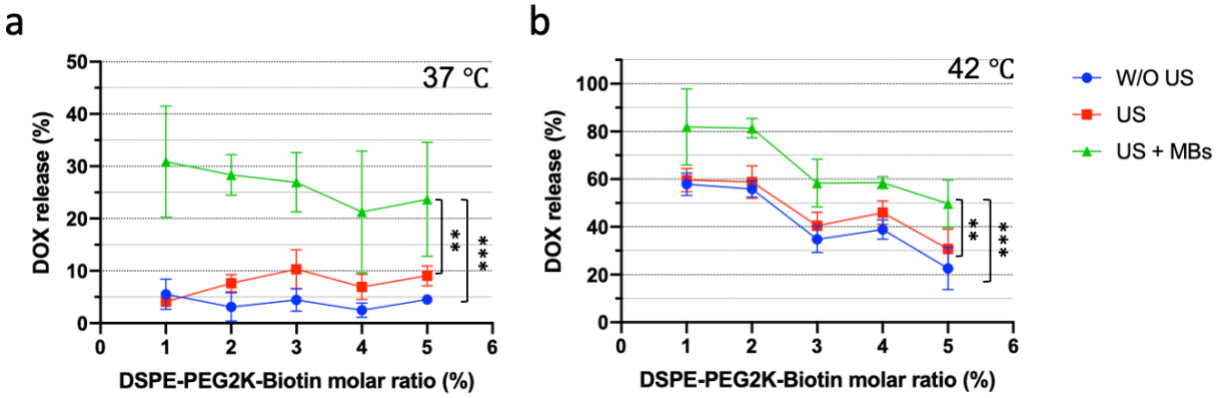

Figure 33 Ultrasound-induced cavitation and DOX release percentage of TSL-DOX with different biotin-lipid molar ratios at (a) 37 ºC or (b) 42 ºC. N = 3. US: ultrasound, MBs: microbubbles. ** P < 0.01; ***P < 0.001

3.5.6 DOX release increased percentage after heating and cavitation

Combining heating and cavitation has been proven to further increase DOX release than heating only. Yet, the enhancement range of DOX release has not been evaluated. Investigating the enhancement range of DOX release helps to further identify how much contribution of improving DOX release is from cavitation. TSL-DOX have been treated with two conditions: heating + ultrasound (blue curve) and heating + cavitation (red curve) at 37 ºC or 42 ºC. Figure 34a showed that TSL-DOX has DOX release percentages increased by 4.56 ± 2.83% when these liposomes were treated with ultrasound and heating at 37 ºC. Similarly, as shown in Figure 34b, when TSL-DOX were heated at 42 ºC for 10 min, enhancement of DOX release increased by 5.12 ± 3.82% after ultrasound exposures. With 5% of the biotinylated lipids on the membrane, DOX

release increased by 8.14 ± 3.39% when TSL-DOX in comparison to that was treated with ultrasound exposure only. When combined cavitation and heating, the enhancement of cumulative DOX release increased by 21.81 ± 8.85% for all types of TSL-DOX at 37 ºC. Increasing the molar ratios of biotinylated lipids of TSL-DOX does not obvious enhance or decrease the DOX release. When combined cavitation and heating, DOX release of TSL-DOX (1% biotinylated lipids) increased by 27.32 ± 5.75%. For TSL-DOX (2~4% biotinylated lipids), the enhancement of DOX releases slightly decreased. However, for TSL-DOX with 5% biotinylated lipids, the enhancement of DOX releases was 27.10 ± 12.61%. The average cavitation-induced enhancement of DOX release for all types of TSL-DOX at 42 ºC was 24.63 ± 9.34%. These results proved that combining cavitation and heating can further enhance DOX release at both 37 ºC and 42 ºC. These results proved that the membrane molar fraction of biotinylated lipids can also affect DOX release.

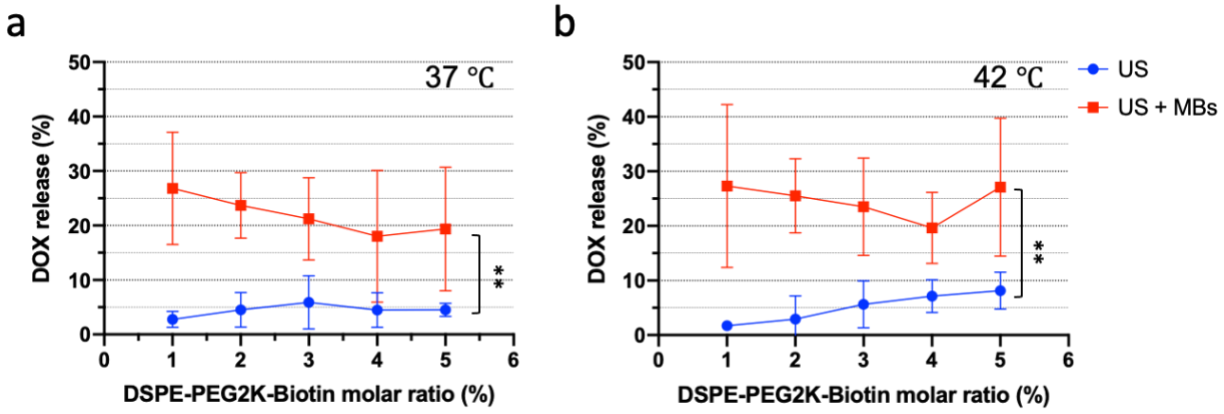

Figure 34 DOX release increased mediated by ultrasound-induced cavitation at (a) 37 ºC or (b)42 ºC. ** P < 0.01.

3.6 DOX-loaded thermosensitive liposomes-conjugated microbubbles (TSL-MB)

3.6.1 Conjugation of DiO-TSL and biotinylated microbubbles

DiO-labeled thermosensitive liposomes (DiO-TSL) were conjugated to the surface of biotinylated microbubbles based on the biotin-avidin-biotin linkage. To eliminate the experimental variables and to minimize the influence from DOX on the biotin-avidin conjugation, in this experiment, I prepared DiO-TSL (5% biotinylated lipids) that is without DOX loading in the core. DiO-TSL are too small to be detected by fluorescent microscopy because of the detection limit. In contrast, the microbubbles can be seen under microscopy. To evaluate the conjugation between TSL and microbubbles, the biotinylated microbubbles were not labeled with fluorescent dyes. The success of conjugation will be proved when the DiO signal was

detected from the surface of microbubbles. As shown in Figure 35a, the fluorescent signals of DiO-TSL showed many green spheres with different diameters at micrometers' level. The result in Figure 35b showed overlaps of the fluorescent-labeled spheres and the non-fluorescent labeled microbubbles (10% biotinylated lipids). This further confirmed that these green spheres were microbubbles. Figure 35c showed a larger view of a DiO-TSL conjugated microbubble and a non-conjugated microbubble. Both were highlighted by yellow circles. Figure 35d shown the cross-sectional fluorescent intensity distribution of two selected microbubbles in Figure 35c. The red curve described the overall fluorescent intensity of the microbubble area that has DiO-TSL conjugated on the surface. As a negative control, another microbubble nearby has no conjugation of DiO-TSL, showing low fluorescent intensity across the microbubble.

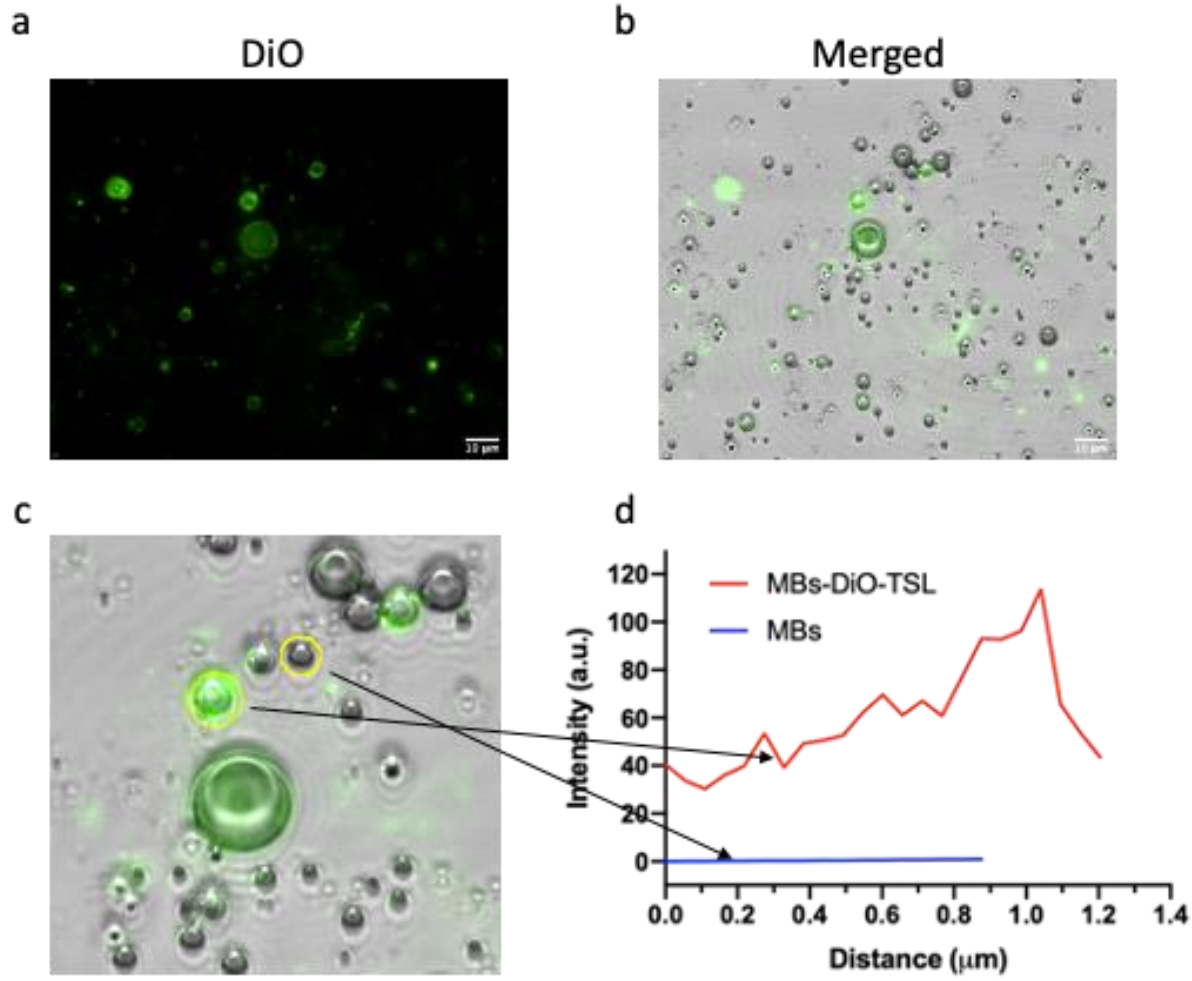

Figure 35 The conjugation of DiO-TSL and biotinylated microbubbles. (a) DiO fluorescent signal (green); (b) Merged view; (c) sectional amplification image; (d) cross-sectional fluorescent intensity

of the conjugated microbubble. TSL: thermosensitive liposomes; MBs: microbubbles. Scale bar = 10 µm

3.6.2 The molar fractions of biotinylated lipids on microbubbles and the conjugations

The conjugation between DiO-TSL and biotinylated microbubbles has been proved in the previous section. After that, it is necessary to find out what is the minimum molar fractions of DSPE-PEG2K-Biotin of microbubbles that can ensure a conjugation. Three types of microbubbles were prepared with the inclusion of 3, 5, and 10 mol% DSPE-PEG2K-Biotin without fluorescent labeling. The DiO-TSL were prepared with 5 mol% of DSPE-PEG2K-Biotin. As shown in Figure 36a-c, under the DiO fluorescent channels, the non-fluorescent-labeled microbubbles were shown as green color. Moreover, in Figure 36d-f, the DiO-TSL conjugated microbubbles were shown as green. Figure 36d-f also showed the merged views of the bright field and the DiO channel. With a 5% molar ratio of biotinylated lipids on the membrane, that most of the microbubbles were conjugated with DiO-TSL, in comparison to the microbubbles with a 3% molar ratio of biotinylated lipids. However, increasing the biotinylated lipids molar ratio to 10% did not obviously increase the numbers of TSL-conjugated microbubbles. Based on these results, a 5% molar ratio of the biotinylated lipids was chosen to prepare biotinylated microbubbles in the next experiment.

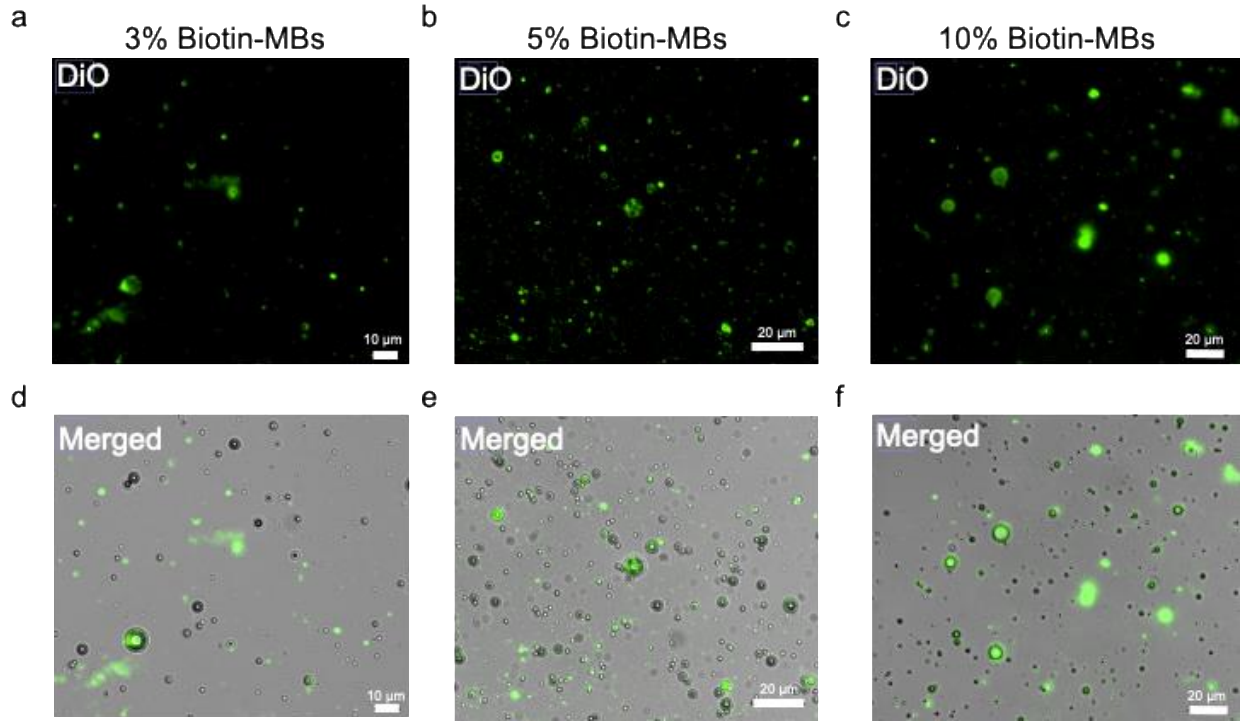

Figure 36 The conjugation of a DiO-TSL and a microbubble with different membrane molar ratio of biotin. MBs: microbubbles. Scale bar = 20 μm.

3.6.3 Biotinylated molar fractions of DiO-labeled TSL-DOX and the conjugation

Changing the membrane inclusion molar ratio of DSPE-PEG2K-Biotin on microbubbles might influence the conjugation between DiO-TSL and microbubbles. It is also important to know whether the inclusion molar ratio of DSPE-PEG2K-Biotin on TSL also influence the conjugation. Whether loading DOX into the core of TSL will affect the conjugations? To answer these two questions, I prepared DiO-labeled doxorubicin-loaded thermosensitive liposomes (DiO-TSL-DOX) with the inclusions of DSPE-PEG2K-Biotin of 1, 3, and 5 mol%. I also prepared non-fluorescent labeled microbubbles with 5 mol% of DSPE-PEG2K-Biotin. The fluorescent signals from DiO and DOX on the microbubbles will be regarded as proof of the conjugation. As shown in Figure 37, fluorescent signals of DiO were shown as green, while fluorescent signals of DOX were shown as magenta. The overlaps of DiO and DOX were shown as white color. The DiO-TSL (green) were shown at the surface of microbubbles, indicating the conjugations. And DOX (magenta) was also shown to overlap with the DiO signals. Both signals of DiO and DOX were shown as white color on the surface of microbubbles in the merged views. These results indicated that DOX and TSL were sharing the same locations after DiO-TSL-DOX were conjugated to microbubbles. Increasing the molar fractions of DSPE-PEG2K-Biotin of DiO-TSL does not improve the numbers of conjugations.

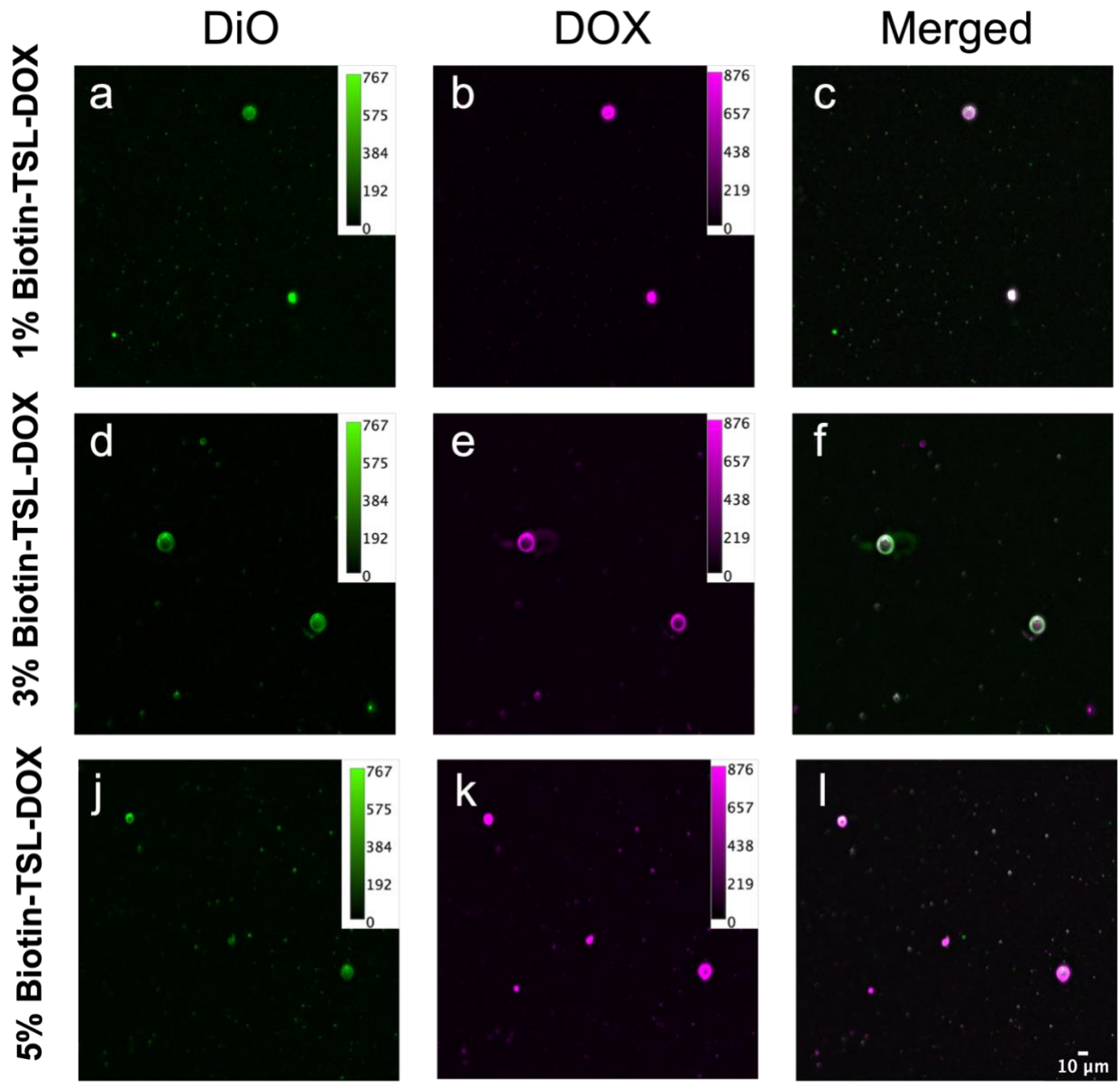

Figure 37 Conjugations between different DiO-labeled TSL-DOX and biotinylated microbubbles. DiO signal: green; DOX signal: magenta. Scale bar = 10 µm.

3.6.4 The conjugation of DiO-TSL-DOX and DiD-labeled microbubbles

The conjugation of a DiO-TSL-DOX and a DiD-labeled microbubble was testified. As shown in Figure 38b-e, the signals of a DiO-TSL-DOX were detected in DiO (green) and DOX (magenta) channels, while the signal of the DiD-MB was detected in DiD (red) channel. Triple colors merged well together, indicating a successful conjugation of a DiO-TSL-DOX and a DiD-MB (Figure 38e). To further confirm the relative

positions of each fluorescent dye on the microbubble, the fluorescent intensity-based spatial cross-correlation of microbubbles was detected. As shown in Figure 38f, the fluorescent intensity profiles of triple dyes across a microbubble were matched at similar positions, which indicate the membrane of the microbubble.

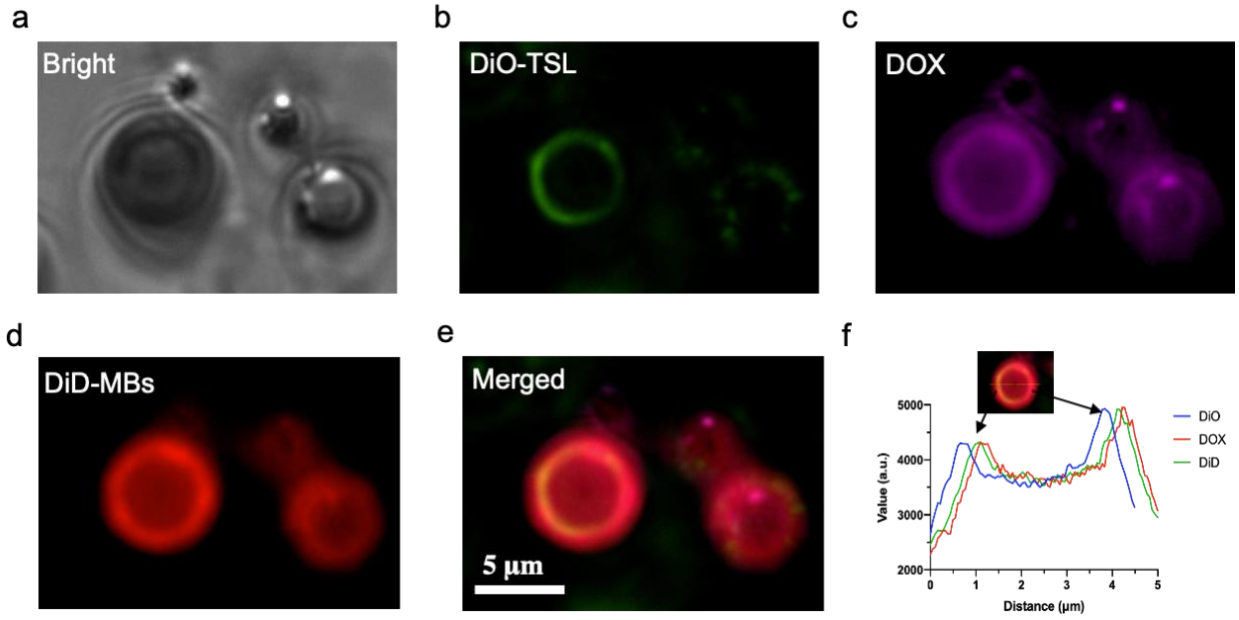

Figure 38 Conjugation of DiO-labeled, DOX-loaded TSL and DiD-labeled microbubble via biotin-avidin-biotin linkage. (a) Bright filed, (b) DiO (green): membrane of the TSL, (c) DOX (magenta): DOX-loading into TSL, (d) DiD (red): membrane of the microbubble, (e) Merged view of DiO, DOX, and DiD channels, (f) Intensity-based spatial cross-correlation of a microbubble.

3.6.5 Fluorescent colocalization of a DiO-TSL-DOX and a DiD-MB

Analyzing the conjugation ratio between a DiO-TSL-DOX and a DiD-MB is based on the fluorescent colocalization. Colocalization analysis describes the overlay level between two fluorescent channels(Adler & Parmryd, 2010). Manders' coefficient (range 0-1) is one of the colocalization coefficients, which is commonly used to describe the overlay level(Adler & Parmryd, 2010). Figure 39 showed the colocalization analysis between the fluorescent channels: DOX and DiO, DOX and DiD, and DiO and DiD. The Manders' coefficient between DOX channel and DiO channel was 0.484. This is similar as the coefficient between DiO and DiD: 0.477. The results indicate the fluorescence colocalization between DOX and DiO is as similar as that between DiO and DiD. The results further proved the conjugation of TSL-DOX and a

microbubble. The Manders' coefficient of DOX and DiD was 0.879, indicating a high overlay of DOX on the membrane of the microbubbles.

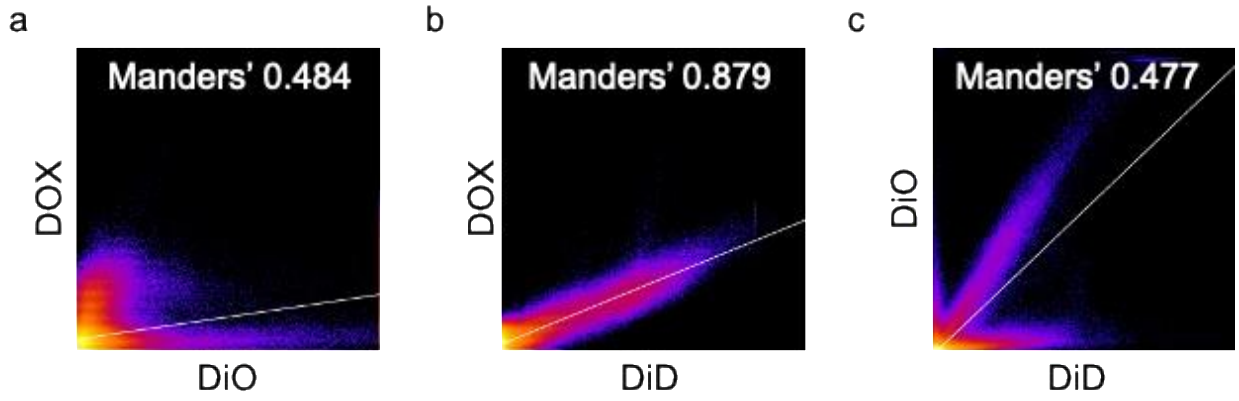

Figure 39 Colocalization analysis between fluorescent channels: (a) DOX and DiO, (b) DOX and DiD, and (c) DiO and DiD.

3.6.6 DOX release of TSL-MB by combining heating and cavitation

DOX release of DOX loaded thermosensitive liposome-conjugated microbubbles (TSL-MB) was evaluated at both 37 ºC and 42 ºC. According to the previous paper, there are ~1000 of TSL-DOX conjugated to one microbubble(Luan et al., 2012). According to this estimation, the sample solutions of TSL-MB (1×10^{10}) can carry drug-loaded liposomes of ~0.6×10^{13}. Both the sample solution of TSL-MB and TSL-DOX were finally diluted with 1X PBS with the same concentration of DOX (2.5 µg/mL). The DOX release percentage was calculated according to Equation 7. As shown in Figure 40, DOX release curves were similar between the groups of TSL treated with heating only (green curve) and heating + ultrasound (red curve) at 42 ºC for 10 min. The cumulative DOX release percentages are closed between three groups: TSL-MB, TSL heating only, and TSL + ultrasound (US) at 42 ºC. However, when only heating at 42 ºC for one minute, TSL-MB released ~ 50% DOX after cavitation, while the other control groups only have < 20% of DOX release. However, when heating for > 5 min, TSL-MB has a cumulative drug release of ~70%. Other research groups: TSL-DOX + US and TSL-DOX + heating only have a similar cumulative drug release of 62~65%. When heating at 37 ºC for different time, DOX release percentages of TSL-MB were <10% even treated with cavitation.

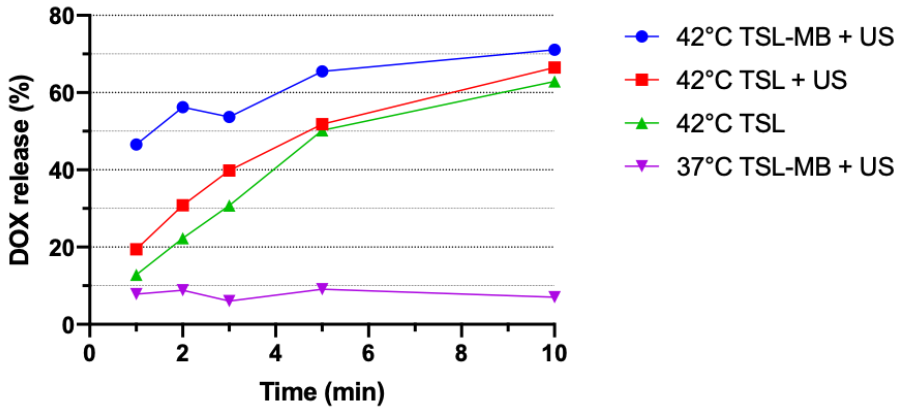

Figure 40 DOX release of TSL-MB by combining cavitation and heating.

3.6.7 Investigate the physical adsorption of the unloaded DOX and the biotinylated microbubbles

To prove that the signal of DOX is from the conjugation via biotin-avidin linkage instead of physical adsorption, the unloaded DOX and avidin were co-incubated with biotinylated microbubbles and then tested. There are two research groups: the TSL-DOX group and the unloaded DOX group. For the TSL-DOX group, DOX was loaded into liposomes; for the unloaded DOX group, the same concentration of free DOX as the TSL-DOX group without liposomal shells. Both the TSL-DOX and the unloaded DOX were added into the biotinylated microbubbles with the same amount of avidin, respectively. As shown in Figure 41a-b, the magenta fluorescence represents the signal of DOX. Most of the biotinylated microbubbles were conjugated with TSL-DOX. However, with the same experimental conditions and range of fluorescent intensity, the fluorescent signal of the unloaded DOX group is low. It was more obvious in the merged view (Figure 41b and Figure 41d) that the biotinylated microbubble was conjugated more with TSL-DOX, in comparison with the unloaded DOX.

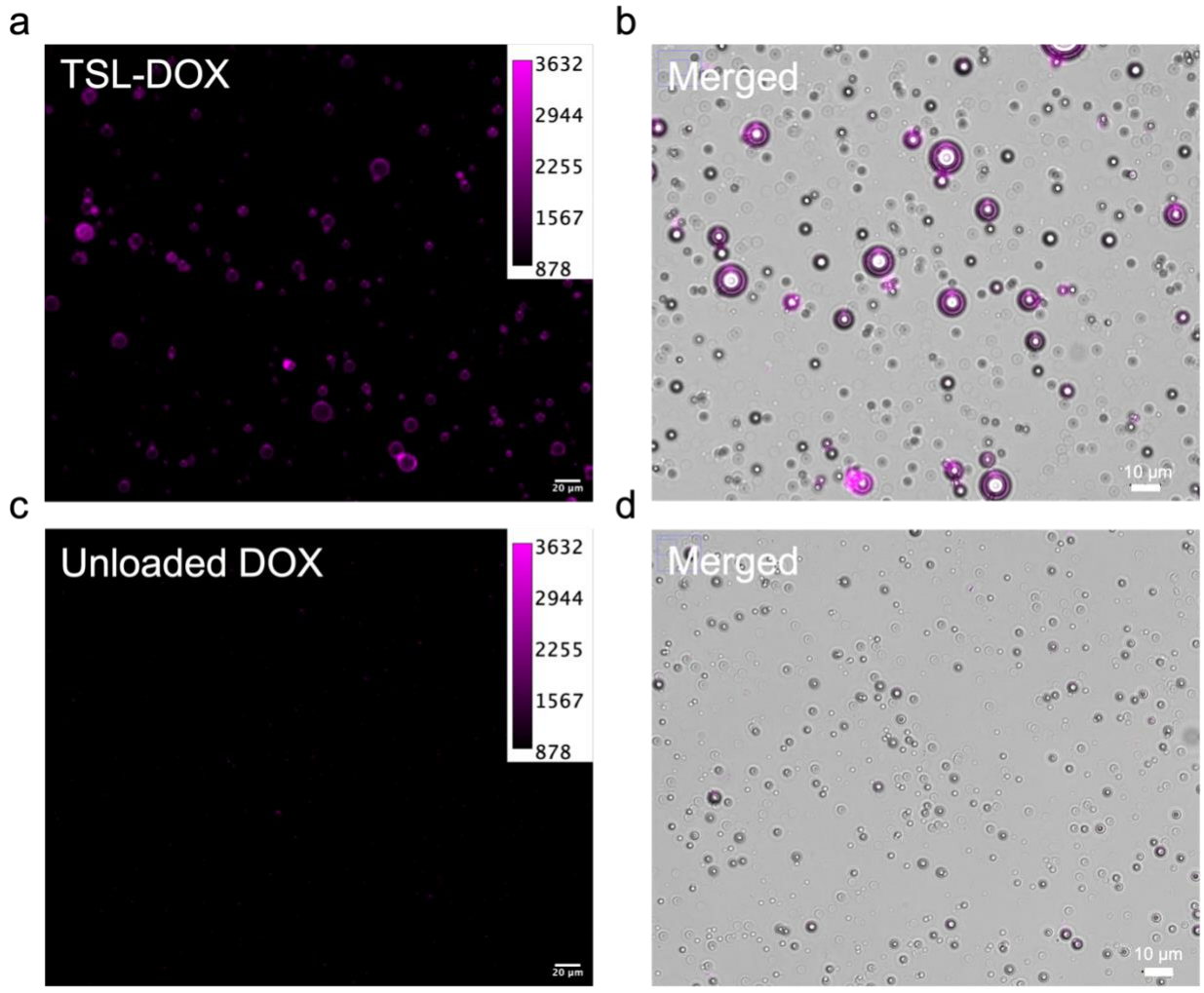

Figure 41 (a) and (b): the TSL-DOX conjugate to the biotinylated microbubbles. (c) and (d): physical adsorption of unloaded DOX and the biotinylated microbubbles in the presence of avidin.

Chapter 4 Interpretations and Significance of Study Findings

4.1 Summary of contributions

Combining ultrasound-induced cavitation and heating can increase the release of loaded drugs from thermosensitive liposomes (TSL) without changing the membrane lipid compositions. Cavitation can induce mechanical disruptions to the lipid membrane of TSL to trigger drug release(Lentacker et al., 2010), and the membrane compositions can change the phase behavior of the lipids, which also impacts the drug

release at a specific temperature(Kneidl et al., 2014). Current studies have proven that heating TSL to the phase transition temperature (T_m) can increase drug release from TSL(Dou et al., 2017). However, it is unknown how much contribution is from cavitation in increasing drug release. Is heating or cavitation the major incentive in increasing drug release when combining these two effects? Moreover, it is also unclear how does the membrane compositions of TSL influence the drug release after treating with heating and cavitation. To answer these questions, I have developed a series of doxorubicin-loaded thermosensitive liposomes (TSL-DOX) with inclusions of 1 to 5 mol% of DSPE-PEG2K-Biotin. The controlled drug release was triggered by heating TSL-DOX to the phase transition temperature (T_m) of 42 ^oC. Cavitation was then applied after heating TSL-DOX to 42 ^oC for 10 min. We found that combing heating and cavitation can further increase DOX release from TSL, in comparison to heating only. While heating to T_m is the main cause for triggering DOX release at T_m, cavitation acts as a secondary factor to further enhance DOX release. When the environmental temperature is lower than T_m, cumulative DOX release from TSL is lower than that were heated at the T_m even they were treated with cavitation. In addition to changing the environmental stimulations (heating and cavitation), changing the membrane compositions of TSL-DOX also affected DOX release percentage. With a higher inclusion of DSPE-PEG2K-Biotin on the membrane, the final cumulative DOX release percentage decreased even when they were treated with both heating and cavitation.

The research findings have supported the hypothesis of this research project: increasing temperature to the T_m is the driving force of DOX release, while cavitation helps to further increase the cumulative DOX release after heating. TSL-DOX, formed by different membrane formulations, will respond differently to cavitation and heating regarding drug release. Since cavitation helps to fully trigger drug release of TSL, it is possible to precisely control drug release by changing the cavitation effect. Controlling the relative distance between microbubbles and TSL could be one of the methods to control the influence of cavitation in drug release. Therefore, this project also developed another drug-carrying system thermosensitive liposomes conjugated microbubbles (TSL-MB) via biotin-avidin-biotin linkage. The successful conjugation has been proved. After heating and cavitation, TSL-MB increased DOX release at the early heating time (< 5 min), in comparison to heating only. Though the final cumulative drug release percentage did not increase, TSL-MB have shown the potential of controlling the drug release kinetics, which might base on the linkage of TSL and microbubbles. In summary, the findings of this research help to develop more novel controlled drug release methods using a thermosensitive liposomal system by combining heating and cavitation.

4.2 Significance of study findings

4.2.1 Preparation of TSL-DOX

The doxorubicin-loaded thermosensitive liposomes (TSL-DOX) have been developed using a staggered herringbone micromixer. By increasing the total flow rate (TFR) of the lipid solution and the $(NH_4)_2SO_4$ buffer, we have prepared thermosensitive liposomes (TSL) with sizes of 150 ~ 170 nm (see Figure 15 and Table 5). The sizes of the prepared TSL were constant in PBS or $(NH_4)_2SO_4$ buffer solutions for near three months (see Table 6). This indicates that the prepared TSL were stable in different buffer solutions. The anticancer drug doxorubicin (DOX) was loaded into TSL to form TSL-DOX. The encapsulation efficiency (EE) of DOX increased from ~42% to ~80% when the TFR was increased to 5mL/min (see Figure 19). This implied that increasing the mixing rate of lipids and buffer can improve the EE of DOX. However, the improvement is limited even we further increase TFR to 10 mL/min. This indicated that DOX loading is not fully dependent on the mixing rate of lipids and buffer. The fluorescent intensity of DOX in TSL-DOX was constant in PBS for one week (see Figure 20). This showed that TSL-DOX can keep stable in the solution without leaking DOX for at least one week.

4.2.2 Trigger DOX release of TSL-DOX by heating

The prepared TSL-DOX release ~ 70% of loaded DOX when they were heated at 42 °C while keeping a low leakage of DOX at 37 °C for 10 min (Figure 21). This indicated that TSL-DOX were rather stable at the human body temperature. TSL-DOX can selectively release the loaded DOX at a hyperthermia level (~ 42 °C). These properties limit the potentially toxic side effect of DOX to the other normal organs during in vivo blood circulation. The DOX release was related to the inclusion molar ratios of DSPE-PEG2K-Biotin. Increasing the inclusion molar ratios of DSPE-PEG2K-Biotin leads to a lower cumulative DOX release at 42 °C. This implied that DSPE-PEG2K-Biotin changed the membrane phase behavior or the membrane fluidities, leading to a less sensitive response of the lipids to 42 °C. Therefore, I investigated the thermal transition range of TSL-DOX by heating them from 37 to 45 °C (Figure 22a). The results further confirmed that the inclusion of DSPE-PEG2K-Biotin rise the transition temperature peak from 42 to 44 °C. TSL-DOX with 1 mol% DSPE-PEG2K-Biotin has a transition temperature peak of 42°C. However, TSL-DOX with 5 mol% DSPE-PEG2K-Biotin has a higher transition temperature peak of 44°C. These results suggested that the decrease of DOX cumulative release is related to the phase behavior. The phase behavior can be adjusted by increasing the inclusion of DSPE-PEG2K-Biotin. A maximum size change also reflects the states of TSL-DOX when they were heated close to the transition temperature peak (Figure 22b). The size changes

of TSL-DOX were reversible when they were cooling to room temperature. This result indicated that DOX release at 42°C does not destroyed the liposomal formulation in the buffer solution.

4.2.3 Triggering DOX release of TSL-DOX by combining heating and ultrasound

As heating to the phase transition temperature can increase DOX release from TSL-DOX. I further investigate whether TSL-DOX will release more loaded drug when they were treated with both heating and ultrasound without adding microbubbles to induce cavitation. Both the ultrasound burst cycles and exposure duration time have been tested. TSL-DOX release small amount of DOX when they were heated at 37 °C for 2 min then treated with ultrasound of different pulse cycles (Figure 27). Similar DOX release percentages of TSL-DOX at 42 °C for 2min were found, even they were also treated with ultrasound after heating. These results indicated ultrasound do not influence DOX release when TSL-DOX were at their early state of heating. The sizes and PDI of TSL-DOX also help to confirm this finding (Figure 28). In comparison to the obvious increase of size (Figure 22), TSL-DOX has no obvious changes of their sizes. The cumulative DOX release is 20 ~ 25%, which is in line with the findings in Figure 21. However, the DOX releases are chaotic when different types of TSL-DOX were heated at 42 °C and treated with ultrasound exposures. To further investigate the influence of ultrasound and heating on drug release, I prolonged the heating time to 10 min, then applied ultrasound to TSL-DOX with different exposure times. Prolonging ultrasound exposure time slightly increase DOX release of TSL-DOX with 1 and 5mol% DSPE-PEG2K-Biotin. However, DOX release percentages are similar for other groups of TSL-DOX with 2~4 mol% DSPE-PEG2K-Biotin. These results indicated that ultrasound has limited influence on further triggering DOX release after heating.

4.2.4 Improve DOX release by combining heating and cavitation

Before inducing cavitation to trigger DOX release from TSL-DOX, the cavitation of microbubbles was first evaluated. Microbubbles were developed and evaluated for their size and morphology (Figure 24 and Figure 25). Increasing the ultrasound pulse cycles or pulse repetition frequencies can increase the destruction rate of microbubbles, which can influence the cavitation effect (Figure 31 and Figure 33). By combining heating and cavitation, TSL-DOX has been proved to further increase doxorubicin (DOX) with a cumulative release of 80~100% (Figure 34). The DOX release induced by heating is ~70% (Figure 21), while the enhancement induced by cavitation is 20~35% (Figure 35). This indicated heating to the phase transition temperature (T_m): 42 ^oC is the primary incentive of increasing DOX release, cavitation is the secondary motive power that helps further enhance DOX release after heating. When TSL-DOX were heated to 37 ^oC and then were

treated with cavitation, the cumulative DOX release was 25~30%, lower than that at 42 ºC. Combining with heating and cavitation, the enhancement of DOX release at 37 ºC is 20~25% (Figure 34 a), which is close to that at 42 ºC(Figure 34 b). Increasing the molar ratios of biotinylated lipids on TSL decreased the cumulative drug release at both 37 ºC and 42 ºC even when these TSL-DOX were treated with cavitation after heating (Figure 33). However, no trend of DOX release changes induced by cavitation (Figure 34). This implied that DOX release at T_m is highly dependent on the membrane chemical properties instead of cavitation, which decide the thermal responsivity of TSL toward heating. In this situation, external stimulations like ultrasound or cavitation have limit influence on the drug release. However, when TSL-DOX were only heated at < T_m, DOX release is less dependent on the phase transition behavior of the membrane lipids. In contrast, the external mechanical disruptions (i.e. cavitation) can increase DOX release from TSL.

4.2.5 Develop a new ultrasound and thermal responsive drug-carrying system

According to the results in the previous section, cavitation and heating have been proved to further increase DOX release from different types of biotinylated TSL-DOX. Based on these findings, to control the relative distance between TSL-DOX and microbubbles, I further designed a new drug-carrying system: thermosensitive liposomes-conjugated microbubbles (TSL-MB). The conjugation was based on biotin-avidin-biotin linkage. Both biotinylated TSL-DOX and microbubbles were successfully prepared and evaluated in the previous sections. DiO-labeled TSL were conjugated to non-fluorescent labeled microbubbles (Figure 36). Increasing the molar fraction of DSPE-PEG2K-Biotin on microbubbles can increase conjugations (Figure 37). This implied that the concentration of DSPE-PEG2K-Biotin can be a key factor that influences the conjugations. Therefore, TSL-DOX with the inclusion of 2~5mol% of DSPE-PEG2K-Biotin were prepared to link to microbubbles (Figure 38). However, increasing the molar fraction of DSPE-PEG2K-Biotin did not improve conjugations. This indicated that DSPE-PEG2K-Biotin on the surface of TSL-DOX has less influence on the conjugations than those was on the surface of microbubbles. This might be related to differences in the surface areas between TSL-DOX and microbubbles. As TSL-DOX only have a surface area of 1.26×10^{-13} m^2, when their average diameter is ~200 nm. The surface area of microbubbles (diameter: 2 μm) is 100 times larger than TSL. Since increasing the molar fraction of DSPE-PEG2K-Biotin decreased the DOX release, 1mol% DSPE-PEG2K-Biotin was selected to prepare TSL-DOX to achieve the highest DOX release after heating and to conjugate to microbubbles. The DiO-TSL-DOX have proven to be conjugated to DiD-labeled microbubbles (see Figure 39). This indicates fluorescent labeling and DOX loading do not impact the conjugation. After that, the physical attachment of

unloaded DOX to biotinylated microbubbles has been tested. The result showed there is no absorption of the unloaded DOX to microbubbles. This indicated that the fluorescent signals of DOX are coming from TSL-DOX instead of the unloaded DOX in the surrounding environment. The unloaded DOX cannot attach to the surface of microbubbles. Combining cavitation and heating increased DOX release (~ 45%) of TSL-MB at 42 ^{o}C in 1 min (Figure 40). However, after treating with cavitation and heating, the cumulative DOX release percentages did not improve, in comparison to the mixed solution of TSL-DOX and microbubbles (Figure 33). These findings indicated that the conjugation between microbubbles and TSL-DOX do not change the final DOX release but might influence the kinetic process of DOX release. However, more independent tests are required for a convincing conclusion.

4.3 Limitations of the proposed method

4.3.1 More evaluations of controlling DOX release by combining heating and cavitation

The results have proved that heating to the phase transition temperature (T_m) is the leading cause of DOX release, while cavitation is another stimulation that helps to further release the loaded DOX from TSL-DOX. Combining heating and cavitation can also increase DOX of TSL-DOX at a temperature that is lower than T_m. Increasing the inclusion of DSPE-PEG2K-Biotin decreased the cumulative DOX release. However, it is unclear how DOX release can be adjusted by changing the other lipids instead of DSPE-PEG2K-Biotin. In addition to changing the chemical properties of TSL-DOX, controlling cavitation and its impacts on DOX release is another key direction that requires further investigation. More ultrasound parameters including ultrasound pressure and intensity should be taken into consideration. By detecting the acoustic pressure field of the ultrasound transducer could help to quantify the ultrasound intensity. This project has finished the development and characterization of thermosensitive liposomes-conjugated microbubbles (TSL-MB) to control the relative distance between TSL-DOX and microbubbles. The cavitation of TSL-MB can also affect the DOX release from the attached TSL-DOX. However, more investigations are required to evaluate DOX release from TSL-MB by combining heating and cavitation.

4.3.2 Acoustic pressure field detection

The acoustic pressure is directly linked to the ultrasound intensity that describes the acoustic energy and heat generation at the target point. Therefore, it is important to detect the acoustic pressure field of the transducer. However, this part of the work has only been partially done. To measure the spatial acoustic pressure field, a stepwise motion stage (XYZ-F140-L-600*600*100, IntelLiDrives, USA), an oscilloscope (DS1104Z, Rigol, Canada), and a hydrophone will be used. As shown in Figure 42, a motion stage will be

controlled by a computer using a MATLAB app that is to control the hydrophone to move in X, Y, and Z directions. The hydrophone transforms the accepted pressure signals of the transducer into electrical signals and passes them to the oscilloscope. The oscilloscope collects and shows the signals from both the signal generator and the hydrophone. These signals can be further calculated as the spatial acoustic pressures and the acoustic intensity in the computer. Based on the results, the 3-dimensional (3D) acoustic pressure and intensity at the focal area of the transducer will be confirmed. Finishing this part of the experiment will help to better control the ultrasound energy that is delivered to the targeted site to induce either cavitation or heating effect.

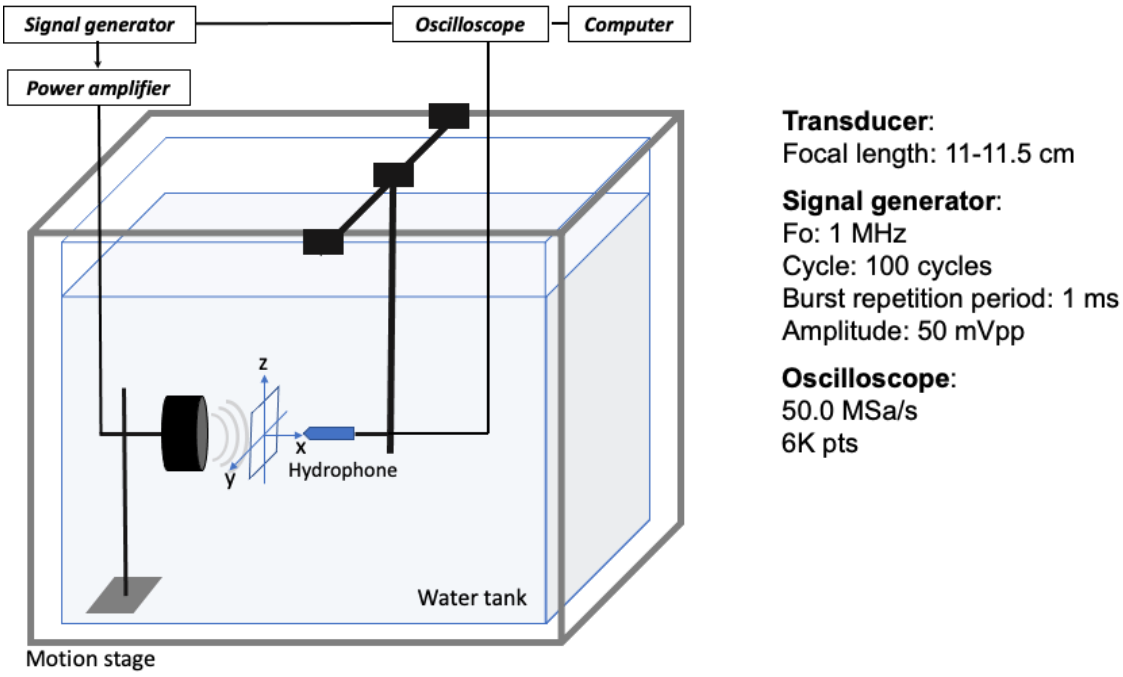

Figure 42 Acoustic pressure field detection of an ultrasound transducer perpendicular toward a hydrophone.

4.4 Future directions

4.4.1 Bubble-enhanced high-intensity focused ultrasound for controlled drug release

In addition to the cavitation effects, ultrasound can also rise the tissue temperature to induce hyperthermia (i.e. 40 ~ 45 °C)(Dromi et al., 2007; Grull & Langereis, 2012). This heating effect increases the local blood

perfusion and the passive diffusion of anticancer drugs to the targeted cells(Lang et al., 1999). Two Phase-I clinical trials have applied high-intensity focused ultrasound-induced hyperthermia (HIFU-HA) to enhance the delivery of Lysol-thermosensitive liposomal doxorubicin (i.e. Thermodox®) to treat breast cancer and liver cancer (i.e. TARDOX study) respectively(de Maar et al., 2020; Lyon et al., 2017). Although the concentration of DOX was increased in the tumor sites, the treatment procedure required up to 60 min of heating because HIFU has only a limited focal region to induce hyperthermia(de Maar et al., 2020). What's more, the heat transport efficiency of ultrasound decreases when the blood perfusion rate in the targeted tissue (e.g. liver) is high(Coussios et al., 2007; Eipel et al., 2010). Interestingly, there are studies shown a higher HIFU-induced heat deposit efficiency of the tissue, enhanced by locally scattering the acoustic energy (e.g. cavitation) (Coussios et al., 2007; Kaneko et al., 2005).

The thermosensitive liposome-conjugated microbubbles (TSL-MB) is a suitable drug-carrying system to investigate the DOX release mediated by the combination of ultrasound-induced cavitation and HIFU-HA, which is also called bubble-enhanced HIFU-HA. As we have found that combining heating and cavitation can increase the DOX release from TSL-DOX at an early heating stage (<5 min), the TSL-MB drug-carrying system can be used to induce bubble-enhanced HIFU-HA to trigger drug release from a thermosensitive drug carrying system.

4.5 Research summary

Investigating the drug release mechanism of smart drug delivery systems is significant in developing new controlled drug release methods. This thesis investigates drug release from doxorubicin-loaded thermosensitive liposomes (TSL-DOX) by combining heating and ultrasound-induced cavitation. To achieve this research goal, we first developed and evaluated drug release TSL-DOX that have different membrane compositions. Secondly, we evaluated DOX release by combining heating and cavitation by adjusting different temperatures and ultrasound parameters. We have found that heating to the phase transition temperature (T_m) is the primary reason of triggering DOX release. When TSL-DOX was heated above T_m, combining cavitation and heating can further enhance drug release without changing the membrane formulations of TSL. Cavitation enhanced DOX release from TSL-DOX at 37 ºC, improving drug release at the targeted site even when the temperature is lower than T_m: 42 ºC. Finally, based on these findings, we further developed and characterized a new functional drug delivery system: doxorubicin-loaded thermosensitive liposomes-conjugated microbubbles (TSL-MB). When applying both heating and cavitation to TSL-MB, we found an increase of DOX release when heating < 5min, in comparison to the TSL-DOX control group. This interesting finding suggested that conjugating TSL-DOX and microbubbles

can adjust the DOX release behavior at the early heating stage. For the future experiment, TSL-MB can be designed to load other therapeutic agents (e.g. genes, peptides, and antibodies) and can control the release of these loaded agents by combining heating and cavitation. Overall, we have proven that combing cavitation and heating will further improve drug release from TSL-DOX. These findings could support more the future investigations of drug release from other liposomal drug carrying systems.

References

Adler, J., & Parmryd, I. (2010). Quantifying colocalization by correlation: The Pearson correlation coefficient is superior to the Mander's overlap coefficient. *Cytometry. Part A: The Journal of the International Society for Analytical Cytology*, *77*(8), 733–742. https://doi.org/10/b8pkqp

Bamber, J. C., & Hill, C. R. (1979). Ultrasonic attenuation and propagation speed in mammalian tissues as a function of temperature. *Ultrasound in Medicine & Biology*, *5*(2), 149–157. https://doi.org/10/dht7bq

Barenholz, Y., Amselem, S., Goren, D., Cohen, R., Gelvan, D., Samuni, A., Golden, E. B., & Gabizon, A. (1993). Stability of liposomal doxorubicin formulations: Problems and prospects. *Medicinal Research Reviews*, *13*(4), 449–491. https://doi.org/10/fdqrhh

Batzri, S., & Korn, E. D. (1973). Single bilayer liposomes prepared without sonication. *Biochimica et Biophysica Acta (BBA) - Biomembranes*, *298*(4), 1015–1019. https://doi.org/10/bmk88r

Boissenot, T., Bordat, A., Fattal, E., & Tsapis, N. (2016). Ultrasound-triggered drug delivery for cancer treatment using drug delivery systems: From theoretical considerations to practical applications. *Journal of Controlled Release*, *241*, 144–163. https://doi.org/10/f88kd7

Bray, F., Ferlay, J., Soerjomataram, I., Siegel, R. L., Torre, L. A., & Jemal, A. (2018). Global cancer statistics 2018: GLOBOCAN estimates of incidence and mortality worldwide for 36 cancers in 185 countries. *CA: A Cancer Journal for Clinicians*, *68*(6), 394–424. https://doi.org/10/gd59tq

Carpentier, A., Canney, M., Vignot, A., Horodyckid, C., Goldwirt, L., Leclercq, D., Delattre, J.-Y., Chapelon, J.-Y., & Idbaih, A. (2015). Temporary disruption of the blood-brain barrier using an implantable ultrasound system for recurrent glioblastoma patients under IV carboplatin chemotherapy: Initial phase 1/2a clinical trial observations. *Journal of Therapeutic Ultrasound*, *3*(1), O14. https://doi.org/10/gkq5r3

Carpentier, A., Canney, M., Vignot, A., Reina, V., Beccaria, K., Horodyckid, C., Karachi, C., Leclercq, D., Lafon, C., Chapelon, J.-Y., Capelle, L., Cornu, P., Sanson, M., Hoang-Xuan, K., Delattre, J.-Y., & Idbaih, A. (2016). Clinical trial of blood-brain barrier disruption by pulsed ultrasound. *Science Translational Medicine*, *8*(343), 343re2-343re2. https://doi.org/10/gfwf34

Carugo, D., Bottaro, E., Owen, J., Stride, E., & Nastruzzi, C. (2016). Liposome production by microfluidics: Potential and limiting factors. *Scientific Reports*, *6*(1), 25876. https://doi.org/10/f8m548

Chang, P. P., Chen, W.-S., Mourad, P. D., Poliachik, S. L., & Crum, L. A. (2001). Thresholds for inertial cavitation in Albunex suspensions under pulsed ultrasound conditions. *IEEE Transactions on*

Ultrasonics, Ferroelectrics, and Frequency Control, *48*(1), 161–170. https://doi.org/10/dc7z9d

Charcosset, C., Juban, A., Valour, J.-P., Urbaniak, S., & Fessi, H. (2015). Preparation of liposomes at large scale using the ethanol injection method: Effect of scale-up and injection devices. *Chemical Engineering Research and Design*, *94*, 508–515. https://doi.org/10/f654c4

Chen, W.-S., Brayman, A. A., Matula, T. J., & Crum, L. A. (2003). Inertial cavitation dose and hemolysis produced in vitro with or without Optison®. *Ultrasound in Medicine & Biology*, *29*(5), 725–737. https://doi.org/10/dfcw26

Chen, X., Wan, J. M., & Yu, A. C. (2013). Sonoporation as a cellular stress: Induction of morphological repression and developmental delays. *Ultrasound Med Biol*, *39*(6), 1075–1086. https://doi.org/10.1016/j.ultrasmedbio.2013.01.008

Cheung, C. C. L., Ma, G., Ruiz, A., & Al-Jamal, W. T. (2020). Microfluidic Production of Lysolipid-Containing Temperature-Sensitive Liposomes. *Jove-Journal of Visualized Experiments*, *157*, e60907. https://doi.org/10/gjrs6j

Chowdhury, S. M., Lee, T., & Willmann, J. K. (2017). Ultrasound-guided drug delivery in cancer. *Ultrasonography*, *36*(3), 171–184. https://doi.org/10.14366/usg.17021

Coussios, D. >C C., Farny, C. H., Haar, G. T., & Roy, R. A. (2007). Role of acoustic cavitation in the delivery and monitoring of cancer treatment by high-intensity focused ultrasound (HIFU). *International Journal of Hyperthermia*, *23*(2), 105–120. https://doi.org/10/fg6476

Couture, O., Foley, J., Kassell, N. F., Larrat, B., & Aubry, J.-F. (2014). Review of ultrasound mediated drug delivery for cancer treatment: Updates from pre-clinical studies. *Translational Cancer Research*, *3*(5). https://doi.org/10.21037/3354

Daeichin, V., van Rooij, T., Skachkov, I., Ergin, B., Specht, P. A. C., Lima, A., Ince, C., Bosch, J. G., van der Steen, A. F. W., de Jong, N., & Kooiman, K. (2017). Microbubble Composition and Preparation for High-Frequency Contrast-Enhanced Ultrasound Imaging: In Vitro and In Vivo Evaluation. *Ieee Transactions on Ultrasonics Ferroelectrics and Frequency Control*, *64*(3), 555–567. https://doi.org/10.1109/TUFFC.2016.2640342

De Cock, I., Zagato, E., Braeckmans, K., Luan, Y., de Jong, N., De Smedt, S. C., & Lentacker, I. (2015). Ultrasound and microbubble mediated drug delivery: Acoustic pressure as determinant for uptake via membrane pores or endocytosis. *Journal of Controlled Release*, *197*, 20–28. https://doi.org/10/f6tbn8

de Maar, J. S., Suelmann, B. B. M., Braat, M. N. G. J. A., van Diest, P. J., Vaessen, H. H. B., Witkamp, A. J., Linn, S. C., Moonen, C. T. W., van der Wall, E., & Deckers, R. (2020). Phase I feasibility study of Magnetic Resonance guided High Intensity Focused Ultrasound-induced hyperthermia, Lyso-

Thermosensitive Liposomal Doxorubicin and cyclophosphamide in de novo stage IV breast cancer patients: Study protocol of the i-GO study. *Bmj Open*, *10*(11), e040162. https://doi.org/10/ghsp5m

Derieppe, M., Rojek, K., Escoffre, J.-M., de Senneville, B. D., Moonen, C., & Bos, C. (2015). Recruitment of endocytosis in sonopermeabilization-mediated drug delivery: A real-time study. *Physical Biology*, *12*(4), 046010. https://doi.org/10/gfv95j

Dong, Q., He, L., Chen, L., & Deng, Q. (2018). Opening the Blood-Brain Barrier and Improving the Efficacy of Temozolomide Treatments of Glioblastoma Using Pulsed, Focused Ultrasound with a Microbubble Contrast Agent. *Biomed Research International*, 6501508. https://doi.org/10.1155/2018/6501508

Dou, Y., Hynynen, K., & Allen, C. (2017). To heat or not to heat: Challenges with clinical translation of thermosensitive liposomes. *Journal of Controlled Release: Official Journal of the Controlled Release Society*, *249*, 63–73. https://doi.org/10/f9zz65

Doxil®—The first FDA-approved nano-drug: Lessons learned. (2012). *Journal of Controlled Release*, 18.

Dromi, S., Frenkel, V., Luk, A., Traughber, B., Angstadt, M., Bur, M., Poff, J., Xie, J., Libutti, S. K., Li, K. C. P., & Wood, B. J. (2007). Pulsed-high intensity focused ultrasound and low temperature sensitive liposomes for enhanced targeted drug delivery and antitumor effect. *Clinical Cancer Research*, *13*(9), 2722–2727. https://doi.org/10/cwcpxg

Dua, J. S., Rana, A. C., & Bhandari, D. A. K. (n.d.). *LIPOSOME: METHODS OF PREPARATION AND APPLICATIONS*. 7.

Duan, L., Yang, L., Jin, J., Yang, F., Liu, D., Hu, K., Wang, Q., Yue, Y., & Gu, N. (2020). Micro/nano-bubble-assisted ultrasound to enhance the EPR effect and potential theranostic applications. *Theranostics*, *10*(2), 462–483. https://doi.org/10/ghcm6d

Duan, X. X., Yu, A. C. H., & Wan, J. M. F. (2019). Cellular Bioeffect Investigations on Low-Intensity Pulsed Ultrasound and Sonoporation: Platform Design and Flow Cytometry Protocol. *Ieee Transactions on Ultrasonics Ferroelectrics and Frequency Control*, *66*(9), 1422–1434. https://doi.org/10.1109/Tuffc.2019.2923443

Duck, F. A. (2007). Medical and non-medical protection standards for ultrasound and infrasound. *Progress in Biophysics and Molecular Biology*, *93*(1), 176–191. https://doi.org/10/dc9f7g

Eipel, C., Abshagen, K., & Vollmar, B. (2010). Regulation of hepatic blood flow: The hepatic arterial buffer response revisited. *World Journal of Gastroenterology : WJG*, *16*(48), 6046–6057. https://doi.org/10/bsmg9r

Escoffre, J.-M., Derieppe, M., Lammertink, B., Bos, C., & Moonen, C. (2017). Microbubble-Assisted Ultrasound-Induced Transient Phosphatidylserine Translocation. *Ultrasound in Medicine and Biology*, *43*(4), 838–851. https://doi.org/10/f938p2

Evers, M. J. W., Kulkarni, J. A., Meel, R. van der, Cullis, P. R., Vader, P., & Schiffelers, R. M. (2018). State-of-the-Art Design and Rapid-Mixing Production Techniques of Lipid Nanoparticles for Nucleic Acid Delivery. *Small Methods*, *2*(9), 1700375. https://doi.org/10/ghxht7

Feshitan, J. A., Chen, C. C., Kwan, J. J., & Borden, M. A. (2009). Microbubble size isolation by differential centrifugation. *Journal of Colloid and Interface Science*, *329*(2), 316–324. https://doi.org/10/d29jzq

Gasca-Salas, C., Fernández-Rodríguez, B., Pineda-Pardo, J. A., Rodríguez-Rojas, R., Obeso, I., Hernández-Fernández, F., del Álamo, M., Mata, D., Guida, P., Ordás-Bandera, C., Montero-Roblas, J. I., Martínez-Fernández, R., Foffani, G., Rachmilevitch, I., & Obeso, J. A. (2021). Blood-brain barrier opening with focused ultrasound in Parkinson's disease dementia. *Nature Communications*, *12*(1), 779. https://doi.org/10/gk5n6q

Goss, S. A., Frizzell, L. A., & Dunn, F. (1979). Ultrasonic absorption and attenuation in mammalian tissues. *Ultrasound in Medicine & Biology*, *5*(2), 181–186. https://doi.org/10/c4t4cx

Grazia Andreassi, M., Venneri, L., & Picano, E. (2007). Cardiac imaging: The biological effects of diagnostic cardiac ultrasound. *Progress in Biophysics and Molecular Biology*, *93*(1), 399–410. https://doi.org/10/c9sm5n

Grull, H., & Langereis, S. (2012). Hyperthermia-triggered drug delivery from temperature-sensitive liposomes using MRI-guided high intensity focused ultrasound. *Journal of Controlled Release*, *161*(2), 317–327. https://doi.org/10/f33qg8

Gu, Y., Chen, C., Tu, J., Guo, X., Wu, H., & Zhang, D. (2016). Harmonic responses and cavitation activity of encapsulated microbubbles coupled with magnetic nanoparticles. *Ultrasonics Sonochemistry*, *29*, 309–316. https://doi.org/10/gmt5wq

Hensel, K., Mienkina, M. P., & Schmitz, G. (2011). Analysis of Ultrasound Fields in Cell Culture Wells for in Vitro Ultrasound Therapy Experiments. *Ultrasound in Medicine and Biology*, *37*(12), 2105–2115. https://doi.org/10/bzfgcm

Hertz, R., & Barenholz, Y. (1977). The relations between the composition of liposomes and their interaction with triton X-100. *Journal of Colloid and Interface Science*, *60*(1), 188–200. https://doi.org/10/cqtkhn

Hu, Y., Wan, J. M., & Yu, A. C. (2013). Membrane perforation and recovery dynamics in microbubble-

mediated sonoporation. *Ultrasound Med Biol*, *39*(12), 2393–2405. https://doi.org/10.1016/j.ultrasmedbio.2013.08.003

Idbaih, A., Ducray, F., Stupp, R., Baize, N., Chinot, O. L., De Groot, J. F., Guyotat, J., Sonabend, A. M., Menei, P., Dufour, H., Weinberg, J., Desseaux, C., Canney, M., Schmitt, C., & Carpentier, A. (2021). A phase I/IIa study to evaluate the safety and efficacy of blood-brain barrier (BBB) opening with the SonoCloud-9 implantable ultrasound device in recurrent glioblastoma patients receiving IV carboplatin. *Journal of Clinical Oncology*, *39*(15_suppl), 2049–2049. https://doi.org/10/gk5n6p

Ignee, A., Atkinson, N. S. S., Schuessler, G., & Dietrich, C. F. (2016). Ultrasound contrast agents. *Endoscopic Ultrasound*, *5*(6), 355–362. https://doi.org/10/ghkrdh

Jahn, A., Reiner, J. E., Vreeland, W. N., DeVoe, D. L., Locascio, L. E., & Gaitan, M. (2008). Preparation of nanoparticles by continuous-flow microfluidics. *Journal of Nanoparticle Research*, *10*(6), 925–934. https://doi.org/10/dsr3gc

Jesorka, A., & Orwar, O. (2008). Liposomes: Technologies and Analytical Applications. *Annual Review of Analytical Chemistry*, *1*(1), 801–832. https://doi.org/10/cznm36

Kaneko, Y., Maruyama, T., Takegami, K., Watanabe, T., Mitsui, H., Hanajiri, K., Nagawa, H., & Matsumoto, Y. (2005). Use of a microbubble agent to increase the effects of high intensity focused ultrasound on liver tissue. *European Radiology*, *15*(7), 1415–1420. https://doi.org/10/c9kqjk

Kneidl, B., Peller, M., Winter, G., Lindner, L. H., & Hossann, M. (2014). Thermosensitive liposomal drug delivery systems: State of the art review. *International Journal of Nanomedicine*, *9*, 4387–4398. https://doi.org/10/f6gtn7

Kotouček, J., Hubatka, F., Mašek, J., Kulich, P., Velínská, K., Bezděková, J., Fojtíková, M., Bartheldyová, E., Tomečková, A., Stráská, J., Hrebík, D., Macaulay, S., Kratochvílová, I., Raška, M., & Turánek, J. (2020). Preparation of nanoliposomes by microfluidic mixing in herring-bone channel and the role of membrane fluidity in liposomes formation. *Scientific Reports*, *10*(1), 5595. https://doi.org/10/ghv47v

Laginha, K. M., Verwoert, S., Charrois, G. J. R., & Allen, T. M. (2005). Determination of Doxorubicin Levels in Whole Tumor and Tumor Nuclei in Murine Breast Cancer Tumors. *Clinical Cancer Research*, *11*(19), 6944–6949. https://doi.org/10/cf7r2h

Landon, C. D., Park, J.-Y., Needham, D., & Dewhirst, M. W. (2011). Nanoscale Drug Delivery and Hyperthermia: The Materials Design and Preclinical and Clinical Testing of Low Temperature-Sensitive Liposomes Used in Combination with Mild Hyperthermia in the Treatment of Local Cancer. *The Open Nanomedicine Journal*, *3*, 38–64. https://doi.org/10/ccx97c

Lang, J., Erdmann, B., & Seebass, M. (1999). Impact of nonlinear heat transfer on temperature control in regional hyperthermia. *IEEE Transactions on Biomedical Engineering*, *46*(9), 1129–1138. https://doi.org/10/bzhtpr

Leighton, T. G. (2007). What is ultrasound? *Progress in Biophysics and Molecular Biology*, *93*(1), 3–83. https://doi.org/10/ct2xrg

Lentacker, I., Geers, B., Demeester, J., De Smedt, S. C., & Sanders, N. N. (2010). Design and Evaluation of Doxorubicin-containing Microbubbles for Ultrasound-triggered Doxorubicin Delivery: Cytotoxicity and Mechanisms Involved. *Molecular Therapy*, *18*(1), 101–108. https://doi.org/10/bc6h89

Leow, R. S., Wan, J. M., & Yu, A. C. (2015). Membrane blebbing as a recovery manoeuvre in site-specific sonoporation mediated by targeted microbubbles. *J R Soc Interface*, *12*(105). https://doi.org/10.1098/rsif.2015.0029

LI, J., YU, X., WAGNER, T. E., & WEI, Y. (2014). A biotin-streptavidin-biotin bridge dramatically enhances cell fusion. *Oncology Letters*, *8*(1), 198–202. https://doi.org/10/ghbk9b

Luan, Y., Faez, T., Gelderblom, E., Skachkov, I., Geers, B., Lentacker, I., van der Steen, T., Versluis, M., & de Jong, N. (2012). Acoustical Properties of Individual Liposome-Loaded Microbubbles. *Ultrasound in Medicine & Biology*, *38*(12), 2174–2185. https://doi.org/10/ghhftc

Lyon, P. C., Griffiths, L. F., Lee, J., Chung, D., Carlisle, R., Wu, F., Middleton, M. R., Gleeson, F. V., & Coussios, C. C. (2017). Clinical trial protocol for TARDOX: A phase I study to investigate the feasibility of targeted release of lyso-thermosensitive liposomal doxorubicin (ThermoDox®) using focused ultrasound in patients with liver tumours. *Journal of Therapeutic Ultrasound*, *5*(1), 28. https://doi.org/10/gg8wgg

Münter, R., Kristensen, K., Pedersbæk, D., Bruun Larsen, J., Bæk Simonsen, J., & Lars Andresen, T. (2018). Dissociation of fluorescently labeled lipids from liposomes in biological environments challenges the interpretation of uptake studies. *Nanoscale*, *10*(48), 22720–22724. https://doi.org/10/gfrqd3

Nelson, T. R., Fowlkes, J. B., Abramowicz, J. S., & Church, C. C. (2009). Ultrasound Biosafety Considerations for the Practicing Sonographer and Sonologist. *Journal of Ultrasound in Medicine*, *28*(2), 139–150. https://doi.org/10/gh64pt

Qin, P., Han, T., Alfred, C. H., & Xu, L. (2018). Mechanistic understanding the bioeffects of ultrasound-driven microbubbles to enhance macromolecule delivery. *Journal of Controlled Release*, *272*, 169–181. https://doi.org/10/gc3vbb

Sapra, P., & Allen, T. M. (2003). Ligand-targeted liposomal anticancer drugs. *Progress in Lipid*

Research, *42*(5), 439–462. https://doi.org/10/fpj8nk

Scott, C. C., Vacca, F., & Gruenberg, J. (2014). Endosome maturation, transport and functions. *Seminars in Cell & Developmental Biology*, *31*, 2–10. https://doi.org/10/f59bnn

Sirsi, S. R., & Borden, M. A. (2014). State-of-the-art materials for ultrasound-triggered drug delivery. *Advanced Drug Delivery Reviews*, *72*, 3–14. https://doi.org/10/f59fcq

Small, E. F., Dan, N. R., & Wrenn, S. P. (2012). Low-Frequency Ultrasound-Induced Transport across Non-Raft-Forming Ternary Lipid Bilayers. *Langmuir*, *28*(40), 14364–14372. https://doi.org/10/f3842k

Small, E. F., Willy, M. C., Lewin, P. A., & Wrenn, S. P. (2011). Ultrasound-induced transport across lipid bilayers: Influence of phase behavior. *Colloids and Surfaces A-Physicochemical and Engineering Aspects*, *390*(1–3), 40–47. https://doi.org/10/b4x8tt

Stride, E., Segers, T., Lajoinie, G., Cherkaoui, S., Bettinger, T., Versluis, M., & Borden, M. (2020). Microbubble Agents: New Directions. *Ultrasound in Medicine & Biology*, *46*(6), 1326–1343. https://doi.org/10/ggtg29

Stroock, A. D., Dertinger, S. K. W., Ajdari, A., Mezić, I., Stone, H. A., & Whitesides, G. M. (2002). Chaotic Mixer for Microchannels. *Science*, *295*(5555), 647–651. https://doi.org/10/b85smb

Suzuki, R., Oda, Y., Utoguchi, N., Namai, E., Taira, Y., Okada, N., Kadowaki, N., Kodama, T., Tachibana, K., & Maruyama, K. (2009). A novel strategy utilizing ultrasound for antigen delivery in dendritic cell-based cancer immunotherapy. *J Control Release*, *133*(3), 198–205. https://doi.org/10.1016/j.jconrel.2008.10.015

Swaay, D. van, & deMello, A. (2013). Microfluidic methods for forming liposomes. *Lab on a Chip*, *13*(5), 752–767. https://doi.org/10/f4krw5

Takahashi, T., Nakagawa, K., Tada, S., & Tsukamoto, A. (2019). Low-energy shock waves evoke intracellular Ca2+ increases independently of sonoporation. *Scientific Reports*, *9*. https://doi.org/10.1038/s41598-019-39806-x

Tu, J. W., Zhang, H., Yu, J. S., Chun, L. F., & Chen, Z. Y. (2018). Ultrasound-mediated microbubble destruction: A new method in cancer immunotherapy. *Oncotargets and Therapy*, *11*, 5763–5775. https://doi.org/10.2147/Ott.S171019

Tung, Y.-S., Vlachos, F., Choi, J. J., Deffieux, T., Selert, K., & Konofagou, E. E. (2010). In vivo transcranial cavitation threshold detection during ultrasound-induced blood-brain barrier opening in mice. *Physics in Medicine and Biology*, *55*(20), 6141–6155. https://doi.org/10/dctzqt

Wang, M., Zhang, Y., Cai, C., Tu, J., Guo, X., & Zhang, D. (2018). Sonoporation-induced cell membrane permeabilization and cytoskeleton disassembly at varied acoustic and microbubble-cell

parameters. *Sci Rep*, *8*(1), 3885. https://doi.org/10.1038/s41598-018-22056-8

Wilhelm, S., Tavares, A. J., Dai, Q., Ohta, S., Audet, J., Dvorak, H. F., & Chan, W. C. W. (2016). Analysis of nanoparticle delivery to tumours. *Nature Reviews Materials*, *1*(5). https://doi.org/10/gcskzm

Yang, F., Gu, N., Chen, D., Xi, X., Zhang, D., Li, Y., & Wu, J. (2008). Experimental study on cell self-sealing during sonoporation. *Journal of Controlled Release*, *131*(3), 205–210. https://doi.org/10/d2d9ws

Yatvin, M. B., Weinstein, J. N., Dennis, W. H., & Blumenthal, R. (1978). Design of liposomes for enhanced local release of drugs by hyperthermia. *Science (New York, N.Y.)*, *202*(4374), 1290–1293. https://doi.org/10/drhs9r

Yu, B., Lee, R. J., & Lee, L. J. (2009). Microfluidic Methods for Production of Liposomes. *Methods in Enzymology*, *465*, 129–141. https://doi.org/10/b8pnsm

Zeghimi, A., Escoffre, J. M., & Bouakaz, A. (2015). Role of endocytosis in sonoporation-mediated membrane permeabilization and uptake of small molecules: A electron microscopy study. *Physical Biology*, *12*(6), 066007. https://doi.org/10/gg2kx2

Zeghimi, A., Uzbekov, R., Arbeille, B., Escoffre, J.-M., & Bouakaz, A. (2012). Ultrastructural Modifications of Cell Membranes and Organelles Induced by Sonoporation. In *2012 Ieee International Ultrasonics Symposium (ius)* (pp. 2045–2048). Ieee. https://doi.org/10.1109/ULTSYM.2012.0511

Zhao, F., Zhao, Y., Liu, Y., Chang, X., Chen, C., & Zhao, Y. (2011). Cellular Uptake, Intracellular Trafficking, and Cytotoxicity of Nanomaterials. *Small*, *7*(10), 1322–1337. https://doi.org/10/c7kzfw

Zhong, W., Sit, W. H., Wan, J. M., & Yu, A. C. (2011). Sonoporation induces apoptosis and cell cycle arrest in human promyelocytic leukemia cells. *Ultrasound Med Biol*, *37*(12), 2149–2159. https://doi.org/10.1016/j.ultrasmedbio.2011.09.012